Thesis for the degree of Doctor of Philosophy

ALL-PHOTONIC CONTROL OF BIORELEVANT PROCESSES USING MOLECULAR PHOTOSWITCHES AND CAGED COMPOUNDS

JESPER R. NILSSON

Department of Chemistry and Chemical Engineering
Chalmers University of Technology
Gothenburg, Sweden 2015

Department of Chemistry and Chemical Engineering
Chalmers University of Technology
SE-412 96 Gothenburg
Sweden
Telephone + 46 (0)31-772 1000

Front Cover:
In ancient Roman tradition, Janus the two-faced God symbolized transitions – from one state to another.

Back Cover:
Photo by Lena Nyberg (or was it Maria or Emma? Thanks for lending me the LOMO, Maxim. It's a fantastic camera.)

ALL-PHOTONIC CONTROL OF BIORELEVANT PROCESSES USING MOLECULAR PHOTOSWITCHES AND CAGED COMPOUNDS

JESPER R. NILSSON

Department of Chemistry and Chemical Engineering
Chalmers University of Technology

Abstract

The development of light-controlled molecular tools for *in situ* regulation of biological activity holds great promise *e.g.* for resolving dynamic aspects of cellular signal transduction and to overcome inherent pharmaceutic limitations such as poor drug selectivity. In this thesis, photoswitchable molecules from the spiropyran, dithienylethene, and azobenzene families as well as an *o*-nitrobenzyl-type caged compound were used in a variety of constellations intended for biological use. The presented research ranges from spectroscopic studies on isolated molecular interactions in solution to photoactivated kinase inhibition in live zebrafish.

The first part of this thesis focuses on novel approaches for photocontrolled drug release, based on a supramolecular competitive binding methodology. Two host-guest systems were investigated for this purpose; a dithienylehtene – porphyrin dimer, and a spiropyran – cucurbit[7]uril (CB7) system. In the first investigated system, it was found that drug release could be reversibly controlled by light. The spectral properties of the release scaffold also provided a fluorescence-based reporting function. In the second system, an unexpected loss of spiropyran bistability was observed upon complexation to CB7. Also, the undesired hydrolysis of the spiropyran photoswitch was completely halted when bound to the macrocycle. The spiropyran hydrolysis reaction was further examined in a separate study, also included in this thesis.

The second and thirds parts focus on photocontrolled small-molecules introduced to living systems. This includes a study on the cytotoxic properties of a DNA-binding spiropyran in live human cancer cells. It was demonstrated how cell-death could be selectively triggered by photoisomerizing the spiropyran to the merocyanine form inside the cells. Part three focuses on photocontrolled inhibition of the, for cancer highly relevant, *RE*arranged during *T*ransfection (RET) kinase. An azobenzene-derived photoswitch and an *o*-benzyl-type caged inhibitor based on the pyrazolopyrimidine scaffold were developed and evaluated. Both compounds exhibited light-controlled RET inhibition in an isolated enzyme- and live cell assay. The caged compound was also used to photonically activate inhibition of RET in live zebrafish, confirming uptake and decaging of the compound inside the live organism.

Keywords: photoswitch, caged compound, drug release, spiropyran, dithienylethene, azobenzene, *o*-nitrobenzyl, kinase inhibitor, live cell, spectroscopy.

List of publications

This thesis is based on the work contained in the following papers:

I   Light-induced cytotoxicity of a photochromic spiropyran
       Jesper R. Nilsson, Shiming Li, Björn Önfelt* and Joakim Andréasson*
       Chemical Communications **47**, 11020–11022 (2011).

II   Switching Properties of a Spiropyran–Cucurbit[7]uril Supramolecular
       Assembly: Usefulness of the Anchor Approach
       Jesper R. Nilsson, Cátia Parente Carvalho, Shiming Li, José Paulo Da Silva,
       Joakim Andréasson* and Uwe Pischel*
       ChemPhysChem **13**, 3691–3699 (2012)

III   Characterization of the Thermal and Photoinduced Reactions of
       Photochromic Spiropyrans in Aqueous Solution
       Martin Hammarson, Jesper R. Nilsson, Shiming Li, Tamás Beke-Somfai and
       Joakim Andréasson*
       Journal of Physical Chemistry B **117**, 13561−13571 (2013)

IV   A Photoswitchable Supramolecular Complex with Release-and-Report
       Capabilities
       Jesper R. Nilsson, Melanie C. O'Sullivan, Shiming Li, Harry L. Anderson
       and Joakim Andréasson*
       Chemical Communications **51**, 847−850 (2015)

V   Design, Synthesis and Inhibitory Activity of Photoswitchable RET Kinase
       Inhibitors
       Rubén Ferreira, Jesper R. Nilsson, Carlos Solano, Joakim Andréasson* and
       Morten Grøtli*
       Accepted for publication in Scientific Reports

VI   A Caged Ret Kinase Inhibitor and its Effect on Motoneuron Development
       in Zebrafish Embryos
       David Bliman, Jesper R. Nilsson, Petronella Kettunen, Joakim Andréasson*
       and Morten Grøtli*
       In revision

Contribution report[†]

Paper I: Carried out and analyzed the spectroscopic measurements. Participated in the imaging experiments. Wrote the manuscript.

Paper II: Planned, performed, and analyzed the spectroscopic experiments together with C. P. C. Did not partake in the mass-spectrometry measurements.

Paper III: Participated in performing and analyzing the spectroscopic experiments. Did not partake in the theoretical calculations.

Paper IV: Designed, performed, and analyzed the experiments. Wrote the manuscript.

Paper V: Designed, performed, and analyzed the spectroscopic measurements and the biological testing. Wrote the manuscript.

Paper VI: Planned, performed, and analyzed the spectroscopic experiments and (together with D.B.) the *in vitro* biological testing. Assisted in the zebrafish experiments. Contributed to writing the manuscript.

Publications not included in this thesis

DNA-Binding Properties of Amidine-Substituted Spiropyran Photoswitches
Martin Hammarson, Jesper R. Nilsson, Shiming Li, Per Lincoln and Joakim Andréasson*
Chemistry – A European Journal **20**, 15855–15862 (2014)

An All-Photonic Molecule-Based Parity Generator/Checker for Error Detection in Data Transmission
Magnus Bälter, Shiming Li, Jesper R. Nilsson, Joakim Andréasson* and Uwe Pischel*
Journal of the American Chemical Society **135**, 10230−10233 (2013)

8-Triazolylpurines: Towards Fluorescent Inhibitors of the MDM2/p53 Interaction
Mariell Pettersson, David Bliman, Jimmy Jacobsson, Jesper R. Nilsson, Jaeki Min, Luigi Iconaru, R. Kiplin Guy, Richard W. Kriwacki, Joakim Andréasson, Morten Grøtli*
In revision

[†] No contribution to the synthesis work was made by this author in the appended papers.

Contents

1 Thesis Introduction

Potent and selective therapeutic compounds are essential tools in clinical medicine. By studying the structure and native function of biochemical targets, biomedical researchers strive to design molecules that are able to interact with and perturb target activity, to yield therapeutic benefits for the patient. Iterative testing-redesign programs are applied to identify the most suitable drug candidate with respect to efficacy and safety, which is then taken through the different phases of clinical trials. This well-established scheme is at the heart of modern rational drug design and has helped build the impressive catalogue of drugs we have on the market today. However, there exists a serious limitation inherent to traditional pharmacotherapy; after distributing the compound, there is no way to regulate when and where the molecule is active – all control over that agent is essentially lost. This intrinsic lack of control combined with imperfect target selectivity in the designed drugs, frequently lead to more or less severe adverse drug reactions and patient suffering.[1] This is particularly recognizable for aggressive therapeutic treatments such as chemotherapy.

The chemical biologist is held back by the same limitation. Signal transduction research relies heavily on the development of strongly interacting and selective small-molecule effectors.[2,3] By studying the cellular response(s) following modulation of biochemical pathways involved in pathophysiological processes, information on how these signaling cascades are interconnected can be extracted. This type of refined knowledge is crucial when trying to understand overall cause-and-effect relationships of drug-target interactions and how to efficiently regulate them. However, since these signaling events are time- and space-dependent processes, valuable information is lost if we cannot control when and where the molecular probe is active.[4]

The above paragraphs are examples meant to highlight the usefulness of developing externally controllable molecular tools. They serve to introduce this thesis, which main objective is to describe how *light* can be used to control molecular structure and how this concept can be applied to create biologically relevant tools and applications. Light is a versatile stimulus able to instantly interact with molecules without having to add additional chemicals. Also, under certain conditions, light to which biological tissue is more or less transparent can be applied to remotely trigger molecular events inside our body.[5] The development of photocontrolled biological tools is primarily motivated by the *increased selectivity* that comes with the spatiotemporal resolution of light. It should be noted that the photocontrolled applications presented in this thesis (in their current state) are far from being useful in any clinical application. Nevertheless, the prospective use of a general photocontrolled system is exemplified from a clinical viewpoint in Figure 1.
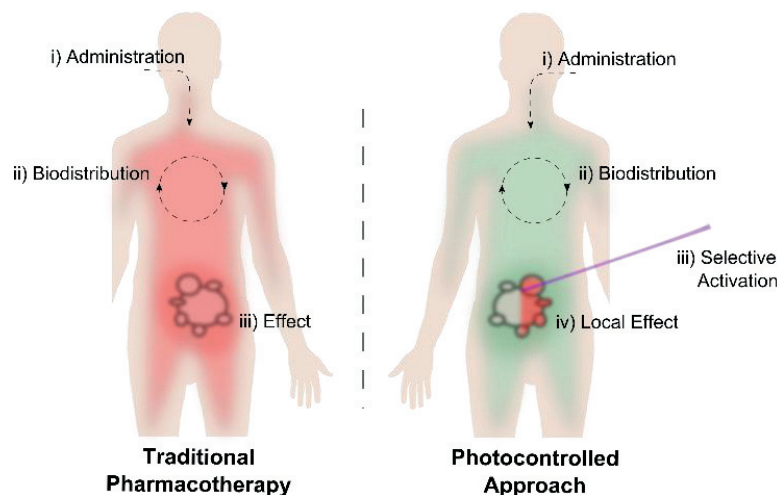
Figure 1. Comparison between traditional pharmacotherapy and a photocontrolled approach. Left panel: In the traditional approach, the administered drug (red color) is typically also the target-interacting drug.‡ Due to more or less inadequate selectivity, regions other than the target area are also exposed to the drug, leading to treatment-related side effects. Right panel: In the photocontrolled approach, the light-responsive drug can be designed to be inactive in the administered form (green color). Upon exposing the target area to light (iii), the drug can be selectively activated (red color) in a highly localized manner.

Two main strategies for inferring light-responsiveness in molecular samples are described in this thesis; using photochromic[4,6-11] and photocaged[4,10-16] compounds. Photocromic compounds, (photoswitches) are a class of molecules that can be reversibly transformed between two or more forms using light. As the name photo*chrome* [*chroma* (χρώμα), greek = color] implies, the molecular transformation is typically accompanied by a change in color of the compound. You may already be familiar with some photochromic devices. The arguably most recognized example is photochromic eyewear, which darken in response to UV light from the sun. What is perhaps less obvious is that the change in color is due to a structural rearrangement in the molecules embedded in the plastic laminate on the glasses. In this case, the color change itself serves a purpose but in fact, virtually all physicochemical characteristics of the photoswitch change to some extent upon light exposure; the size, shape, structural flexibility, polarity, redox properties, *etc.* One may say that light has created an entirely new molecule. In this thesis, the focus is not so much on the color change but rather on how to harness the other properties that come with it, to afford for instance photoswitchable binding affinity and biological activity. As mentioned above, a photo*caged* strategy has also been explored. Caged compounds are photoresponsive molecules that, in contrast to the *reversible* nature of photoswitches, are *irreversibly* transformed by light.

---

‡ One exception is the use of so-called *prodrugs*, which are activated in the metabolic process in the body.

This general introduction is followed by two chapters, in which some underlying theoretical considerations related to light-matter interactions are introduced (chapter 2), along with a brief account on the main experimental techniques (chapter 3) used in the appended research. This should hopefully provide an adequate theoretical foundation for the comprehension of the presented results. Readers well-accustomed to the language of physical chemistry may perceive parts of these chapters as more-than-comprehensible, and should approach them as they see fit.

Further on, in chapter 4, an overview of the existing strategies for controlling biological systems with light are outlined. This includes a description of the working principle of photoswitches and photocages, along with a brief account on strategies for extending the usability of photoresponsive compounds through supramolecular arrangements with non-photochromic molecules. Protein kinases fulfills an important role as a biological target in this thesis. Therefore, a description of their overall function is also included.

The original research presented in this thesis is based on the six appended papers (from here on referred to as Papers I-VI). The results are summarized in chapter 5, which is organized into three parts. The first part (section 5.1) focuses on fundamental intermolecular interactions between photoswitches and non-photochromic molecules. It includes two projects exploring a drug displacement methodology to achieve photoswitchable drug release systems. These systems rely on supramolecular interactions between a spiropyran photoswitch and the cucurbit[7]uril macrocycle (Paper II), as well as a dithienylethene photoswitch and a porphyrin dimer (Paper IV). Also presented in the first part is a kinetic characterization study of a series of photoswitches from the spiropyran family in buffer solution (Paper III). In particular, the unwanted hydrolytic reaction of spiropyrans is scrutinized on.

The results in the second and third parts of chapter 5 (sections 5.2 and 5.3, respectively) lie closer to the field of molecular biology, as they both include studies on living systems. In part two, the light-induced cytotoxic- and uptake properties of a spiropyran were studied in a human cancer cell-line (Paper I). Part three focuses exclusively on photocontrolled enzyme inhibition. There, an azobenzene-derived photoswitch (Paper V) and *o*-nitrobenzyl-type caged compound (Paper VI) for gaining photonic control over the inhibition of a receptor tyrosine kinase are described.

2 Fundamentals

There is no simple way of explaining how light interacts with matter and any attempt to thoroughly do so is well beyond the scope of this thesis. Nevertheless, as most of the concepts discussed herein involves light-matter interactions, a brief account on selected qualities is presented below. The latter part of this chapter is dedicated to host-guest chemistry, since a significant part of my work revolves around these concepts. This includes the supramolecular strategies described in Papers II and IV, as well as kinase inhibition in Papers V and VI.

2.1 Light

Light is successfully described as two things at once. One often refers to the *wave-particle duality* of light, where it on one hand is described as an oscillating electromagnetic wave propagating through space, and on the other hand as a flow of discrete, (rest-) massless energy particles. The wave description depicts light as consisting of two periodically oscillating components, one electric and one magnetic, on a right angle to each other and the direction of propagation (Figure 2). Light was shown to possess a wave-like character as early as the 1600's through the work of Hooke, Huygens and Euler. It was not until the 1860's, however, that Scottish physicist James Clerk Maxwell was able to propose a comprehensive set of differential equations, effectively assigning co-varying electric and magnetic properties to light.[17]
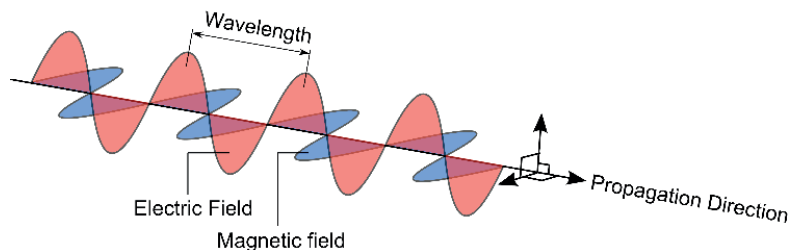
Figure 2. The electromagnetic wave-description of light.

The familiar graphic representation shown in Figure 2 is a consequence of the Maxwell equations, which (although derived solely from classical physics) remain extraordinarily accurate in predicting experimental outcomes where light can be regarded purely as a wave. In the year 1900, inspired by his studies on black body radiation, Max Planck postulated that all systems that emit light do so in discrete units of energy – *quanta*.[18] The proportionality constant is called Planck's constant (h), and it follows that the energy (E) of quanta can be calculated according to equation [1].

$$E = h\nu \qquad [1]$$

Here ν is the frequency of oscillation. For light with wavelength λ travelling at a constant speed (c), the energy can be calculated according to equation [2].

$$E = \frac{hc}{\lambda} \qquad [2]$$

The concept of discrete energy packets (*photons,* as they were later termed)[19], did not resonate with the established wave-description of light. Nevertheless, Heinrich Hertz's[20] and Einstein's[21] contemporary experiments on the photoelectric effect strongly supported Planck's ideas on quantized energy. An important contribution in reference to the wave-particle discussion was put forward in 1924 by French physicist Louis de Broglie,[22] in which he proposed that all particles (at the time he was referring to the electron) in fact moves like waves – *matter-waves*. The de Broglie hypothesis further muddled the distinction between energy, particles, and waves, highlighting the need for a unified theory of light and matter. Today, following the paradigm shift of the quantum revolution and years of subsequent refinements, we have arrived at a quantum mechanical description of light in which the abovementioned aspects can be accounted for. The notion of wave-particle duality still holds, however, and the two representations are used interchangeably.

2.2 Matter

In the Bohr atom model, which emerged in 1913, the atom was proposed to consist of a positively charged nucleus around which electrons orbit at set distances – *shells*, representing energy levels.[23] Moving an electron between these shells proceeds in concert with absorption or emission of light. With this model, Bohr was able to justify the mathematical equations explaining atomic spectral line patterns observed for instance in electric discharge experiments (*e.g.* the Rydberg formula), and show that the proportionality did in fact adhere to the abovementioned Planck relation. The requirement for light to exactly match the energy difference between an initial state (i) and a final state (f) in an atom or molecule is therefore called the *Bohr frequency condition* and can be expressed according to equation [3].

$$E_f - E_i = h\nu \qquad [3]$$

Based on the Bohr model and the de Broglie matter-wave hypothesis, *wave mechanics* (largely based on the work of Erwin Schrödinger),[24] emerged as a quantum mechanical adaptation for describing the quantum nature of matter. The wave-description of matter, in combination with Heisenberg's uncertainty principle,[25] changed the

perception of electron motion in atoms. Instead of orbiting the nucleus (as in the Bohr model), the electrons were depicted as residing within nuclei-centered probability distributions – *orbitals*. The atomic orbitals are obtained by solving the Schrödinger equation for the atom in question. What determines the properties of an atom is the number of protons and neutrons in the nucleus and how the atomic orbitals are populated by electrons *i.e.* the electron configuration.

Molecular orbitals, depicting the electron density across an entire molecule, can in turn be approximated by linear combinations of the involved atomic orbitals. The ground state electron configuration of atoms and molecules are worked out by pairing electrons in the orbitals according to the *Aufbau principle, Pauli exclusion principle* and *Hund's rule*. The relative energies and electron occupancy of molecular orbitals can provide insights into photophysical processes. Of particular importance are the highest occupied- and the lowest unoccupied molecular orbitals (HOMO and LUMO, respectively) which are central in the so called *Frontier Molecular Orbital theory.*[26] Depending on the number of electrons and relative energies of the available orbitals, unpaired electrons may occur, resulting in different *spin multiplicities*. The by far most frequent scenario in the ground state is to have a spin multiplicity of 1. This occurs when the molecule contain spin-paired electrons, and the state is called a *singlet*. For molecules with two unpaired electrons, the spin multiplicity is 3 and the corresponding state is called a *triplet*. Triplets are very uncommon in the ground state of a molecule but exceptions exists, for instance molecular oxygen.

Each electronic state in a molecule contain several vibrational states and each vibrational state several rotational states, all of which are quantized. This implies that there are large differences in the energy required to stimulate these transitions. By applying the *Boltzmann distribution* to calculate the relative occupancy of these states in the absence of light at room temperature, it can be concluded that a typical small-molecule in solution populates the lowest vibrational state of the lowest electronic state.

2.3   Photoexcitation

The mathematical framework of quantum mechanics provides a concise (albeit abstract) means of describing not only the state of a molecule, but also the mechanisms with which it transfers from one state to another. The probability for a molecule to absorb light can be said to depend on how well the incident light resonates with the change in the electronic landscape of the molecule. In quantum mechanics, *perturbation theory*[27] can be used for approximating the responses of molecules to weak disturbances. *Fermi's golden rule*, as stated in equation [4], gives the probability (P_{fi}) per unit time of a perturbation-induced transition from an initial state (Ψ_i) to final state (Ψ_f).

$$\frac{dP_{fi}}{dt} = 2\pi\rho \left| \langle \Psi_f | \hat{H}' | \Psi_i \rangle \right|^2 \qquad [4]$$

The integration implied in the bra-ket notation is taken over all space, and ρ is the density of final states. When the perturbation is induced by light, the perturbing Hamiltonian ($\hat{H}'$) can be approximated by the scalar product between the electric field[§] of light, $\bar{E}(t)$, and the *dipole operator* ($\hat{\mu}$), as shown in equation [5].

$$\frac{dP_{fi}}{dt} = 2\pi\rho \left| \langle \Psi_f | \bar{E}(t) \cdot \hat{\mu} | \Psi_i \rangle \right|^2 \qquad [5]$$

Here, $\hat{\mu}$ evaluates the charge-weighted distances of all species in the molecule according to equation [6].

$$\hat{\mu} = \sum_j q_j \bar{r}_j \qquad [6]$$

Assuming the electric field is uniform over the molecule,[**] the time-dependent probability can be written according to equation [7].

$$\frac{dP_{fi}}{dt} = \frac{2\pi(\bar{E}_0 \cdot \bar{\mu}_{fi})^2}{h^2} \rho_v(v_{fi}) \qquad [7]$$

Here, $\bar{E}_0$ is the amplitude and $\rho_v(v_{fi})$ the number of oscillation modes of the electric field at the transition frequency v_{fi}. The *transition dipole moment* ($\bar{\mu}_{fi}$) is also introduced in equation [7]. This molecule- and transition-specific parameter can be interpreted as a vector pointing in the direction of the net electron flow as the molecule is excited. It is defined in terms of the dipole operator according to equation [8].

$$\bar{\mu}_{fi} = \langle \Psi_f | \hat{\mu} | \Psi_i \rangle \qquad [8]$$

From the above exercise (see in particular equation [7]), two factors can be identified as determining the intensity of light absorption. First, the transition dipole moment squared ($\bar{\mu}_{fi}{}^2$), also referred to as the *dipole strength* and second, the scalar product

---

[§] Due to the relative difference in strength (electric interactions are significantly stronger than magnetic) it is often considered sufficient to include only interactions between the electric field component of light and the electric charges of the molecule, while a full treatment would also require the magnetic field component to be taken into account.

[**] The wavelength of the oscillating light used in molecular spectroscopy is significantly longer (for example *ca.* 200-800 nm in UV/vis spectroscopy) than the corresponding molecular spatial dimension (*ca.* 1-10 nm), justifying the assumption of uniformity.

$\bar{E}_0 \cdot \bar{\mu}_{fi}$, which infers a cosine squared directionality condition between the incident electric field vector and the transition dipole moment vector. The theoretically deduced dipole strength is directly proportional to the *molar absorption coefficient*, $\varepsilon(\nu)$. Molecules with appreciably large molar absorption coefficients in the visible electromagnetic region are called *chromophores*. This parameter and its relation to molar absorption are discussed further in section 3.1.

2.4   Excited State Processes

The excited state processes described in this section are those of a typical chromophore in solution. It is by no means an exhaustive description of all possible excited state processes. Note in particular that intermolecular excited state reactions are not considered. Upon photon absorption, a molecule (M) is promoted from the ground state (S_0) to an electronically excited state (S_n). This can be denoted as shown in reaction [9].

$$M + h\nu_1 \rightarrow M^* \qquad\qquad [9]$$

In molecules, the destination state is typically a vibrationally excited state within the S_n electronic state, making the absorption event a *vibronic* transition. The available processes through which a molecule dissipate absorbed energy, can be summarized in a *Jablonski dagram* (Figure 3).
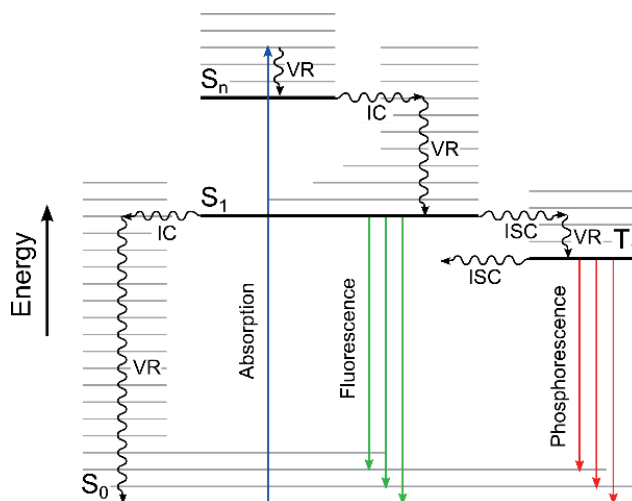
Figure 3. Jablonski diagram illustrating absorption and excited state deactivation processes. Electronic states are shown as bold horizontal lines, these include singlet states (S_0, S_1, S_n) and a triplet state (T_1). Vibrational states are shown as gray horizontal lines. All radiative processes are represented by straight arrows. These are absorption (blue), fluorescence (green), and phosphorescence (red). The non-radiative processes are depicted as wavy arrows and include vibrational relaxation (VR), internal conversion (IC), and intersystem crossing (ISC).

Following excitation to S_n, the molecule typically relaxes to the lowest vibrational state of S_1 through a combination of very efficient non-radiative processes. The relaxation processes leading to the S_1 state occur on a much shorter time scale than the corresponding processes depopulating S_1 (due to the *Energy gap law*). Excited state processes are therefore approximated as proceeding exclusively from S_1. This is often referred to as *Kasha's rule*.[28] Once in S_1, the molecule can relax to the ground state *via* one of the following three routes. *(1)* Non-radiative relaxation. This involves *internal conversion* (IC), a horizontal (isoenergetic) transition between electronic states of the same multiplicity, followed by dissipation of energy to solvent molecules through *vibrational relaxation* (VR). *(2)* Through the triplet state. For this to occur the molecule has to first undergo a spin-forbidden horizontal transition (*inter system crossing, ISC*) to the triplet state, T_1. From T_1 the molecule can return to S_1 either by emitting a photon or by relaxing non-radiatively. Emissive relaxation from a triplet state to a singlet state is called *phosphorescence*. *(3)* Radiative relaxation. The spin-conserved emission of a photon is called *fluorescence* and, analogous to the word chromophore (for visible light absorbers), fluorescent molecules are called *fluorophores*. Emissive decay, either *via* fluorescence of phosphorescence, can be written according to reaction [10].

$$M^* \rightarrow M + h\nu_2 \qquad [10]$$

To express the fraction of molecules relaxing *via* a specific pathway a *quantum yield* (Φ) is defined. The quantum yield for a specific process is simply the number of process-specific events per absorbed photon. It follows that the rate (k_i) with which process i proceeds can be used to define the quantum yield, as shown in equation [11].

$$\Phi_i = \frac{\#\ events\ of\ type\ i}{\#\ photons\ absorbed} = \frac{k_i}{\sum_j k_j} \qquad [11]$$

Here, the sum $\sum_j k_j$ denotes the rates (including k_i) with which S_1 is depopulated. Another important property of a molecule is how for long it stays in the excited state. The *excited state lifetime* (τ_f) of a molecule is defined according to equation [12] and describes the average time the molecule spends in the excited state.

$$\tau_f = \frac{1}{\sum_j k_j} \qquad [12]$$

Two quantum yields are particularly relevant in this thesis; the fluorescence- and isomerization quantum yields, Φ_f and Φ_{iso}, respectively. The latter is discussed in section 2.4.2.

2.4.1   Excitation Energy Transfer (EET)

Under certain conditions, the excited state of a molecule can be depopulated by transferring its excitation quanta to an adjacent molecule. Following the convention of reactions [9] and [10], this can be expressed according to the following series of reactions, involving the donor (D) and acceptor (A) of the quanta.

$$D + A + h\nu_1 \overset{1}{\rightarrow} D^* + A \overset{2}{\rightarrow} D + A^* \overset{3}{\rightarrow} D + A + h\nu_3 \qquad [13]$$
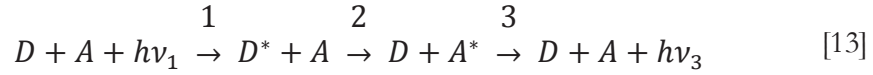
The energy transfer step (reaction [13], step 2) can occur either *via* electron exchange (*Dexter energy transfer*) or *Förster resonance energy transfer*, FRET.[29] While the Dexter mechanism requires orbital overlap (direct contact), FRET can occur over larger distances (up to *ca.* 100 Å). The rate of excitation energy transfer *via* FRET (k_{FRET}) can be expressed according to equation [14].

$$k_{FRET}(r) = \frac{1}{\tau_{f,D}} \left(\frac{R_0}{r} \right)^6 \qquad [14]$$

In this equation, $\tau_{f,D}$ is the fluorescence lifetime of the donor in the absence of acceptor, and r the distance between donor and acceptor. The *Förster distance* (R_0) is the donor-acceptor distance at which 50% of the donor molecules relaxes *via* FRET. The *energy transfer efficiency, $E(r)$*, can therefore be expressed in terms of R_0 and r, according to equation [15].

$$E(r) = \frac{R_0^6}{R_0^6 + r^6} \qquad [15]$$

Note how the efficiency of energy transfer depends on the donor-acceptor distance to the inverse power of six. This strong distance dependence makes FRET an excellent method for measuring the proximity of D-A pairs. Finally, the Förster distance can be written as a function of the donor fluorescence quantum yield ($\Phi_{f,D}$) the orientation factor (κ^2), the overlap integral between the normalized emission spectrum of the donor, $F_D(\lambda)$, and the molar absorption coefficient of the acceptor, $\varepsilon(\lambda)$, according to equation [16].

$$R_0^6 = \frac{9000\Phi_{f,D}(ln10)\kappa^2}{128\pi^5 n^4 N_A} \int F_D(\lambda)\varepsilon(\lambda)\lambda^4 d\lambda \qquad [16]$$

In this equation, n is the refractive index of the intervening medium (typically the solvent), and N_A Avogadro's number. The Förster distance (to the power of six) is in other words dependent on FRET-pair specific parameters and directly proportional to κ^2. The orientation factor, in turn, depends of the relative orientation between the transition dipole moments of the donor and acceptor and ranges from 0 (for perpendicular arrangement) to 4 (linearly aligned). For randomly oriented FRET-pairs, κ^2 equals 2/3.

2.4.2 Photochromism

The photochromic reaction is central to this thesis. According to the IUPAC Gold Book it is defined as "a reversible transformation of a molecular entity between two forms, A and B, having different absorption spectra, induced in one or both directions by absorption of electromagnetic radiation. The spectral change produced is typically, but not necessarily, of visible color and is accompanied by differences in other physical properties."[30] The overall process according to the above definition can be written as shown in reaction [17] where r_{AB} and r_{BA} denote the reaction rates.

$$A \underset{r_{BA}}{\overset{r_{AB}}{\rightleftharpoons}} B \qquad [17]$$
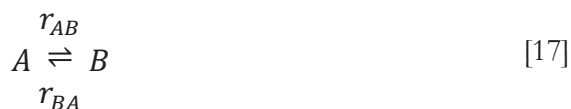
Since photochromic reactions are initiated by the absorption of light and thus are excited state process, the isomerization quantum yield (Φ_{iso}) can be defined analogous to equation [11], to yield equation [18];

$$\Phi_{iso} = \frac{\#\ isomerization\ events}{\#\ absorbed\ photons} \qquad [18]$$

The reaction rate r_{AB} (r_{BA} is defined analogously) can be expressed as the product of the light intensity, $I(\lambda)$, molar absorption coefficient, $\varepsilon(\lambda)$, and Φ_{iso} according to equation [19].

$$r_{AB} \propto [A]I(\lambda)\varepsilon_A(\lambda)\Phi_{iso}^{AB} \qquad [19]$$

For a photochromic reaction performed with a wavelength where both species A and B have non-zero molar absorption, a *photostationary distribution* (*PSD*), where $r_{AB} = r_{BA}$, is reached. Assuming wavelength-independent Φ_{iso}, the PSD can be written according to equation [20].

$$PSD = \frac{[A]}{[B]} = \frac{\varepsilon_B(\lambda)\Phi_{iso}^{BA}}{\varepsilon_A(\lambda)\Phi_{iso}^{AB}} \qquad [20]$$

Equation [20] is particularly useful for selecting a suitable wavelength to perform the photoswitching. Neglecting any wavelength dependence of Φ_{iso}, the isomeric ratio at photoequilibrium can be controlled by applying an irradiation wavelength where the ratio between the molar absorption coefficients of the two isomeric forms correspond to the desired PSD.

2.5 Host-Guest Chemistry

Host-guest chemistry relates to non-covalent interactions *e.g.* hydrogen bonding, hydrophobic forces, van der Waals forces, electrostatic interactions, metal coordination *etc.*, where the molecular species can be regarded as discrete units and the interactions between them are treated statistically. In particular, host-guest chemistry describes binding interactions where two types of molecules denoted host (H) and guest (G) self-assembles to form a supramolecular complex, *e.g.* $H@G$.[††] Included in this section are the two most common $H{:}G$ binding stoichiometries; 1:1, and 1:2. Common host molecules include cucurbiturils,[31] cyclodextrins,[32,33] and porphyrins[34] to mention a few. Reversible enzyme-ligand interactions (*e.g.* Type I, II, and III kinase inhibition, see section 4.4) can also be treated as host-guest binding events, and therefore, some theoretical aspects on this topic is included in this section. The defining parameter of host-guest binding is the *equilibrium binding constant* (K), representing the strength of the complex formation. It can be assessed by observing changes in equilibrium complex concentration(s) in the presence of varying concentrations of the guest. Experimentally, this is most often achieved through spectroscopic titration experiments.[35]

2.5.1   1:1 Binding Stoichiometry

The most basic complexation is where one guest binds to one host. This is referred to as *1:1 complex formation*, which can be written according to reaction [21].

$$H + G \underset{k_{-1}}{\overset{k_1}{\rightleftharpoons}} H@G \qquad [21]$$

---

†† Here, the @-sign represents the non-covalent, reversible nature of the complex interaction.

Here, k_1 and k_{-1} are the rate constants for the forward and backward reaction, respectively. In the case of 1:1 binding, K_{11} is defined according to equation [22].

$$K_{11} = \frac{[H@G]}{[H][G]} = \frac{k_1}{k_{-1}} \tag{22}$$

For a 1:1 complex, the concentration of unbound host and guest can be expressed in terms of the total concentration of host ($[H]_{tot}$) and guest ($[G]_{tot}$) according to the mass balance equations [23] and [24].

$$[H]_{tot} = [H] + [H@G] \tag{23}$$

$$[G]_{tot} = [G] + [H@G] \tag{24}$$

The equation system consisting of [22], [23], and [24] has one relevant solution for $[H@G]$, this is shown in equation [25].

$$[H@G] = \frac{1}{2}\left([G]_{tot} - [H]_{tot} + \frac{1}{K_{11}}\right) - $$
$$\sqrt{\left([G]_{tot} - [H]_{tot} + \frac{1}{K_{11}}\right)^2 + 4[H]_{tot}[G]_{tot}} \tag{25}$$

Since $[H]_{tot}$ and $[G]_{tot}$ are generally known, equation [25] implies that if the binding situation is such that the complex formation is exclusively of 1:1 character, and $[H@G]$ can somehow be monitored, K_{11} is the only unknown parameter and can easily be determined. Conversely, if the binding constant is known, the equilibrium concentration of all species in solution (*via* equations [23] and [24]) can readily be calculated.

2.5.2 1:2 Binding Stoichiometry

The 1:1 stoichiometry can be expanded to describe binding interactions where the host can bind two guests or *vice versa*.‡ In 1:2 binding, two dynamic equilibria (reaction [26]) are maintained. Thus, two binding constants (equations [27] and [28]) are needed to characterize the equilibrium concentrations.

---

‡ Which of the molecular species is denoted *host* and which is denoted *guest* is arbitrary from a theoretical point of view, 2:1 binding stoichiometry can be defined analogously to 1:2 binding.

$$H + 2G \underset{k_{-1}}{\overset{k_1}{\rightleftharpoons}} H@G + G \underset{k_{-2}}{\overset{k_2}{\rightleftharpoons}} H@G_2 \qquad [26]$$
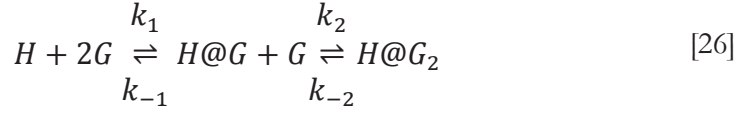
$$K_{11} = \frac{k_1}{k_{-1}} = \frac{[H@G][G]}{[H][G]^2} = \frac{[H@G]}{[H][G]} \qquad [27]$$

$$K_{12} = \frac{k_2}{k_{-2}} = \frac{[H@G_2][G]}{[H][G]^2} = \frac{[H@G_2]}{[H][G]} \qquad [28]$$

The mass-balances in the case of 1:2 binding are defined analogously to the 1:1 binding, as shown in equations [29] and [30].

$$[H]_{tot} = [H] + [H@G] + [H@G]_2 \qquad [29]$$

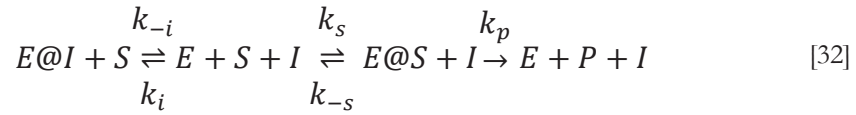$$[G]_{tot} = [G] + [H@G] + 2[H@G]_2 \qquad [30]$$

For the equation system composed of equations [27]-[30] above, the concentrations cannot be solved analytically. Instead, iterative algorithms must be employed to solve the resulting cubic equation [31].

$$[G]^3 K_{11}K_{12} + [G]^2(K_{11}(2K_{12}[H]_0 - K_{12}[G]_0 + 1)) +$$
$$[G](K_{11}([H]_0 - [G]_0) + 1) - [G]_0 = 0 \qquad [31]$$

The theoretical framework for host-guest binding situations can easily be expanded to account for more complicated stoichiometries, as long as equilibrium expressions and mass-balances can be defined, to match the number of unknown parameters. Once these systems of equations are in place, obtaining numerical solutions is also generally feasible. What typically proves more demanding, however, is to design experiments to accurately determine the involved binding constants, particularly in cases where the physicochemical observables (*e.g.* absorption spectra) of the different complexes in solution are similar.

2.5.3   Competitive Enzyme Inhibition

Non-covalent competitive enzyme inhibition (*e.g.* Type I and Type II kinase inhibition, section 4.4) can be treated as a series of connected equilibria where the enzyme-catalyzed product (P) formation in the presence of substrate (S) and competitive inhibitor (I), can be written according to reaction [32].

$$E@I + S \underset{k_i}{\overset{k_{-i}}{\rightleftharpoons}} E + S + I \underset{k_{-s}}{\overset{k_s}{\rightleftharpoons}} E@S + I \overset{k_p}{\rightarrow} E + P + I \qquad [32]$$

Assuming that the enzymatic reaction without inhibitor present follows *Michaelis-Menten kinetics*, the rate of substrate turnover (V_0) can be derived as a function of the maximum rate (V_{max}), and the substrate- and inhibitor concentrations according to equation [33].

$$V_0 = \frac{V_{max}[S]}{K_m(1 + K_i[I]) + [S]} \qquad [33]$$

Here, K_m is the *Michaelis-Menten constant, i.e.* the substrate concentration at which $V_0 = V_{max}/2$ in the absence of inhibitor, and $K_i = k_i/k_{-i}$ is the inhibitor binding constant. It is common practice to report IC_{50}-values as a measure of inhibitor potency. The IC_{50}-value is defined as the inhibitor concentration at which the enzyme activity is suppressed 50% *in vitro*. For competitive inhibitors, it can be related to the inhibitor-to-enzyme binding constant (K_i) according to the Cheng-Prusoff equation:[36]

$$IC_{50} = K_i\left(1 + \frac{[S]}{K_m}\right) \qquad [34]$$

3 Methodology

This chapter presents the main experimental techniques used in the papers comprising this thesis. These are without exceptions spectroscopic techniques, and therefore rely on light-matter interactions. The underlying theoretical considerations are described in the previous chapter 2.

3.1 Absorption Spectroscopy

In this thesis, absorption spectroscopy refers to the *steady-state* experimental technique. As such, it records the average absorption of an ensemble of randomly oriented molecules in solution as a function of incident light wavelength. Figure 4 shows the experimental setup of an absorption spectrometer.
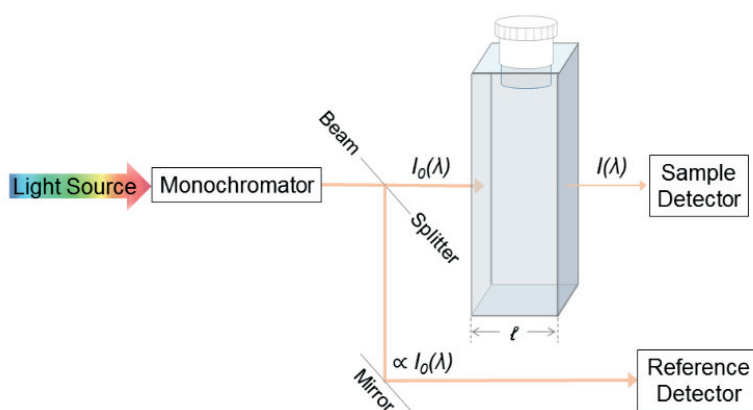

Figure 4. Schematic layout of a typical absorption spectroscopy setup. The beam-path, monochromator, cuvette sample compartment, and detectors are specified.

By measuring the light intensity before and after the sample, a measure on the absorption as a function of the wavelength of the probing light is obtained according to equation [35].

$$A(\lambda) = \log\left(\frac{I_0(\lambda)}{I(\lambda)}\right) \qquad [35]$$

Here, $A(\lambda)$ is the wavelength-dependent absorption and $I_0(\lambda)$ and $I(\lambda)$ the light intensities before and after the sample, respectively. An absorption *spectrum* is collected by probing the absorption while scanning the sample with a range of wavelengths. Absorption spectroscopy, although basic in its experimental layout, is a powerful and versatile technique for studying molecules in solution. An important reason for this is the straightforward relationship between absorption and molar concentration (C) provided by the *Lambert-Beer law*, as shown in equation [36].

$$A(\lambda) = \varepsilon(\lambda)C\ell \qquad\qquad [36]$$

Here, ℓ is the sample path length (Figure 4) and $\varepsilon(\lambda)$ the molar absorption coefficient (typically expressed in $M^{-1}cm^{-1}$). Molar absorption is an additive property in the sense that if N absorbing species is present in solution, the molar absorption coefficient-weighted concentration of each species make up the total absorption according to equation [37].

$$A(\lambda) = \ell \sum_{j}^{N} \varepsilon_j(\lambda)C_j \qquad\qquad [37]$$

For studying photochromic reactions, UV/vis absorption spectroscopy (typically probing the 200 - 800 nm wavelength region) is an exceptionally suitable technique as it provides a convenient means of monitoring the isomerization while requiring small amounts of sample.

3.2   Fluorescence Spectroscopy

Fluoresence spectroscopy is a collective term for a number of techniques probing the emissive properties of molecules. As in the preceding description of absorption spectroscopy, fluorescence spectroscopy herein refers to the steady-state technique, *i.e.* the average emission from an ensemble of randomly oriented molecules in solution. Figure 5 shows the principal components of a typical experimental setup.
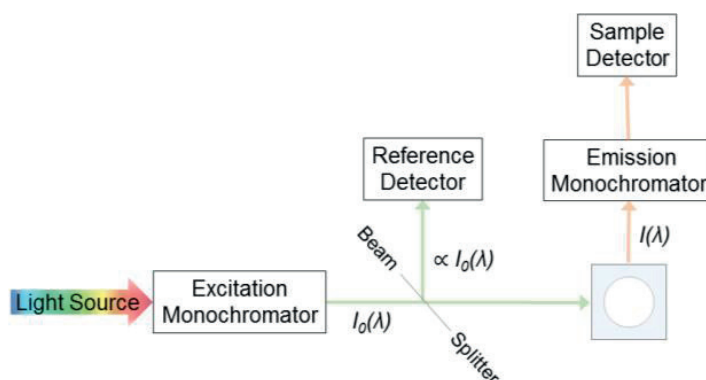

Figure 5. Schematic layout of a typical fluorescence spectroscopy setup. The beam-path, monochromators, cuvette sample compartment, and detectors are specified.

Two key modes of operation in steady-state fluorescence spectroscopy are *emission-* and *excitation* mode. They differ in the way the monochromators are operated. In emission mode, the excitation monochromator is fixed, while the emission monochromator is scanned over the different wavelengths. Thus, information on the relative fluorescence

intensities of the emitted light is obtained. The result is presented as an *emission spectrum*, displaying fluorescence intensities as a function of emitted wavelengths. In excitation mode, the roles of the monochromators are reversed, providing information on the absorptive origin of the emitting species. Typically, emission is collected at a right angle to the excitation light§§ in order to minimize the amount of light from the excitation source reaching the detector.

With this setup, fluorescence can be used as a highly sensitive analytical tool for probing *e.g.* changes in the microenvironment of a fluorophore. The absolute intensity ratio of incident *vs.* emitted light is strongly instrument-dependent and therefore rarely presented in the literature. Instead, the fluorescence intensity of a compound is typically referenced to existing standards and presented as a fluorescence quantum yield. A comprehensive description of various fluorescence-based techniques and their applications can be found in the textbook "Principles of Fluorescence Spectroscopy" by Lakowicz.[37]

3.3 Confocal Microscopy

Fluorescence microscopy is an imaging technique where emission from added or naturally existing fluorophores is observed through an optical system to create magnified images. This differs from conventional wide field microscopy where contrast instead is obtained through sample differences in *e.g.* opacity or refractive index. In fluorescence microscopy, an excitation source is needed to excite the fluorophores. Lasers are typically used for this purpose as they produce monochromic light while allowing regulation of the intensity. A schematic of a *laser scanning confocal microscope* (*LSCM*) setup is shown in Figure 6.

---

§§ Front face detection, collecting emitted light at a very small angle to the exciting light beam, can be used for highly concentrated samples or films.
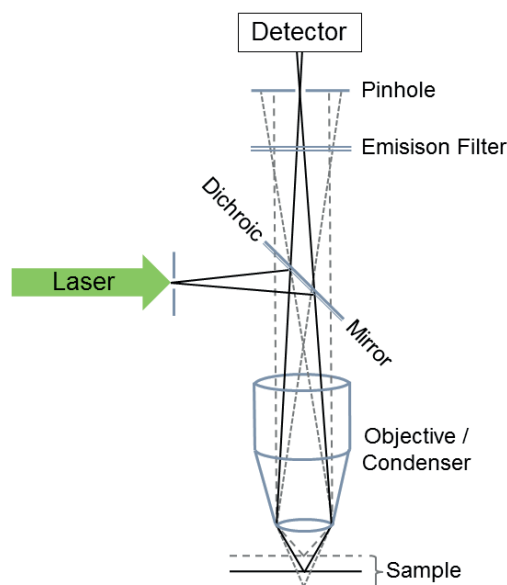
Figure 6. Schematic representation of the principles of confocal microscopy. Note how only light from the focal plane of the sample (solid black line) reaches the detector.

Most LSCMs in life science today are operated in so called "epi-mode", meaning that the emission is observed from the same side as the incident excitation originated. This means that excitation light and emitted light partly travels in the same beam path, through the same components. In particular, the *objective* for the exciting light becomes the *condenser* for the emitting light. Further components in the confocal setup includes the *dichroic mirror*, which reflects excitation light while transmitting emitted light; the *emission filter(s)*, which further excludes remaining excitation light and enables multiple emission output channels, and the *detector*. What actually makes the microscope "confocal", is the *pinhole* aperture. By placing a pinhole in a conjugate plane to the sample focal plane, out-of-focus fluorescence is blocked from the detector and only light originating from the focal plane is detected. The "scanning" part of LSCM refers to the function of the *scanning mirrors* (not shown in Figure 6). They are incorporated in the beam-path and are responsible for directing the excitation volume to achieve point-by-point illumination of the sample, facilitating generation of the 2D emission intensity histogram that is the image. The resolution of an LSCM is diffraction limited,[***] however several super resolution techniques (*e.g.* stimulated emission depletion, STED)[38] are advancements stemming from the confocal setup. Readers interested in a more thorough description of confocal microscopy in biological imaging are referred to the comprehensive textbook "Handbook of Biological Confocal Microscopy" by Pawley.[39] Related to this thesis, confocal microscopy was used to image bio-structures

---

[***] The theoretical limit (the *Abbe diffraction limit*) for what light microscopy can resolve is around 250 nm.

(cells and neurons) in Papers I and VI, as well as for delivering *in situ* photoswitching stimulus in Paper I.

4 Controlling Biology with Light

As briefly mentioned in the introduction to this thesis, two fundamental components are required to realize a photocontrolled system. The first is an optical system producing light. Several properties inherent to light makes it superior as external stimulus. *(1)* Light propagates with a speed of *ca.* 300 000 km/s, which means that the application intended for control can be more or less instantly triggered. *(2)* Light can be focused to very small volumes. There are microscopy techniques in use where the excitation focal volume is controlled with femtoliter (10^{-15} L) precision, allowing for a highly localized site of activation. *(3)* Under certain conditions, light is *bio-orthogonal*, meaning that it has minimal effect on the native systems of the body. It is also waste-free, as no chemicals are added or produced.

For light to be able to interact with molecules inside the body, a fundamental requirement is that it can sufficiently penetrate the skin and underlying tissue.[†††] Light-scattering and overlapping absorption from heme-groups in blood severely limits the penetration depth of light with wavelengths below 650 nm. For longer wavelengths ($\lambda > 900$ nm), absorption attributed to vibrational modes of water molecules becomes a limiting issue. This effectively creates a window where interfering absorption is minimal, called the *therapeutic optical window*.[5,40,41] It should be noted, however, that most of the photocontrolled systems published in the literature today (including a majority of the papers this thesis is based on) are operated using light with wavelengths outside the therapeutic optical window. Because of this (at least for applications in tissue samples), they have to be regarded as proof-of-principle studies. Several techniques (*e.g.* multiphoton-excitation, and photon upconversion), can be applied to overcome the limitations imposed by the optical window.

The second requirement in a photocontrolled system is the photoresponsive component.[6,10,11] There are two main classes of photoresponsive compounds used in this line of research – photoswitches and photocages. One may also include photosensitizers in this category, in particular photosensitizers for generating reactive oxygen species, as utilized in *photodynamic therapy* (*PDT*). PDT has proven highly successful for treating a range of medical conditions (*e.g.* superficial cancers[42]) and is a prime example of a phototriggered technique that has made it far into clinical practice. In this thesis, PDT is omitted from further discussions mainly because the effect controlled by light invariably is of non-specific kill/no kill character.

Based on the photoswitchable and photocaged building blocks, a number of strategies for obtaining photonic control of biological systems have been devised. As expected when trying to summarize a rapidly evolving research field, absolute distinctions are sometimes hard to make out. Nevertheless, for the purpose of this

---

[†††] A complementary method circumventing this requirement is the endoscopic use of optical fibers for direct light-exposure. However, this compromises the overall non-invasive character attributed to the photocontrolled approach.

chapter, an organization inspired by that proposed in a recent publication by Kramer has been adopted (Figure 7).[43] In that work, the strategies for obtaining optical control over native signaling proteins are exemplified for the field of neuroscience.
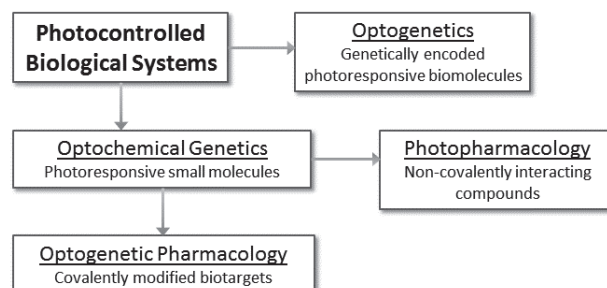

Figure 7. A schematic overview of the strategies for controlling biological systems.

The first branching in Figure 7 separates the purely genetic approach that is optogenetics from the opto*chemical* genetics approach. Optogenetics, as developed by among others Miesenböck[44] and Deisseroth[45], is based on genetically introducing light-sensitivity to biomolecules and cells, typically *via* expression of light-responsive opsin-based proteins, *e.g.* channelrhodopsins.[46] This technique has evolved immensely since its discovery and a testament to its massive impact is the appointment of optogenetics as Nature Methods' "Method of the year" in 2010.[47] It was also recognized in a "Breakthrough of the decade" article in Science Magazine from the same year.[48]

In contrast to optogenetics, opto*chemical* genetics (as coined by Trauner and co-workers in 2011)[9] relies on exogenous introduction of synthetic photoresponsive units. The second branching in Figure 7 maps out the two main strategies for this; optogenetic pharmacology and photopharmacology.⧧ In optogenetic pharmacology, a photosensitized biomolecule is achieved by covalently attaching the photoresponsive unit to a genetically tagged protein. In practice, this is most often done by attaching azobenzene photoswitches to genetically encoded thiol groups at the site of interest, resulting in so-called photochromic tethered ligands.[49,50] The bioconjugate will in this way be addressable by light, thus combining the absolute selectivity of genetic design with the resolving power of light. Both optogenetics and optochemical genetics have had a tremendous impact on, in particular, neuroscience. However, both strategies suffer from the necessity of having to genetically modify the target, which typically requires tedious viral gene-infusion protocols, hampering the general applicability of these approaches.

The remaining category in Figure 7 is photopharmacology.[6] It differs from the previously discussed methods, as no genetic manipulation is required. Neither does it

---

⧧ It seems that "photophamacology" and "*opto*pharmacology" is used interchangeably in the literature.

lead to a permanently modified target, due to the non-covalent nature of the interaction. To a large extent, this makes photopharmacology similar to traditional pharmacotherapy, but (as pointed out in the introduction to this thesis) with the exceptional added value of external photocontrol. Because the targeted structures and systems are completely unmodified, an additional advantage is that the observed effects will be those of a truly native system. Compared to the genetics-based techniques, which have existed since the turn of the millennium, photopharmacology is significantly older, with pioneering contributions presented in the 1960s and 1970s.[51,52]

The above organization mainly describes how light-control can be achieved on a whole-cell or even organism level. In addition to this, there is a tremendous amount of research done on simplified models, and/or synthetic analogs of isolated biomolecules. A well-explored strategy for elucidating basic functions of biomolecules and how it can be controlled by light is by synthetic incorporation of photoswitchable or caged motifs into biomolecules.[8] With this scheme, bio-relevant events such as the duplex-formation of DNA,[53-55] protein folding,[56-58] and RNA hybridization[59,60] have been controlled with light.

The content of this thesis in relation to the above classification system stretches from basic photochromic research (Papers II, III, and IV) to photopharmacology (Papers I, V and VI). It could be argued that the pursued drug release systems presented in Papers II and IV (upon successful implementation in a biological context) would qualify to the photopharmacology category. However, no such attempt is presented here.

4.1   Molecular Photoswitches

In this section, the general principles of molecular photoswitches and some reflections relating to their use are described. The detailed function and characteristics of the three types of photoswitches used in this thesis (spiropyrans, azobenzenes, and dithienylethenes) is expanded on in the contained subchapters.

Molecular photoswitches are compounds with the rare ability to utilize excitation energy from light to reorganize chemical bonds and relax into a stable conformer with a different structural arrangement. In many cases, this *isomerization* can be reversed by exposing the sample to light of a different wavelength, targeting the new conformer.§§§ In this way, one molecule can be reversibly isomerized between two different forms using nothing but photonic stimuli. In terms of executing a specific task, the challenge is then to design the photoswitch in such a way that one isomer induces the desired

---

§§§ The theoretical on photochromism was covered in the previous section 2.4.2.

effect, while the other does not. Successful molecular design according to this criteria would then allow for a photoreversibly controlled application.
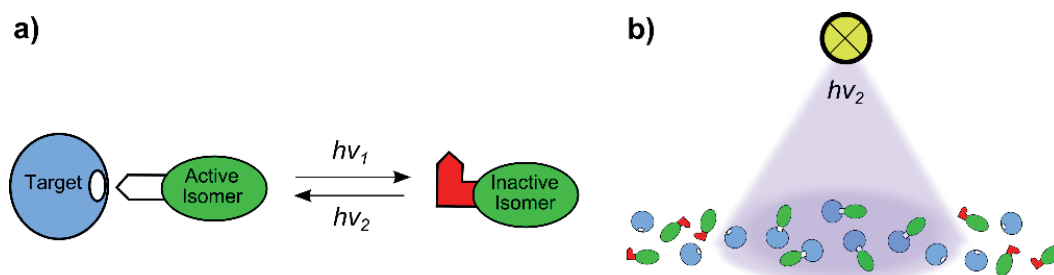

Figure 8. The principle of photoswitchable target affinity. **a)** The photoswitch can be reversibly isomerized between two forms with light. Due to the difference in molecular shape, only one isomer is able to bind to the target. **b)** A localized effect can be selectively triggered by exposing a subset of the target population to light. Changing the exciting light-frequency to v_1 reverses the binding event.

There exists a limited number of photoswitchable core-structures (*e.g.* azobenzenes, diarylethenes, spiropyrans, spirooxazines,[61] *etc.*), each with its own characteristic set of properties. In many cases, however, substituents can be introduced without compromising the overall photoswitching ability of the compound, allowing for tailor-made photoswitches and/or insertion of the photoswitchable moiety into larger molecular constructs[8]. This versatility has led to the development of numerous photoswitchable molecules and systems for use in biology.[4,6-8,10,11,62]

For application in a biological contexts, a thorough understanding of the physicochemical properties of the photoswitch in aqueous solution is key. Some important questions to address regarding photoswitch design are discussed below. *(1)* To what extent can light enrich the sample in the respective isomeric form? For optimal effect, it is often highly desirable to be able to quantitatively convert the sample between the two forms. However, due to overlapping absorption (in particular for the UV induced process), this is rarely possible. Instead, a photostationary distribution (PSD) for the respective photoinduced reaction is reached. The PSD reflects the isomeric composition at photoequilibrium (section 2.4.2 elaborated on this), which in turn defines the *action spectrum* of the photoswitch, *i.e.* the response-extremes between which the photo-operated system can exhibit control. *(2)* How stable are the two isomeric forms toward thermal (dark) isomerization? Typically, a *bistable* compound is wanted, *i.e.* a compound that, once photoswitched, retain the isomeric composition over time in the dark until photonically addressed again. It should be noted, however, that there are also applications which instead rely on the exact opposite, *i.e.* spontaneous deactivation of the photoswitch.[63] *(3)* Does the compound degrade in its intended environment? Photoswitch degradation can for instance be induced by solvent molecules[64] or cell reductants, *e.g.* glutathione.[65] The rate of degradation as well

as the nature of the potential degradation products are of importance, in particular for extended use in aggressive environments. *(4)* Is the photoswitch degraded by light? Photodegradation (or *photofatigue*) presents another potentially limiting factor that needs to be considered.

4.1.1 Spiropyrans

The spiropyran photoswitch consists of a chromene connected to an indoline moiety *via* a spiro-carbon. The resulting molecule is the ring-closed spiro-form (SP). A general spiropyran structure and its photochromic reaction to the colored merocyanine form (MC) is shown in Figure 9.
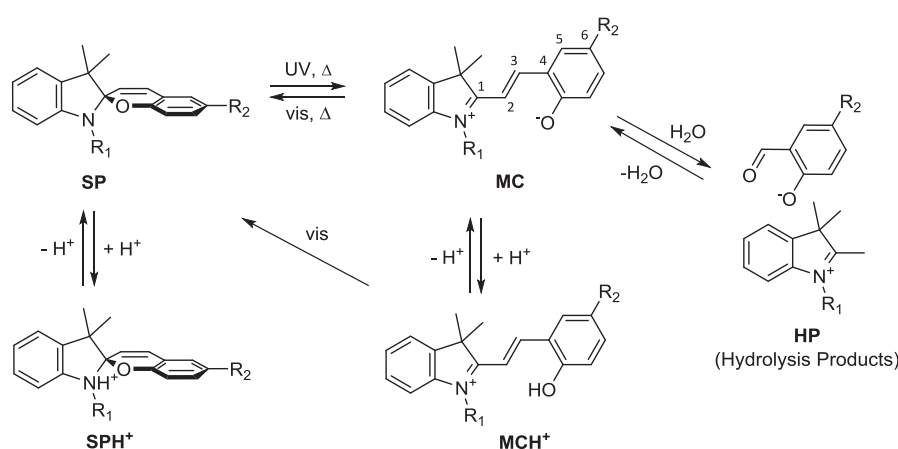

Figure 9. Photonic and thermal interconverison pathways of a general spiropyran photoswitch.

The by far most commonly used spiropyran is the spiro[2*H*-1-benzopyran-2,2'-indoline] (BIPS), and in particular the nitro-substituted 6-nitro-BIPS (Figure 9, $R_1 = $ Me, and $R_2 = NO_2$). Theoretical investigations[66] and spectroscopic studies[67-69] of how the photoisomerization of spiropyrans proceeds have been presented. In general terms, an initial photo-induced cleavage of the C_1-O bond is followed by a *cis/trans* isomerization (over the C_2-C_3 bond) in the course of SP → MC conversion. This transformation brings about a large shift in dipole strength from *ca.* 2-5 D to 20 D.[69] With the isomerization follows substantial steric changes as the molecule is transformed from the bulky SP to the planar, electronically conjugated MC. This extended conjugation is responsible for the intense visible absorption of MC (Figure 10).
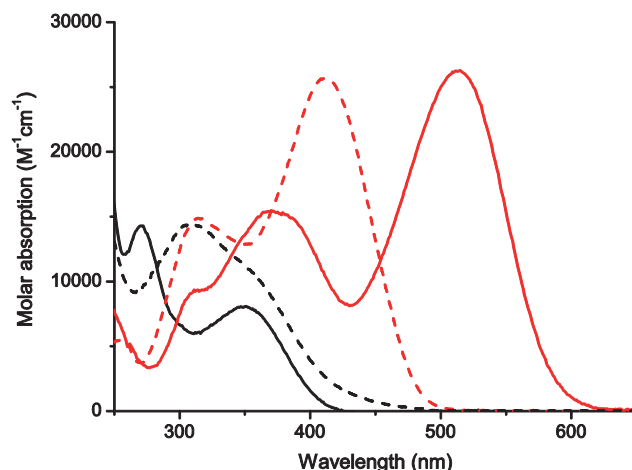
Figure 10. Absorption spectra of the SP (solid black), SPH+ (dashed black), MC (solid red) and MCH+ (dashed red) forms of a spiropyran in water. Here, R_1 = $C_3H_6NMe_3Br$, R_2= NO_2, as used in Paper III.

Due to the zwitterionic nature of the MC form, it is stabilized water. Therefore (as opposed to organic solvents), an SP $\rightleftharpoons$ MC thermal equilibrium with a significant contribution from MC is established in water at room temperature.[67] The rate with which the thermal equilibrium is established in water varies with substituents, but typically occurs on the hour timescale. Both the SP- and MC-forms can be protonated in water to yield SPH+ (pK_a *ca.* 0-3*)* and MCH+ (pK_a *ca.* 3-5), respectively (Paper III). The protonation has been proposed to occur on the indoline nitrogen and phenolate oxygen on SP and MC, respectively, and conveys changes in both absorption spectra and photochromic properties.[70] While SPH+ is neither thermo- nor photochromic, the MCH+ $\rightarrow$ SP interconversion can be triggered with visible light. The tunability of acidity constants (*via* substitution, see Paper III) and the general acidochromic features of spiropyrans makes them eligible for combinatory applications where acid and light inputs can be combined to condition for instance energy transfer or DNA binding.[71,72] On the negative side, the spiropyran photoswitch is known to suffer from hydrolytic instability, which seriously limits extended use in aqueous solutions.[64] The hydrolysis has been proposed to proceed as a retro-aldol reaction initiated by a nucleophilic attack on C_3 of MC. The MCH+ on the other hand, is completely stable toward hydrolysis. This is discussed in further detail in the appended Paper III, where it is concluded that in the pH-range 5-9, water (rather than hydroxide ions) is the hydrolysis-inducing reactant, and that the phenolate oxygen of MC plays a key role in the hydrolytic mechanism.

Compared to the main body of photoswitchable compounds, the spiropyran stands out due to the exceptionally large shift in polarity and steric profile. In particular, the bulky-to-flat rearrangement upon SP $\rightarrow$ MC isomerization has seen it included in several photoreversible DNA-binding applications by the group of Andréasson,

31

typically utilizing the intercalating properties of the open form.[71,73-75] Its properties when covalently linked to the phosphate backbone of DNA has also been reported on, although with mixed results in terms of photoactivity.[76-78] Other biological targets include RNA, the binding to which was photoreversibly controlled by the group of Deiters[79] and Tian.[80] There have also been reports on covalent modification of channel proteins to afford light-controlled pore opening, and content release.[81] This reversible "nano-valve" effect was proposed to be due to disruption of the helix arrangements in the protein due to electrostatic repulsion caused by the MC form. As for triggering SP → MC isomerization through the optical therapeutic window, Marriott and co-workers showed that two-photon induced isomerization to the fluorescent MC isomer could be triggered with 720 nm and used for Optical Lock-In Detection imaging in live *Xenopus* neurons.[82]

4.1.2 Azobenzenes

The archetypical azobenzene consists of two azo-bridged benzene rings, and exists in two isomeric forms; the thermally favored E-form and the Z-form, as shown in Figure 11a. Azobenzenes form one of the largest class of photoswitchable molecules and for biological applications, it is by some distance the most frequently used.[49,83] The reasons for this likely include the convenient "straight-to-bent" structural change, comparatively easy synthesis, and fatigue resistant photoswitching.[84]
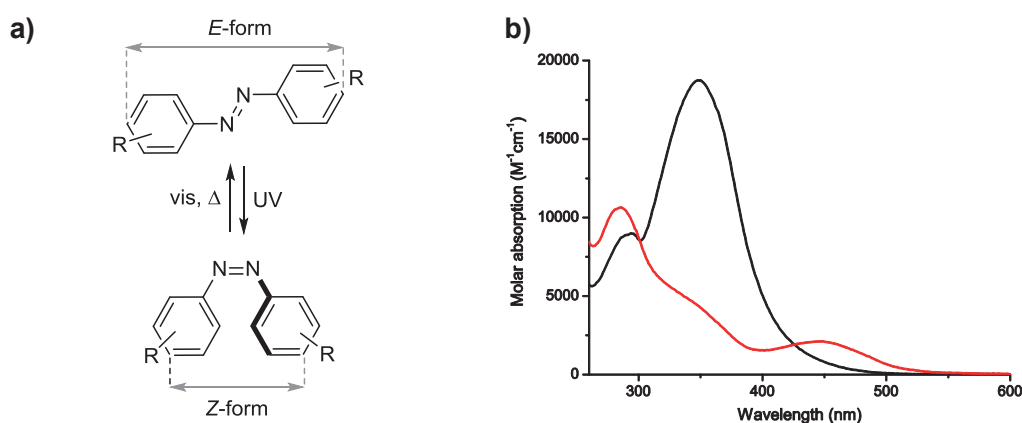

Figure 11. a) Photonic and thermal reactions of the azobenzene photoswitch, emphasizing the difference in end-to-end distance of the isomers. **b)** UV/vis absorption spectra of the azobenzene-derived **I3** in water, as used in Paper V (see Figure 34a on page 63 for structure). The thermally stable E-form (black line) can be photonically converted to the Z-form (red line, 87% Z-form) using UV light.

The absorption spectrum of the near-planar E-form is characterized by a strong π-π^* and weak n-π^* transition (Figure 11b, black line at *ca.* 350 nm and 450 nm, respectively) Excitation into the former band typically allows for substantial Z-form enrichment.

The resulting *Z*-form adopts a bent conformation, with the phenyl ring at a 55° angle to the plane of the azo-group.[85] With the isomerization follows an increase in dipole strength from *ca.* 0 to 3D, and a decrease in end-to-end distance (Figure 11a, *ca.* 3.5 Å difference).[85] The *Z*-form reverts thermally to the *E*-form, but this reaction can also be triggered with light, targeting the n-π^* transition of the *Z*-isomer (Figure 11b, red line at *ca.* 450 nm). Theoretical-[86] and experimental studies[87] have been performed to elucidate how the photoinduced $E \rightarrow Z$ isomerization proceeds, resulting in several mechanistic explanations.[83]

The thermal instability toward isomerization associated with the *Z*-form is often described (along with UV operation) as the main limiting characteristic of azobenzenes. This rate can be rationalized based on the proposed dipolar transition state.[88] Therefore, it can be said with some generality that the rate of thermal $Z \rightarrow E$ isomerization increases with solvent polarity.[89] Introducing substituents on the phenyl rings can drastically affect the rate of this reaction.[90] Stabilization of the *Z*-isomer can for instance be achieved by introducing substituents in the *ortho*-position, as demonstrated by *e.g.* the groups of Hecht[91,92] and Woolley.[93,94] This was also shown to separate the normally overlapping n-π^* bands of the *E*- and *Z*-isomers, allowing for near-quantitative photoswitching in both directions.

Regarding two-photon techniques for photoswitching azobenzenes using for instance red light, the cross-section for two-photon absorption of both isomers is generally small (0.1-5 GM).[95] One strategy for overcoming this limitation is to attach a two-photon absorption sensitizer to the azobenzene, which then facilitates photoswitching by transferring excitation energy to the azo switching unit in an antenna-like fashion, as shown in a dendrimeric sample by Jiang *et al.*[96] This concept was expanded on in a recent study by Izquierdo-Serra *et al.* where light-control over the action of a glutamate receptor in live cells on the basis of two-photon azobenzene switching was achieved.[97]

The numerous reports on the use of azobenzenes in biological settings have been extensively reviewed and will not be covered in detail here.[49,56,83,94,98] In this thesis, the azobenzene switching motif was used to gain photoswitching ability of a small molecule effector (kinase inhibitor, Paper V), in line with the photopharmacology approach previously described in this chapter. For introducing photoreversible steric bulk in small-molecules, the azo unit is a widespread choice. A testament to the general popularity of this type of structural modification is the term "azologization" recently coined by Trauner and co-workers.[99] Photoswitchable small-molecule effectors have in this way been prepared to control the activity of a multitude of biological targets[52,99-102]

A noteworthy drawback regarding the use of azobenzenes in biological environments is the tendency of the azo bridge to be reduced in the presence of thiols, *e.g.* glutathione.[65]

4.1.3 Dithienylethenes

Dithienylethenes (*DTEs*) are a subgroup of the broader chemical class diarylethenes (*DAEs*), which consist of two aryl groups linked by an ethene bridge. In general terms, the DAE photoswitches are renowned for their exceptional thermal bistability, high photoswitching yields, and substantial changes in energetics.[103-106] The overall steric changes upon photoswitching, however, are small. One example of a DAE is stilbene, having two ethene-connected phenyls.[****] The thermally stable *E*-form of stilbene can be photoswitched to the *Z*-form, which upon further photonic excitation can undergo a *6π*-electrocyclic ring-closing reaction with subsequent oxidation to yield the stable product phenantrene (Figure 12).[107]
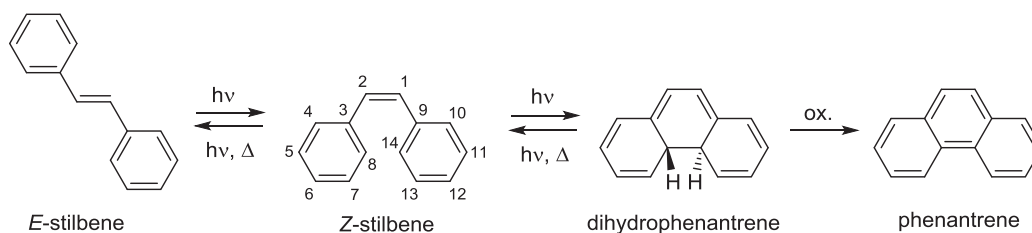

Figure 12. Photothermal reactions of stilbene, leading to the irreversible formation of phenantrene.

By introducing methyl groups in the 8- and 14-positions of stilbene however, the irreversible oxidation reaction can be suppressed, allowing for bidirectional photoswitching between the ring-open and ring-closed form. Furthermore, incorporating heteroatoms (most often sulphur or nitrogen) in the aromatic ring systems, lowers the aromatic stabilization energy of the open form.[108] This effectively reduces the rate of thermal ring-opening and therefore increases the thermal stability of the closed form, yielding a bistable photoswitch. Finally, to prevent photoinduced $Z \to E$ isomerization from competing with the photocyclization reaction, the ethene group is incorporated into a cycloalkene structure, *e.g.* a maleimide[109] or perfluorocyclopentene.[110] The structure and absorption spectra of a typical DTE photoswitch are shown in Figure 13.

[****] Although formally diarylethenes, stilbenes are often considered as a separate class of photoswitches.
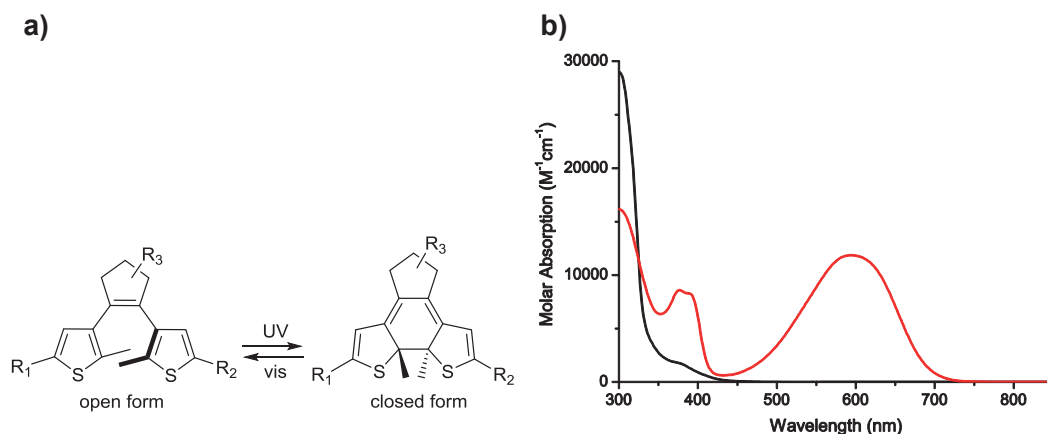
Figure 13. a) Structure and photoisomerization scheme of a general DTE photoswitch. **b)** UV/vis absorption spectra of the open (black line) and closed (red line) form of a DTE in toluene. Here, $R_1 = R_2 = C_5H_4N$ (pyridine), $R_3 = F_6$, as used in Paper IV.

The propeller-shaped open isomer absorbs light mainly in the UV region (Figure 13b, black line), with electron density localized mostly on the two thiophene rings. Exposing the open form to UV light stimulates the ring-closing reaction, resulting in the more or less planar closed form. Due to the extended electronic conjugation in the ring-closed isomer, the absorption band is dramatically red-shifted, leading to intense visible light absorption (Figure 13b, red line). The isomerization reaction can be rationalized on the basis of the Woodward-Hoffman orbital symmetry selection rules,[111] which means that only open isomers with the thiophene rings in an antiparallel arrangement (the photoactive antiparallel arrangement is implied in Figure 13a) can undergo the symmetry-allowed conrotatory photocyclization reaction. As the energy barrier for the parallel ⇌ antiparallel reorganization in the open isomer generally is low, the two conformers exist in a racemic mixture in solution, why the quantum yield of ring-closing is limited to 0.5. However, asymmetric DTEs ($R_1 \neq R_2$) or stereogenic substituents can shift this equilibrium, to increase the ring-closing quantum yield.[109,112] There have also been reports on the use of chiral binding strategies (*e.g.* using DNA[113] or cyclodextrins[114]) to achieve enantiomeric excess upon ring-closing. The cycloreversion reaction is stimulated by visible light, which completely converts the sample to the open isomer, albeit with significantly lower quantum yield. For a comprehensive description of the fundamental properties and recent developments of DTEs, the interested reader is referred to the very recent review by Irie.[104]

In this thesis, the exploited attribute of the DTE is the change in conformational flexibility – the open form being significantly more flexible than the ring-closed ditto. We used this to control the DTE binding mode to a Zn-porphyrin dimer, and thereby realize phototriggered drug release (Paper IV).

As for use in biology, DTEs are not as common as *e.g.* the azobenzene or spiropyran. This is likely due to its relatively recent discovery,[115] possibly in

combination with the limited change in geometry upon photoswitching (which arguably is the most attractive feature for biological applications), and lagging development of water soluble derivatives. That said, there are still plenty of examples of DTEs used in biological applications, *e.g.* as fluorescent probes,[116,117] photoswitchable inhibitors,[118,119] and even as a regulator of paralysis in live *C. Elegans*.[120] DTE-type switching units have also been synthetically incorporated into biomolecules, for instance DNA,[121,122] by the groups of Wagenknecht and Jäschke. In the latter work, the DNA duplex melting temperature and transcription were controlled by photoswitching a DTE-derived pyrimidine nucleotide.[122]

4.2 Photocaging

Photocaging (or just *caging*) refers to the method of covalently linking activity-compromising photocleavable groups to molecules and thereby gaining photonic control over their original function.[4,10-16] An unfortunate (yet common) metaphoric misconception regarding the terminology is that "caged" implies a geometrical confinement of the active molecule, for instance in cage-like inclusion complexes. This, however, is normally not the case. Figure 14 shows a schematic of the concept of caging.
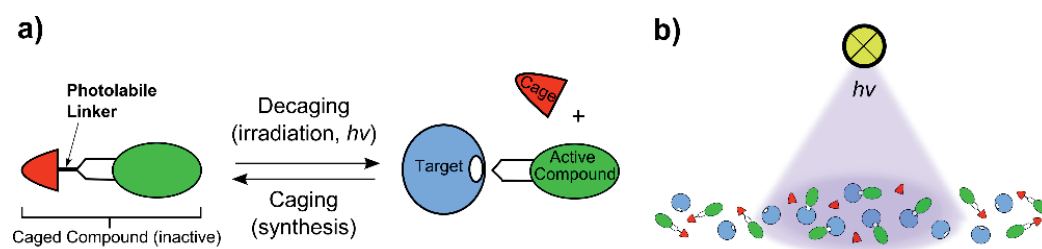

Figure 14. The concept of caging and decaging. **a)** Caging: Synthetic efforts yield the activity-compromised, photoresponsive compound. The presence of the caging group prevents interaction with the target. Decaging: Irradiation breaks the photolabile linker, restoring the active molecule. **b)** A localized effect can be achieved by exposing a subset of the target population to light.

As seen in Figure 14, once the active compound has been liberated, there is no way of photonically regenerating the caged (inactive) form. This irreversibility is the main difference between caging and the previously described photoswitching approach.

The strategy for designing caged compounds typically departs from a known bioactive molecule or binding motif and focuses either on introducing steric bulk and/or in other ways disrupting key affinities between the active compound and its target. This approach has been highly successful and produced a large number of photocontrolled compounds, primarily within the field of cell biology.[10,11,13,14,123] The first reports date back to 1977 and the work of Engels and Schlaeger in which an

o-nitrobenzyl caging group was attached to the phosphate group of cAMP.[51] One year later, adenosinetriphosphate (ATP) was caged by Kaplan *et al.* This work was also where the expression "caging" was coined.[124] Since then, a number of important biomolecules have been caged, including; glutathione,[125] glutamate,[126] biotin[127] and γ-aminobutyric acid (GABA).[128,129]

Regarding the choice of photolabile group, structural variants of nitroaryl- and coumarin-type caging groups seem to be the most widespread in the literature. In particular, dimethoxy-substituted *o*-nitrobenzyls (*e.g.* 6-nitroveratryloxycarbonyl, NVOC, a derivative of which was used in the appended Paper VI) finds regular use.[11,16] The mechanism for NVOC-decaging has been studied by computational means as well as transient absorption spectroscopy.[130,131] A proposed mechanism is shown in Figure 15.
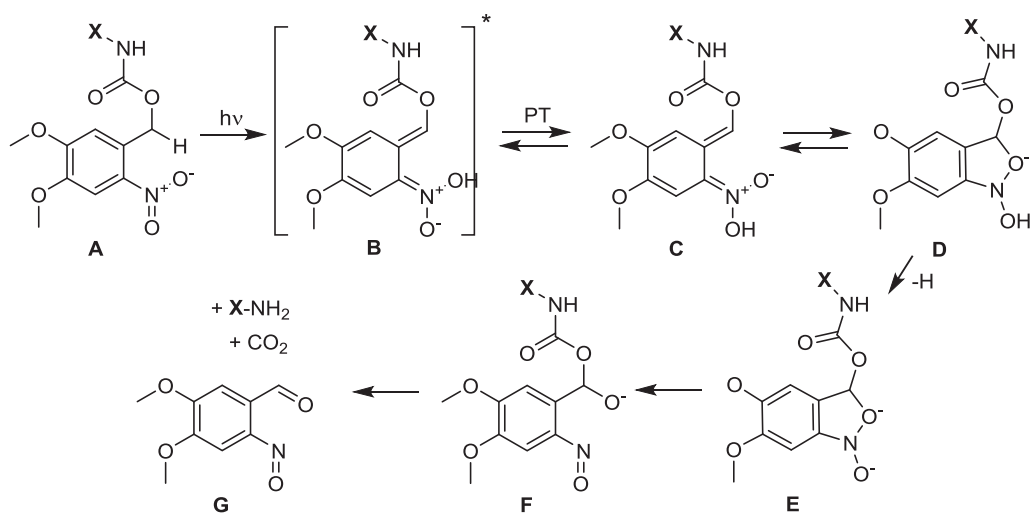

Figure 15. Mechanism of the photoinduced decaging of NVOC-functionalized compounds.[130,131] The compound to be released is indicated as **X**, while PT denotes a solvent-mediated proton transfer.

Factors to consider when selecting caging groups include molar absorption coefficient and quantum yield of photolysis, as these are key parameters for the overall rate of the release. It is also preferable if the release event can be triggered with light sufficiently low in energy (preferably above 350 nm) to avoid potential damage to the biological matrix or the active compound itself.[15,16] Caging groups from the *o*-nitrobenzyl family typically exhibit red-shifted absorption when substituted with electron-withdrawing substituents such as methoxy groups. There are also several recent examples where decaging has been achieved through the therapeutic optical window using *e.g.* two-photon excitation,[128,129,132,133] or *via* photon upconversion strategies.[134,135]

Looking at the concept of caging as such, a few general issues require attention; *(1)* Decaging not only liberates the active compound, but also the caging group. This

may or may not be a problem for the intended application, depending on the reactivity of the caging group toward the target and/or surrounding tissue. Evaluating the effect on the investigated system in the presence of caging group alone with/without light is one way to rule out such interfering processes. *(2)* Caged compounds are invariably larger than the released active compound. This poses a potential challenge for whole-cell and/or organism studies where biological barriers typically need to be traversed, as (diffusional) uptake typically is size-dependent. *(3)* For potent effectors (for instance inhibitors in the pM – nM regime), small amounts of residual active compound from the synthesis (Figure 14a, the "Caging" step) may be sufficient to cause a significant effect in the absence of light. This imposes high demands regarding purity.[12] *(4)* The caged compound needs to be stable toward solvent-induced- and enzymatic decaging. Potential decaging enzymes include *e.g.* esterases.

4.3 Supramolecular Approaches for Extending Photochromic Properties

The preceding sections 4.1 and 4.2 describe how clever design of photoswitches and cages has resulted in a range of photocontrolled compounds and applications for use in biology. With these strategies, however, the attainable biological effects are restricted to those inducible by the isomeric forms of the photoswitch or the decaging products. A convenient way of extending the effects of a photoswitchable system beyond the properties of the available isomers is by introducing additional (not necessarily photoresponsive) components, with which the photoswitch can interact. Such interactions can either be facilitated by linking the two units covalently (typically requiring extensive synthetic efforts), or by designing self-assembled supramolecular systems, as focused on below.[136]

In principle, if a compound has a certain activity in the presence of one isomeric form of a photoswitch, and a different activity in presence of the other, the photoswitching ability can be regarded as *transferred* to the non-photochromic unit. A biorelevant implementation of this concept was recently shown by the group of Feringa, where a metal-coordinating DTE photoswitch was used together with a Zn-porphyrin.[137] In solution, the DTE-unit and Zn-porphyrin self-assembled to form a supramolecular complex. As a result of differences in energies between the DTE isomers, excited state quenching of the Zn-porphyrin (with concomitant loss of sensitizing ability) could be reversibly controlled by photoswitching the DTE-unit. This example shows how properties not associated with the photoswitch (here: generation of singlet oxygen) can be photocontrolled. Another very recent report on this strategy was presented in the work by Presa *et al.*, in which the cancer cell

cytotoxicity of Pt-based compounds were brought under photonic control; again using a metal-coordinating DTE.[138] The change in toxicity was proposed to be due to differences in DNA-binding affinities between the open and closed form of the DTE, when bound to the Pt-complexes.

An alternative approach for extending the effects of photoswitches is to use them as drug-displacement agents. By designing a supramolecular system where a drug of choice is encapsulated in a synthetic "host molecule", release of the drug can be reversibly controlled if the photoswitch fulfills certain host-binding criteria. Specifically, a significant difference in host-binding affinity between the two isomeric forms of the photoswitch is required. Thus, in a typical drug release application, the weakly binding form of the photoswitch is distributed together with the encapsulated drug. Upon photoswitching to the high affinity isomer, the drug is displaced from the host due to competitive binding, and free to induce its intended effect. The advantage with this approach is that photoactivation can be accomplished without the drug itself having to be photoresponsive.

Several studies on photoreversible complex-formations that could potentially be used in this manner have been reported, such as the photoreversible binding involving the macrocyclic hosts cucurbiturils[139,140] and cyclodextrins.[141,142] An interesting variation on this approach was published in 2013 by Han *et al.,* where a photoswitchable "coordination-cage" composed of Pd-coordinated DTE-units was used to reversibly control the release of an inorganic guest in solution.[143] In that work, the host molecule itself was photoswitchable, and able to reversibly displace its content in response to light as a result of changes in the size of the inclusion cavity.

In this thesis, photoswitchable displacement strategies for photocontrolled drug release were studied in Papers II and IV.

4.4 Targeting Kinases

Protein kinases are defined by their ability to catalyze the transfer of a phosphate group from ATP (or GTP) to a serine, threonine, tyrosine, or histidine residue of another protein – the substrate. The reverse process is catalyzed by protein phosphatases; the two processes are shown in Figure 16 below.
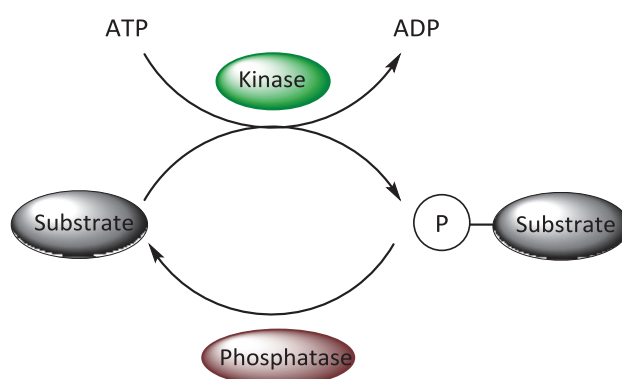
Figure 16. Enzyme-catalyzed substrate phosphorylation/dephosphorylation, showing the role of kinases for facilitating the transfer of phosphate groups.

There are over 500 protein kinases encoded in the human genome and they are implicated in virtually all biochemical cascades in our body by mediating signals and/or regulating the activity of other enzymes. In mammalian cells, three distinct classes of kinases have been identified based on their substrate preference.[144] They include; serine/threonine kinases (S/TKs), tyrosine kinases (TKs), and the dual function kinases (DFKs), which have the combined substrate affinity of the former two.[145,146] The catalytic domain of protein kinases is structurally well conserved and consists of 12 subdomains arranged into a *C*-terminal (consisting mainly of α-helices) and *N*-terminal lobe (anti-parallel β-sheets).[147] A defining binding interaction for ATP occurs in the so called *hinge region* located between the two lobes, where the kinase backbone makes hydrogen bonds to N^2 and 6N of the ATP adenine moiety, as shown in Figure 17.[147]
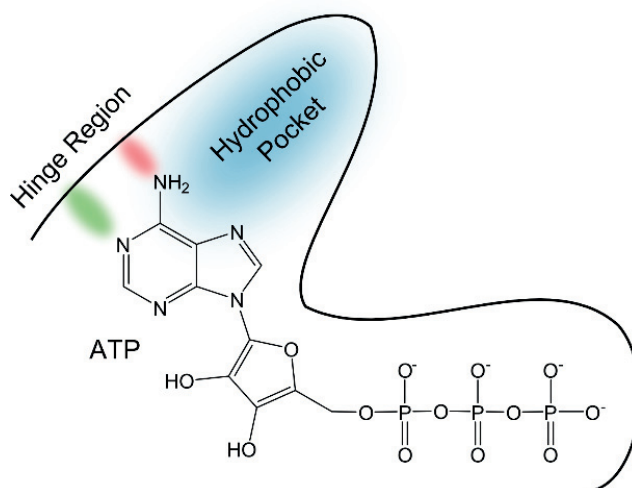

Figure 17. Schematic representation of the binding characteristics of ATP in the kinase catalytic domain. The alternating H-bond acceptor/donor pattern (green/red) making up the hinge region, along with the hydrophobic pocket (blue), are highlighted.

40

Many kinases have been found to be intimately connected to processes leading to tumor cell proliferation and survival. As a result, oncology drug research has focused considerable attention to the development of kinase inhibitors for cancer treatment.[148] Kinase inhibitors are divided into four subcategories based on their binding interaction.[148]

- *Type I* inhibitors are ATP competitive and bind to the active conformation of the kinase active site.
- *Type II* inhibitors are also ATP competitive, but recognizes the inactive conformation of the kinase active site.
- *Type III inhibitors* (or *allosteric* inhibitors) bind outside the ATP binding site and reduces kinase activity, often by changing the active site conformation.
- *Covalent inhibitors* bind irreversibly to the kinase active site.

The majority of kinase inhibitors are ATP competitive (Type I or Type II), and thus mimics the binding of ATP in the active site. Despite being a recognized biomedical target, examples of photocontrolled small-molecule kinase inhibitors are few. This is somewhat surprising, as emergence of photocontrolled analogs could be expected to correlate with general biomedical trends. The so far reported examples are caged variants.[149,150] As for reversibly photocontrolled kinases, two examples of peptidomimetic approaches have been reported by the group of Liskamp.[151,152] Regarding photoswitchable small-molecule kinase inhibitors, Paper V shows the only existing example to date.

4.4.1 Receptor Tyrosine Kinases and the RET Kinase

The *RE*arranged during *T*ransfection kinases (*RET*) belong to the receptor tyrosine kinases (*RTKs*).[†††][153] The RTKs are single pass, transmembrane kinases with the overall function to transduce signals across the cell membrane; they are necessary for development, maturation and maintenance of a number of cell types in the human body. An RTK signaling event is initiated by the binding of growth-factor to an extracellular receptor-site of the kinase, causing dimerization of two kinase units in the cell membrane. The dimerization is then followed by autophosphorylation on tyrosine residues of the kinase, activating the kinase binding pocket on the intracellular side. Once activated, the kinase mediates downstream signaling pathways inside the cell,

---

††† The name "Rearranged during Transfection" relates to the initial discovery of the gene coding for the RET kinase, which was found to rearrange upon transfection with DNA from human lymphoma cells.

leading to cell proliferation and/or differentiation.[154] A conceptual schematic of RTK signal transduction is shown in Figure 18.
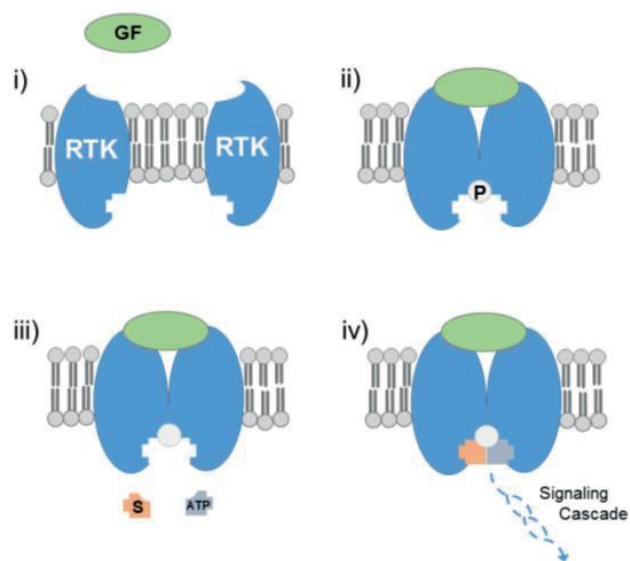

Figure 18. A schematic of receptor tyrosine kinase (RTK) signal transduction. i) Growth factor (**GF**) binds to the extracellular receptor site of the RTK, stimulating dimerization of two membrane bound RTK-units. ii) Autophosphorylation (**P**) occurs (typically in multiple sites), activating the kinase binding domain on the intracellular side. iii-iv) Substrate (**S**) phosphorylation propagates the signal on the intracellular side, completing its membrane passage.

In particular, RET has been shown to be important in the development and maintenance of neurons of the central and peripheral nervous systems.[155] If the normal function of RET is compromised, for instance by point-mutations leading to constitutive activity and/or overexpression of the kinase, uncontrolled (tumorous) cell growth may result. Accordingly, dysregulation of RET has been intimately connected to several types of human cancers, most notably in the thyroid gland and kidney.[146,155,156] In addition, the recent discovery that RET is important in breast cancer is likely a contributing factor to the increased interest in RET signaling, as breast cancer is the most common cancer form.[157] For these reasons, RTKs in general and RET in particular have emerged as attractive therapeutic targets for small-molecule kinase inhibitors.

5 Original Work

The following chapter presents a commented condensation of the results from the papers on which this thesis is based. It is my intention that the "biological complexity" of the studied systems should increase throughout the three parts of this chapter; starting with basic spectroscopic studies of isolated photochromic systems in solution and ending with phototriggered inhibition in a live organism.

5.1 Characterization and Supramolecular Interactions of Photoswitches in Solution

This first section cover Papers II, III, and IV and describes how supramolecular complexes based on photoswitchable components can be used to tune photochromic properties and/or realize novel drug release systems. It also includes a kinetic study of the thermo- and acidochromic reactions of a series of spiropyran photoswitches in water, with particular emphasis on hydrolysis.

5.1.1 Supramolecular Systems for Photocontrolled Drug Release

Described in this section are two examples where a photoswitch was combined with a non-photochromic host molecule to realize photocontrolled drug release on the basis of competitive binding. In the first part, the supramolecular interactions between a pyridine-appended DTE photoswitch and a diethyne-linked porphyrin dimer were exploited to reversibly control the concentration of the neurotransmitter 4-aminopyridine in toluene solution. The second part outlines a similar attempt, using an aminoalkyl functionalized ("anchor-equipped") nitro-spiropyran together with a cucurbit[7]uril (CB7) macrocycle in water. However, due to the loss of bistability of the spiropyran in the presence of CB7, we were unable to realize the proposed release system. Instead, the complexation-induced thermo-, photo-, and acidochromic reactions, as well as hydrolytic properties of the spiropyran complex were characterized. The principles for the herein intended photocontrolled drug displacement systems are shown in Figure 19.
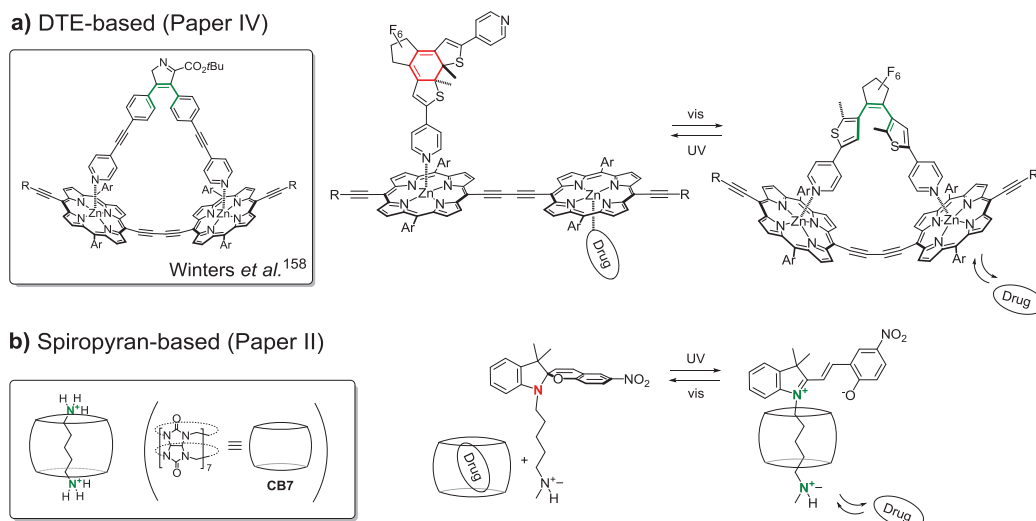
a) DTE-based (Paper IV)

Winters *et al.*[158]

b) Spiropyran-based (Paper II)

CB7

Figure 19. Photoswitchable supramolecular scaffolds for dynamic drug displacement. Based on the binding interactions of known static binders to macromolecular host molecules (framed), two potentially photoswitchable approaches were devised. **a)** The static bidentate binder presented by Winters *et al.*[158] motivated the design of a pyridine appended DTE photoswitch. The increased structural flexibility of the ring-open DTE-isomer allows coordination to both Zn-center in the porphyrin dimer, with increased binding affinity compared to the singly coordinating closed form. Here, R = 3,5-di(*tert*-butyl)phenyl, Ar = $Si(C_6H_{13})_3$. **b)** The strong binding interactions between CB7 and protonated cadaverine (1-5-diaminopentane, $K_{1:1}$ = 1.4×10^7),[159] inspired the design of an aminoalkyl-linked spiropyran. The cadaverine-like motif (both nitrogens positively charged) is only present in the open merocyanine form. It was hypothesized that this isomer would bind stronger to CB7 than the corresponding spiro-form.

The characterization of the two systems are described separately in the following sections 5.1.2 and 5.1.3, starting with the porphyrin-DTE scaffold.

5.1.2 Porphyrin Coordination – Drug Release with a Twist

In 2007, Winters *et al.* published a study showing how the rate of electron transfer from a porphyrin dimer to a covalently linked C_{60} electron acceptor could be controlled by selectively exciting different rotamers of the dimer.[158] In that study, a static pyridine-appended bidentate ligand was used to bind to the two Zn-centers of the dimer, thereby forcing a coplanar arrangement of the porphyrin macrocycles (Figure **19**a, framed). The changes in the absorption spectrum accompanying the planarization (discussed in section 5.1.2.2 below) were later exploited in a photoswitchable system by Kärnbratt *et al.* to realize a light-operated logic memory device with non-destructive readout capabilities.[160] Based on the latter system, we turned to investigate the possibility to use the same scaffold to reversibly control compound concentration in toluene solution, as outlined in Figure 19a above.

To assess the potential for the photoswitch to exert control over guest concentration, it is imperative to establish the binding stoichiometry and affinities of the isomeric

forms of the DTE derivative in the presence of the porphyrin dimer $\mathbf{P_2}$ (see Figure 20 below for structures). To this effect, UV/vis absorption titrations were carried out. The structures and fitted binding constants of the involved compounds are shown in Figure 20.
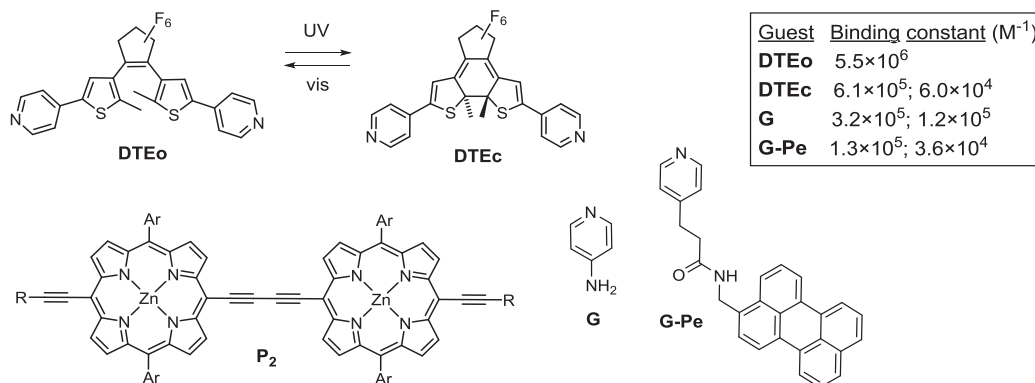

Guest	Binding constant (M^{-1})
DTEo	5.5×10^6
DTEc	6.1×10^5; 6.0×10^4
G	3.2×10^5; 1.2×10^5
G-Pe	1.3×10^5; 3.6×10^4

Figure 20. Structures and binding constants (K_{11}; K_{12}, to $\mathbf{P_2}$ in toluene) of the compounds included in the porphyrin release scaffold. Here, R = 3,5-di(*tert*-butyl)phenyl, Ar = Si(C$_6$H$_{13}$)$_3$. All guests bind to $\mathbf{P_2}$ in a consecutive 1:2 (H:G) manner except **DTEo**, which formed 1:1 complexes. The guest molecules 4-aminopyridine (**G**) and perylene-appended **G-Pe** were used as model drugs for demonstrating the release event (see text below).

The titrations reveal formation of consecutive 1:2 complexes (H:G) for all guests except **DTEo**, which instead forms a 1:1 complex. As for binding strength, the **DTEo** binds significantly stronger to $\mathbf{P_2}$, due to the conformational flexibility, which allows it to stretch and coordinate to both Zn-centers.

5.1.2.1 Photoreversible Release

To demonstrate the release event, a fluorescent model drug (**G-Pe**) was synthesized, as an analog to the bio-relevant neurotransmitter 4-aminopyridine (**G**).[161] When coordinated to $\mathbf{P_2}$, the spectral overlap of the $\mathbf{P_2}$ absorption and **G-Pe** emission assures effective quenching of **G-Pe** emission *via* FRET (R_0 = 66 Å). Therefore, any observed emission originates from the released compound. Predicting the equilibrium concentrations as a function of binding constants and/or total concentrations requires solving a set of coupled mass-balances and equilibrium conditions (see the earlier section 2.5). Based on the results from such an exercise, we prepared a cocktail of 280 µM $\mathbf{P_2}$, 300 µM **DTE** and 1 µM **G-Pe** to illustrate the photoreversible guest release. The results are shown in Figure 21.
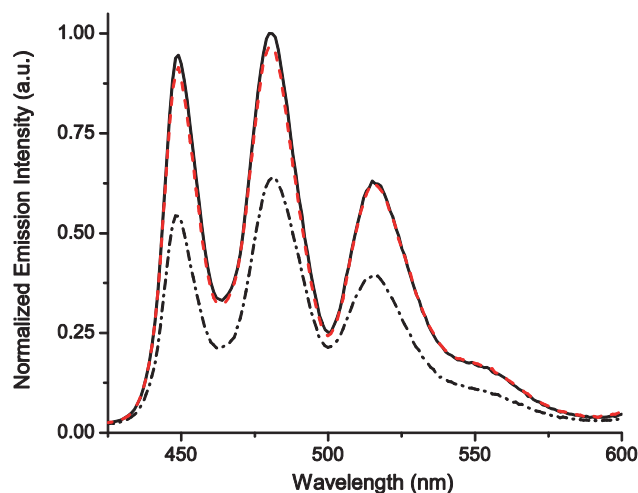
Figure 21. Photoreversible release of **G-Pe**. The applied concentrations were [**P₂**] = 280 μM, [**DTE**] = 300 μM, [**G-Pe**] = 1 μM. Initially, the photoswitch was in the open form, **DTEo** (solid black line). UV exposure for 2 min (302 nm) triggers isomerization to **DTEc** (dash-dotted black line). Subsequent visible-light irradiation isomerizes the sample back to **DTEo** (λ > 550 nm, 3 min, dashed red line).

An initial solution containing **P₂**, **DTEo**, and **G-Pe** gives rise to high emission, as the strongly coordinating **DTEo** occupies both Zn binding-sites in **P₂**. Subjecting the solution to UV light causes **DTEo → DTEc** isomerization, whereafter each DTE-unit cannot coordinate more than one Zn-center. In response, **G-Pe** binds to the liberated coordination site, and the emission is quenched. Subsequent visible light restores the high emission by reforming **DTEo** and displacement of **G-Pe** from **P₂**. This effectively illustrates the ability of the scaffold to reversibly release the guest into solution, using only light stimuli.

5.1.2.2 Report Function

The absorption spectrum of **P₂** changes significantly upon guest coordination (Figure 22a). In particular, ligand-induced **P₂** planarization (here, *via* coordination to **DTEo**) causes a substantial increase and red-shift of the 600 nm – 750 nm absorption band of **P₂** (Figure 22a, black → solid blue line). This was used in the present study to monitor the state of the release scaffold. Since detection of the planarized complex signals "drug released", we probed the inherent **P₂** emission (Figure 22a, dashed blue line) by exciting the mixture at 790 nm, where **P₂** is the sole chromophore.
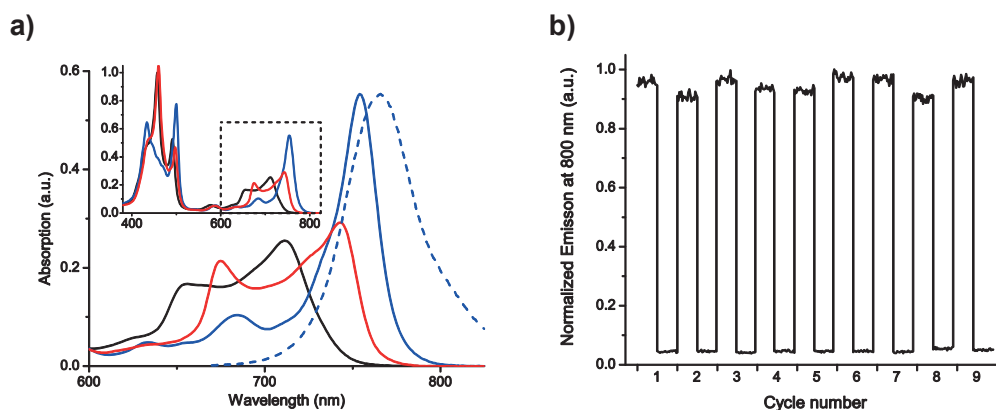
Figure 22. Report function of the **P₂** release scaffold. **a)** Absorption spectra of the supramolecular **P₂**-complexes in toluene: **P₂** (black line), **2G@P₂** (red line), and the planarized **DTEo@P₂** (blue line). The dashed blue line shows the **DTEo@P₂** emission spectra (λ_{exc} = 510 nm). Inset: Absorption from 380–825 nm. **b)** Photoswitching performance, as monitored *via* the report function, *i.e.* emission intensity at 800 nm (λ_{exc} = 790 nm). Applied concentrations: [**P₂**] = 280 μM, [**DTE**] = 300 μM, [**G**] = 1 μM. Each cycle starts with the photoswitch in the open form, **DTEo**, (high intensity). UV exposure triggers isomerization to **DTEc** (low intensity). Subsequent visible light isomerizes the sample back to **DTEo**.

This shows that the release event can be confirmed by fluorescence means, as the drug release proceeds concurrently with a dramatic increase in **P₂** emission, in accordance with the absorption spectral shift of **P₂** (Figure 22a, red → blue line). Therefore, the presented release scaffold fulfills the criteria for an all-photonic release-and-report system.

5.1.3 Spiropyran Complexed to CB7 – Altered Stabilities

The barrel-like host molecules cucurbit[*n*]urils, and in particular the water soluble homolog CB7 (Figure 23), have attracted considerable attention the last twenty years, mainly due to advancements in the synthesis of this class of compounds.[31] Its documented usefulness as a delivery vehicle[162,163] in combination with low cell toxicity[164] has seen it included for instance in a supramolecular approach for staining RNA in live cells.[165] Preferred guests for CB7 inclusion are organic species with two suitably spaced (the depth of CB7 is 9.1 Å) cationic ends. This is due to the combined interactions with the two carbonyl rims and hydrophobic interior of the macrocycle (Figure 23a).
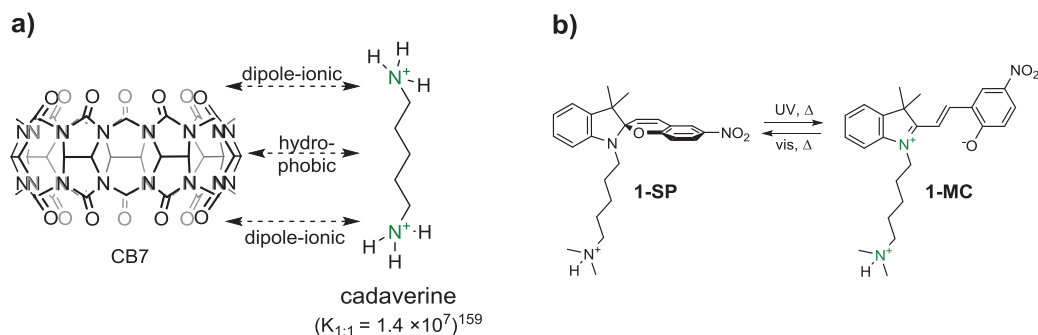
Figure 23. a) Structures of CB7 and protonated cadaverine (1,5-diaminopentane). The dashed arrows indicate attractive forces between the two molecules.[159] **b)** Structures and isomerization scheme of **1**, highlighting the structural resemblance of the aminoalkyl tail to cadaverine.

To determine the potential of **1** to function as a phototriggered drug displacement agent (as conceptually outlined in Figure 19b), the binding of the isomeric forms of the spiropyran to CB7 were investigated. Upon addition of CB7 to a water solution containing the closed SP-form, however, a dramatic acceleration of the thermal SP → MC isomerization was observed. The apparent rate of ring-opening was increased 70-fold, as shown in Figure 24.
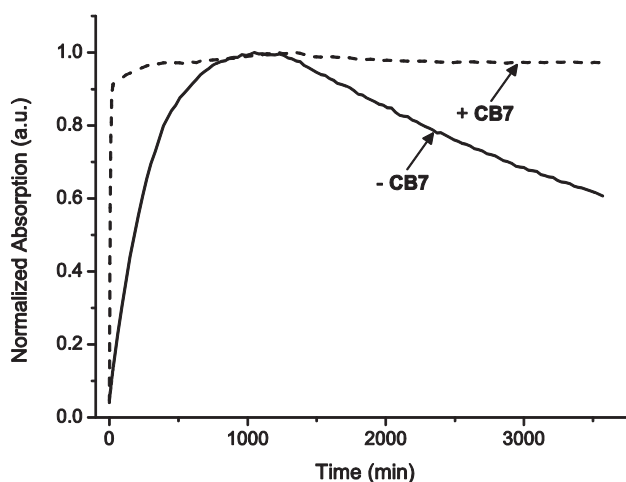

Figure 24. UV/vis time-trace monitoring the MC-form (λ_{obs} = 501 nm) as a function of time in the dark. At the start of the experiment, **1** (10 μM) was in 100% SP-form. The thermal opening was then monitored in the absence (solid line) and presence (dashed line) of 200 μM CB7.

This unexpected loss of bistability seriously limited the potential of the **1**-CB7 system as a photocontrolled drug release scaffold, as any distributed SP-isomer would be converted to the corresponding MC-form on the minute timescale, even in the absence of light. In addition to the rapid isomerization, several other physicochemical parameters of the photoswitch changed as a result of CB7 complexation. Of particular note, the hydrolytic degradation, commonly observed on the hour timescale for spiropyrans was completely halted in the presence of CB7.

5.1.3.1   Anchor-directed CB7 complexation

In parallel to our research on the **1**-CB7 system, reports from the group of Biczók emerged, describing spiropyran inclusion effects in CB8[166] and CB7[167]. In their work with the CB7 homolog, the complexation to a spiropyran without an amino anchor group (Figure 25a) was studied. There, no binding of the MC-form and thus no change in hydrolytic behavior (hydrolysis targets the MC-isomer only) was reported. To illustrate the necessity of equipping the spiropyran with an "anchor-group" for obtaining the herein described effects, we performed kinetic experiments with a small series of spiropyrans having different anchor lengths. The results are shown in Figure 25.
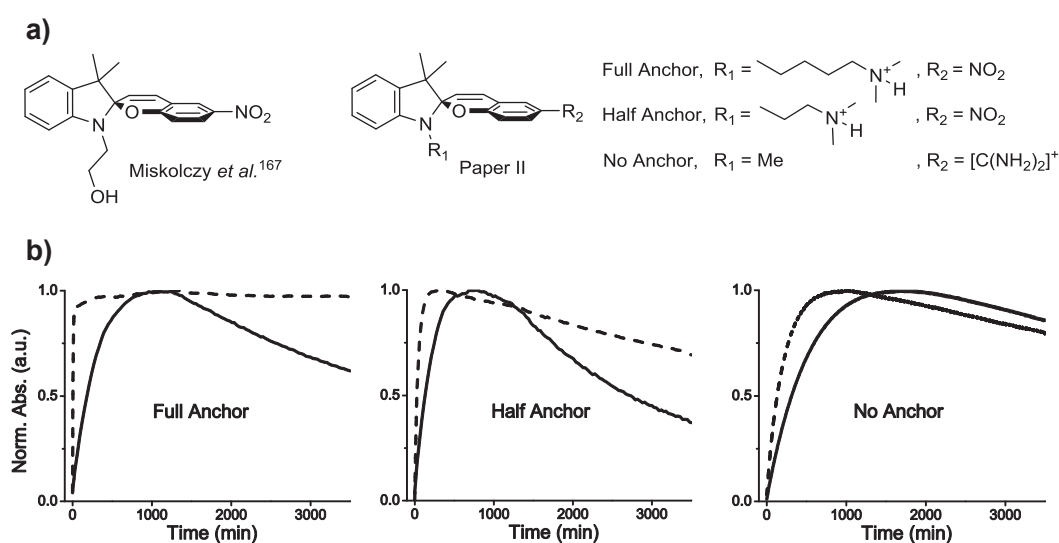

Figure 25. a) Structures of the spiropyrans included in the CB7 kinetics study. **b)** UV/vis time-trace monitoring the MC-form at the respective A_{max} as a function of time in the dark. At the start of the experiment, the compounds (10 μM) were in 100% SP-form. The thermal opening was then monitored in the absence (solid line) and presence (dashed line) of 200 μM CB7.

This clearly shows that both the accelerated SP → MC isomerization and the hydrolytic stability is significantly more pronounced for the "full-anchor" equipped spiropyran. Regarding the CB7 binding mode and -strength, UV/vis absorption titrations with **1-MC** and **1-MCH⁺** revealed the formation of an initial 1:1 complex followed by a significantly weaker binding of a second CB7.‡‡‡ Supported by NMR and ESI-MS experiments, we attributed the initial strong complex formation to anchor immersion

---

‡‡‡ The binding constants of **1-MC** and **1-MCH⁺** to CB7 were $K_{1:1} = 1.2 \times 10^5$ M⁻¹; $K_{1:2} = 1.3 \times 10^3$ M⁻¹ and $K_{1:1} = 7.9 \times 10^5$ M⁻¹; $K_{1:2} = 8.6 \times 10^3$ M⁻¹, respectively. Assessment of **1-SP** binding characteristics were complicated by the rapid thermal ring-opening and overlapping absorption from CB7. Titration experiments under constant visible-light irradiation (continuously reconverting MC to SP) showed spectral similarities to the open form titrations. However, no binding constants could be extracted.

into the macrocycle, while the weaker binding was thought to be an *exo*-complex, where the CB7 binds to the indole ring-system of the photoswitch.

With this binding arrangement, the CB7-induced acceleration of the ring-opening was explained by a stabilizing interaction occurring between the partial negative charge on the CB7 carbonyls, and the positive charge on the indolenium nitrogen of **1-MC**, which likely is formed in an intermediate step in the course of SP → MC isomerization. This is further supported by the CB7-induced lowering of the apparent activation energy for the reaction (E_a = 109 kJ/mol → 88 kJ/mol). The cessation of hydrolysis is proposed to be due to electrostatic repulsion between the water molecules (see section 5.1.4 on hydrolysis of spiropyrans) and the carbonyl oxygens of the CB7 rim. Importantly, and in contrast to what has been reported for spiropyran immersion in CB8,[166] the photoswitching behavior of **1** was not compromised upon binding to CB7. This highlights the usefulness of the anchor approach, as it retains the photoswitching properties of the spiropyran when bound to the CB7 host.

5.1.4   Spiropyrans in Aqueous Solution – a Kinetic Study

This section provides a brief account on the thermal and hydrolytic processes of spiropyrans in aqueous solution, as studied in Paper III. Since the first description of the hydrolysis of spiropyrans in the communication by Stafforst and Hilvert from 2009,[64] little has been done to systematically scrutinize on the behavior of this photoswitch in water. In Paper III, we proposed a complete kinetic model that accounts for the thermal interconversions of the spiropyran photoswitch over a broad pH interval in water. The model was validated using kinetic experimental data for a series of six spiropyrans designed to bestow the spiropyrans with varying acidities (*vide infra*). The proposed kinetic scheme along with the structures of the compounds included in this study are shown in Figure 26.
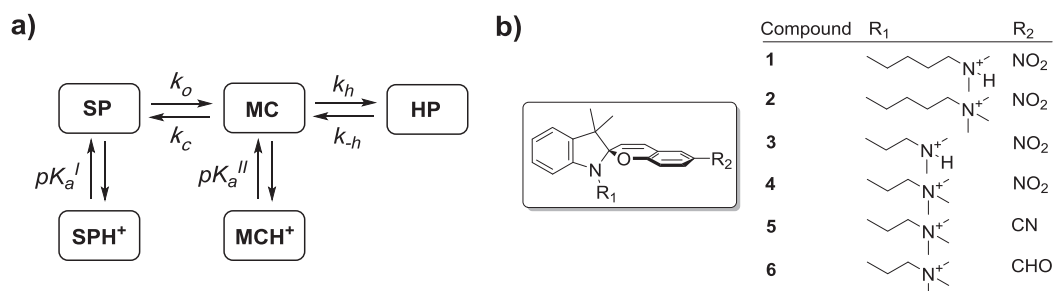
Figure 26. a) The proposed kinetic scheme of the thermal processes of spiropyrans in aqueous solution. Here, the interconversions between the spiro- (SP), and merocyanine (MC) isomers, their respective protonated forms (SPH$^+$ and MCH$^+$), and the hydrolysis products (HP) are shown. For the representative molecular structures, see section 4.1.1, Figure 9. The rate constants for the opening- (k_o), closing- (k_c), hydrolysis-, (k_h) and condensation reaction (k_{-h}), as well as protonation constants (pK_a^I and pK_a^{II}) are indicated. The condensation reaction ("reverse hydrolysis") is motivated in the text below. **b)** Structures of the spiropyrans included in Paper III.

5.1.4.1 Protonation Constants

The first step in this characterization study was to determine in detail the influence of substituents on pK_a^I and pK_a^{II}. Due to the distinct spectral differences of SP $vs.$ SPH$^+$ and MC $vs.$ MCH$^+$ (section 4.1.1, Figure 10), this information could be readily extracted from UV/vis pH-titrations. The collected acidity constants of **1**-**6** are shown in Table **1**.

Table 1. pK$_a$-values of SPH$^+$ (pK_a^I) and MCH$^+$ (pK_a^{II}) for **1-6**.

Compound	1	2	3	4	5	6
pK_a^I	1.4	1.6	0.4	0.4	0.4	0.4
pK_a^{II}	4.2	4.4	4.2	3.7	4.4	4.5

From these results, it was concluded that the length of the aminoalkyl tail in the R$_1$-position significantly affected pK_a^I, while it had no effect on pK_a^{II}. The lower pK_a^I observed for the amino-functionalized spiropyrans with a three-carbon tail compared to five-carbon tail was attributed to the proximity of the cationic nitrogen to the protonation site, leading to more effective electrostatic proton repulsion. This is an important finding, since the protonated spiro-form (SPH$^+$) is non-photochromic.[70] Thus, lowering pK_a^I effectively extends the functional pH-range of the photoswitch. It should be noted that the corresponding pK_a^I-value for spiropyrans with a methyl in the R$_1$-position is significantly higher (*ca.* 2.3).§§§§ As for substituents in the R$_2$-position, it was seen that substituting the strongly electron-withdrawing nitro-group for the

---

§§§§ Unpublished results.

moderately deactivating cyano-group or aldehyde, causes an increase in pK_a^{II} of *ca.* 0.8 pH-units. Also, the applied R₂-substitutions did not alter pK_a^I, which indicates that the two acidity constants can be controlled independent of each other.

5.1.4.2 Thermal Kinetics

The pK_a-values (Table 1) show that for pH 6-10, very little protonated form is present in solution. Therefore, in this pH-range, the equilibria shown in reaction [38] prevails.

$$SP \underset{k_c}{\overset{k_o}{\rightleftharpoons}} MC \underset{k_{-h}}{\overset{k_h}{\rightleftharpoons}} HP \qquad [38]$$

To investigate how these rate constants varied with pH for the different compounds, we initiated a kinetic investigation where the rate of formation and subsequent degradation of the MC-isomer[*****] was monitored using UV/vis spectroscopy. Under these circumstances, the SP-form is thermally isomerized to the MC-form whereafter the MC-isomer reacts to form the respective hydrolysis products. Kinetically, this renders a bi-exponential "rise-and-decay" profile (Figure 27) from which two *apparent* rate constants can be extracted.
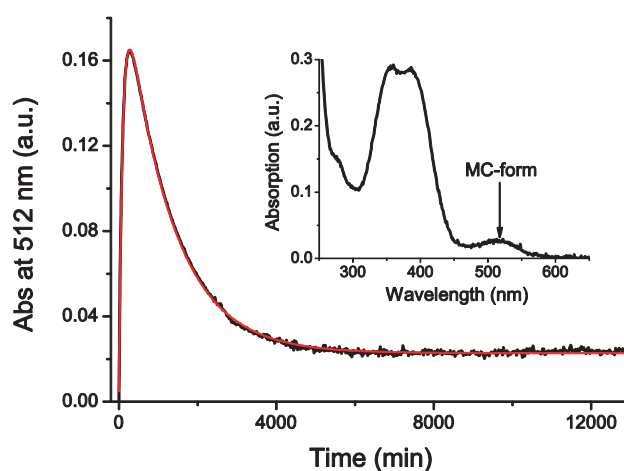

Figure 27. UV/vis absorption time-trace of the thermal SP → MC isomerization, and subsequent hydrolysis at 25 °C, pH 7 (black line, the red line shows the bi-exponential fit), here exemplified for **4**. At $t = 0$, the spiropyran is 100% in the SP-form. Inset: absorption spectrum recorded at $t = 12000$ min, clearly showing the presence of MC-form at equilibrium.

As the kinetic curve leveled off at a non-zero value, it is clear that the hydrolysis is reversible (Figure 27). This motivates the inclusion of the reverse hydrolysis reaction in the kinetic scheme. From the rate expressions for [SP], [MC] and [HP] and the two

---

[*****] The corresponding kinetic investigation at lower pH instead monitored the MCH⁺-form.

fitted *apparent* rate constants (Figure 27, red line), the intrinsic rate constants depicted in reaction [38] can be extracted analytically using a Laplace transform method.[168] To give a representative example; the kinetic experiment of **4** (Figure 27), renders intrinsic rate constants [min^{-1}]; $k_o = 3.5 \times 10^{-3}$, $k_c = 5.1 \times 10^{-3}$, $k_h = 2.2 \times 10^{-3}$, and $k_{-h} = 9.8 \times 10^{-5}$. The corresponding experiment was made for compounds **4**-**6** at pH 6, 7, 8, 9, and 10.[†††††] The results showed that k_o and k_c, although varying between the compounds, remained constant over the pH-range 6-9. Also, k_h was the same for all investigated compounds and did not change with pH. The concentration of hydroxide ions changes 1000-fold over this pH-range, while the observed rate of hydrolysis remains virtually constant. This strongly suggests that water (rather than the hydroxide ion) is the main nucleophile in this regime. This notion was further supported by computational means.

The same methodology as described for pH 6-9 above was applied to determine the rate constants also at pH 0-1, where the kinetic scheme can be reduced to include only SP, SPH$^+$ and MCH$^+$. It was seen that the extracted rate constants k_o and k_c agreed very well to those determined for pH 6-9. Thus, the near-identical k_o and k_c from pH 0 to 10 strongly suggests that no direct acid-induced SP $\rightarrow$ MCH$^+$ reaction takes place, but rather that MCH$^+$ is formed by SP $\rightarrow$ MC isomerization followed by immediate protonation of MC.

Finally, the intermediate pH-range 2-4, where the full kinetic model must be applied, was investigated. We were unable to find an analytical solution to the full kinetic scheme, why a numerical assessment was performed instead. It was seen that combining the intrinsic rate constants extracted for pH 5 with the determined pK_a-values (Table 1), resulted in a kinetic trace that agreed very well with the experimental results, thus verifying the proposed kinetic model also in a pH-range where the full model is required.

In summary; the kinetic investigation shows that one set of intrinsic rate constants can be applied to describe the thermal kinetics of a spiropyran in aqueous solution over a wide pH-range (pH 0-9), according to the proposed kinetic scheme (Figure 26a). Furthermore, the differences in the *apparent* rate of hydrolysis between the spiropyrans is not due to different inherent hydrolytic rate constants (k_h). Rather, it is determined by the protonation constants (Table 1) and differences in the rate constants of ring-opening and closing (k_o and k_c, respectively), which in turn governs the concentration of the hydrolysable MC-isomer in solution.

---

†††††† The complete set of extracted rate constants are summarized in the SI of the appended Paper III.

5.1.5 Discussion and Conclusions

The research summarized in section 5.1 focuses on basic molecular interactions in solution. Compared to the results described later in the present chapter, this research is of more fundamental character. It is therefore worth reiterating that the above described principles, *e.g.* for how a drug release strategy can be developed, requires several steps of refinements before they may be applicable in a biological setting.

Regarding the **P₂**-**DTE** drug release study, it is concluded that the concentration of drug in solution can be effectively controlled by photoswitching the **DTE** unit in the presence of **P₂**. Also, the spectral changes inherent to the release scaffold allow for fluorescence-based readout to determine the status (*i.e.* bound or unbound) of the drug. This combined all-photonic ability to reversibly release drugs and simultaneously report back to the user, could be of tremendous use for triggering and monitoring drug release *e.g.* in a microscopy setup. A particularly attractive feature with the presented system is that both the release- and report function can be triggered with low energy photons (up to *ca.* 700 nm), in compliance with operation in the therapeutic optical window.

Three limitations in the **P₂**-**DTE** system are obvious. First, for solubility reasons, the study was performed in toluene. It should be noted, however, that water-soluble versions of a similar porphyrin dimer[169] and DTE photoswitch[113] have been presented and used in biological matrices. It is acknowledged that other solvents (such as water) likely would affect the affinities of guests to **P₂**, and therefore the performance of the release scaffold. Second, the ratio bound/unbound drug upon photoswitching is *ca.* two-fold. It is debatable if this change in guest concentration is sufficient to induce a significant response in a biological system. Third, the required concentrations of the scaffold-components, [**DTE**] [**P₂**], are substantial compared to [**G**], (*ca.* 300 μM *vs.* 1 μM). Such high operating concentrations raise general concerns regarding for instance solubility and/or toxicity toward the exposed matrix.

As for the second pursued system for drug release, involving the CB7-spiropyran couple, the loss of bistability of the photoswitchable system coincided with the serendipitous discovery of the CB7-induced stabilization toward hydrolysis of the spiropyran unit. The ensuing characterization study allowed for the following conclusions to be drawn. *(1)* The hydrolytic degradation of spiropyran **1** is completely halted when bound to **CB7**. *(2)* The **1-SP → 1-MC** isomerization is accelerated by a factor of 70 with (compared to without) **CB7** present. *(3)* The spiropyran binds to **CB7** by immersion of the cadaverine-derived anchor substituent. *(4)* The anchor binding-mode is necessary for obtaining the observed complexation effects, whilst maintaining

55

unhindered photoswitching capabilities. The benefit of stabilizing the photochromic system toward hydrolysis is obvious. Also, as briefly discussed in section 4.1, a spontaneously reverting photochromic system may for some applications be advantageous, or even necessary. However, further studies are needed to clarify the physicochemical characteristics attributed to photoswitching of the CB7-spiropyran complex, to aid the design of novel applications based on this system.

In the third presented study, on spiropyran hydrolysis, a comprehensive kinetic scheme for the thermal reactions of spiropyrans in aqueous solution was proposed and validated. This general kinetic framework is expected to provide useful guidelines when designing spiropyrans for biological use. The results should be of interest *e.g.* when selecting substitution pattern for applications where the relative concentrations of the spiropyran isomers (and in particular their respective protonated forms) are important.

5.2 Live-cell Study of Spiropyran Cytotoxicity

This section describes how the cytotoxicity of a photochromic spiropyran can be regulated by light. The results and discussion in this section are largely based on the work contained in Paper I.

5.2.1 Motivation – Photoswitchable DNA-binding

There are few reported examples of photoreversibly controlled biological processes where the effects can be observed on a whole-cell or organism level. An important contribution emerged in 2009 when Branda and co-workers demonstrated the use of a DTE photoswitch for reversible control of paralysis in *C. Elegans* nematodes.[120] Azobenzenes have also been used in similar studies, for instance to photocontrol the motility of *Xenopus tropicalis* tadpoles *via* an allosteric modulator of metabotropic glutamate receptor, mGlu$_5$.[101] Another noteworthy example using an azobenzene is the photoswitchable propofol analog developed by the Trauner group, which was used to reversibly trigger anesthesia in *Xenopus laevis* tadpoles.[102]

Small-molecule DNA-binders hold great promise for disrupting DNA-dependent cellular processes and thereby inducing toxic effects in cells. Given that selectivity toward unhealthy cells can somehow be achieved, this type of compounds could be used to target for instance fast replicating cancer cells. In the work by Andersson *et al.* from 2008, photoswitchable DNA-binding was demonstrated.[73] More specifically, a photochromic spiropyran (Figure 28, **4**) was proposed to bind significantly stronger to DNA when in the open isomeric form, compared to the corresponding closed spiro-form. Later, in 2010, Hammarson *et al.* used a similar spiropyran derivative to demonstrate that the DNA-binding in fact depends on the protonation state of the

open isomer (MC/MCH⁺, see section 4.1.1), and that efficient DNA-binding occurs only after protonation of the phenolate oxygen on the MC-isomer.[71] This was suggested to allow for a dual control mechanism for DNA-binding, as both an external trigger (light) and an internal acidity control (cancer cells typically exhibit lower pH than healthy cells[170]) would be required. Apart from the herein appended Paper I, the only spiropyran toxicity study published to date is that of Movia *et al.*[171] where an 8-methoxy-6-nitro BIPS (Figure 28, **1**) spiropyran was shown to be non-toxic for up to 72 h in the low micromolar concentration regime. In that study, however, no attempts were made to investigate the effects of photoswitching in the cells. Based on the research presented above, we turned to investigate the cellular effects of photoswitching the spiropyran to the DNA-binding open form inside live human cancer cells, in an attempt to realize selectively triggered cell-death.
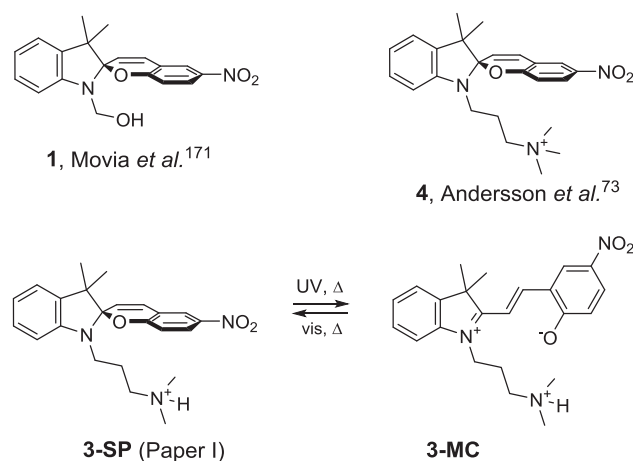

Figure 28. Structures of previously studied spiropyrans **1** and **4** and isomerization scheme of **3**.

5.2.2 Physicochemical Properties

Early attempts suggested that **4** was not appreciably taken up by the human embryonic kidney (HEK293T) cell-line, possibly due to the permanent charge on the quaternary aminoalkyl functionality.⧺⧺⧺ Therefore, we instead turned our attention to the structurally very similar **3** (Figure 28), differing only by carrying a tertiary amine instead of quaternary amine on the indoline tail group. **3-SP** can be photoswitched to the colored **3-MC** (see Figure 29 for spectra) using 254 nm UV light, and the PSD reached is *ca.* 40/60 **3-SP/3-MC**. Visible light stimulates the reverse reaction, and converts the sample to virtually 100% SP-form. Left in the dark, a 50/50 thermal equilibrium isomeric distribution is established with a time constant of *ca.* 6 h. Spiropyran hydrolysis is also observed, although on a significantly longer timescale (time-constant

---

⧺⧺⧺ Unpublished results

ca. 50 h). An important characteristic of **3** in terms of imaging is the fluorescent properties of the MC-form (Φ_f = 0.01), which is the only emissive isomer. This allowed for localization of **3-MC** by means of fluorescence microscopy.
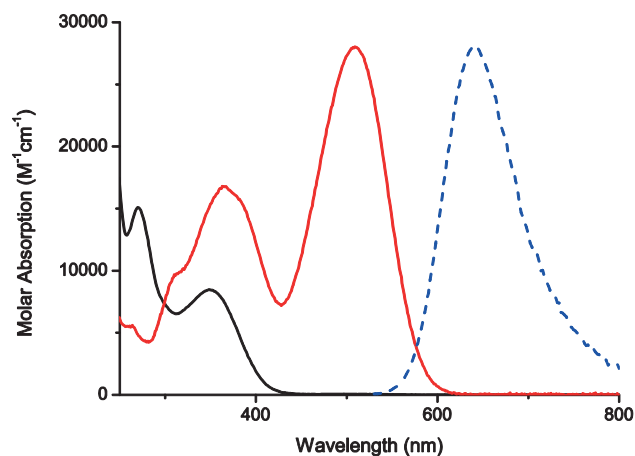

Figure 29. UV/vis absorption spectra of **3-SP** (black), **3-MC** (red) in water. The emission spectra of **3-MC** is shown in dashed blue.

5.2.3 Cell Uptake and Localization

DNA is primarily located in the nuclei of cells.§§§§§ To be effective as a DNA-binding cytotoxic agent it is therefore necessary to be able to penetrate not only the cellular membrane but also the nuclear envelope. To assess the uptake ability of **3**, a solution at thermal equilibrium (50/50 isomeric ratio) was distributed to HEK293T cells and incubated for 15 min at 37 °C. The sample was then mounted on a confocal microscope stage and probed for **3-MC** emission using 488 nm laser excitation. As shown in Figure 30a, little or no fluorescence was observed from inside the cells at this point, indicating the absence of internalized **3-MC**. After exposing the entire field of view to 3 s UV light, the sample was again probed for **3-MC** emission, resulting in intense fluorescence from inside the cells (Figure 30b).

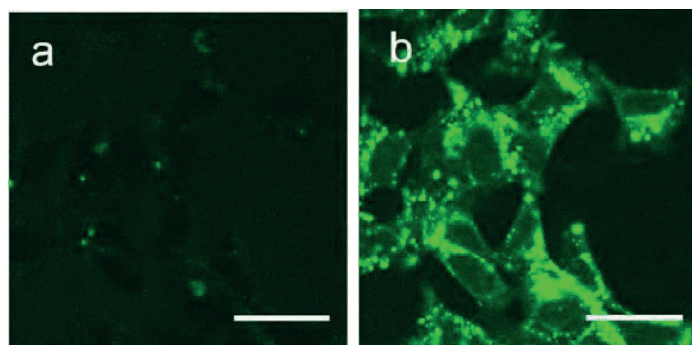§§§§§ There is also DNA in the cytoplasmic mitochondria organelle.

Figure 30. Confocal microscopy images (λ_{exc} = 488 nm) of HEK293T cells incubated for 15 min with **3** (6 μM) at thermal equilibrium, *i.e.* at 50/50 isomeric ratio **a)** before and **b)** immediately after exposing the entire field of view to 10 s UV light. The UV light was filtered out from the microscope mercury lamp (300 nm < λ < 400 nm). Scale bar is 30 μm.

This shows that **3-SP** is the only isomer able to pass the cell membrane and that intracellular SP → MC isomerization can be triggered photonically. Judging from the charge distribution of the respective isomers (the MC-form is zwitterionic and significantly more polar than the SP-form), the discrimination in uptake is not surprising, as increased size and polarity generally has a negative effect on cell uptake. Also, a similar uptake pattern was observed for the corresponding incubation at 4 °C, suggesting mainly a passive diffusion rather than endocytotic uptake mechanism. As for intracellular localization, it is clear from Figure 30 that fluorescence intensity from the cell nuclei is low. This suggests that neither form of **3** is able to effectively penetrate the nuclear envelope (or is efficiently quenched) under the applied conditions. Some binding preference seems to exist, however, as evidenced by the punctuate staining of the cytosol.

5.2.4 Cytotoxic Response

Having confirmed uptake of the photoswitch, the next step was to investigate the cellular effect of photoswitching **3-SP → 3-MC** inside the cells. As discussed throughout this thesis, phototriggered applications are often motivated by the superior target selectivity that comes with the directability of light. To illustrate this principle in the present study a preparation identical to that of the uptake study was followed by UV light-exposure of parts of the cell population (marked by circles in Figure 31). The response to the applied light dose was monitored by collecting microscope images with one minute interval. Selected images are shown in Figure 31 and the progression is described as follows; Immediately after the UV light-dose, the exposed **3**-incubated cells detached from the glass surface, "rounded up", and commenced extensive membrane blebbing, (Figure 31b). This was followed by a phase where the effected

cells ceased to bleb and re-assumed a spherical shape. Finally, *ca.* 2 h after UV exposure, the cell membrane of the effected cells (Figure 31c, red arrows) burst.[******]
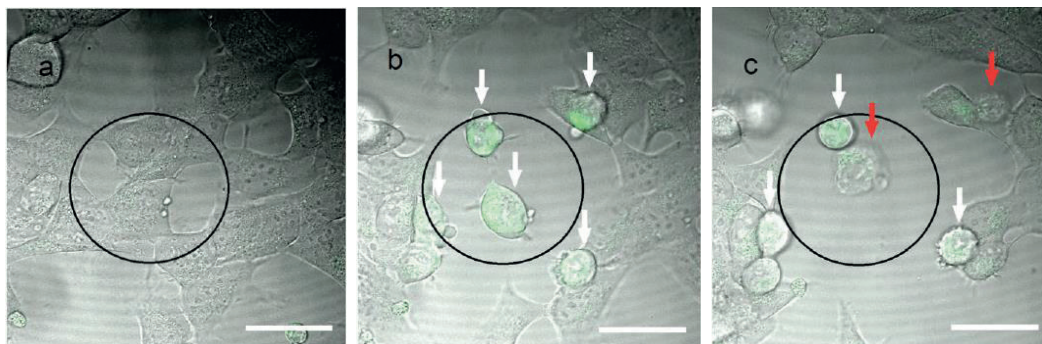

Figure 31. Confocal microscopy images (λ_{exc} = 488 nm) of HEK293T cells incubated for 15 min with **3** (6 μM) at thermal equilibrium, *i.e.* at 50/50 isomeric ratio. After incubation, 10 s UV-light (300 nm < λ < 400 nm) was applied exclusively to the circled region, where after an image time-lapse, collecting images every 60 s, was initiated. The displayed images are **a)** just before UV light-exposure, **b)** 29 min post UV, and **c)** 118 min post UV. The arrows show the cells initially hit by light, red arrows indicate ruptured cells. Scale bar is 30 μm.

Importantly, neither UV light alone, nor extended incubation with the spiropyran in the absence of light caused comparable effects, indicating the necessity of both photoswitch and light for the cytotoxic effect to occur. The effect was also investigated on larger populations of cells, showing a 52 ± 9 % *vs.* 3 ± 2 % incidence of membrane blebbing for incubated and non-incubated cells, respectively. As for the features of the cellular response, the morphological changes exhibited by the effected cells strongly resembles the stages described as being trademark signs of apoptosis.[172] This suggests that a cytosolic apoptotic pathway may have been triggered upon photoswitching. Inducing apoptosis, being a controlled dismantling of the cell, is typically preferred to the more traumatic necrotic cell death, as the latter is known to cause an inflammatory response in surrounding tissue and cells.

5.2.5 Discussion and Conclusions

It was concluded that an apoptotic-like cytotoxic response could be selectively phototriggered in spiropyran-incubated human cancer cells using light and drug doses that in themselves do not harm the cells. The specific cellular process intervened with to cause the observed cell-death is currently unknown. However, the uniformity in the morphological response of the irradiated cells suggest that the cells may commit to the same type of death-program. This may in turn indicate a specific disruptive binding of

---

[******] For a compiled video capture of the entire cytotoxic event, see Supporting Information for Paper I, provided online by the RSC.

the MC-form in the cytosol. It should be noted, however, that nitro-substituted spiropyrans are known to isomerize on the triplet surface and thus are eligible candidates for generation of reactive oxygen species, why this possibility cannot be excluded.[68] A notable strength with the applied spiropyran is the preferential uptake of the non-toxic SP-form, and the slow thermal isomerization to the MC-form in the cytosol, effectively holding back spontaneous buildup of the MC-isomer in the cell.

5.3 Two Tools and Three Model Systems for Studying RET Inhibition

This section is based on the work contained in Papers V and VI. Three model systems, *i.e.* studies on the isolated enzyme, live-cells, and zebrafish, have been used to characterize photoresponsive inhibitory activity against the RET kinase. Two strategies for gaining photocontrol of the inhibition event are presented; using a photoswitch and caged compound. They are described side by side in the ensuing text.

5.3.1 Inhibitor Design

In 2012, Grøtli and co-workers published a study on 3-substituted pyrazolopyrimidine kinase inhibitors for suppressing the activity of RET in an ATP-competitive manner.[173] Crystal structures of the RET kinase (PDB: 2IVV) with bound inhibitor **I1** (Figure 32) inspired the design of a series of modified inhibitors aimed at improved inhibitor-kinase interactions by better utilizing the hydrophobic pocket in the ATP binding site (see section 4.4 for details on kinase binding sites).[174] The best inhibitor, **I2**, showed potent RET inhibition *in vitro* ($IC_{50} = 8$ nM), and was shown to attenuate phosphorylation of ERK1/2, (a downstream reporter for RET activity) at nanomolar concentrations in MCF-7 breast cancer cells.[173]
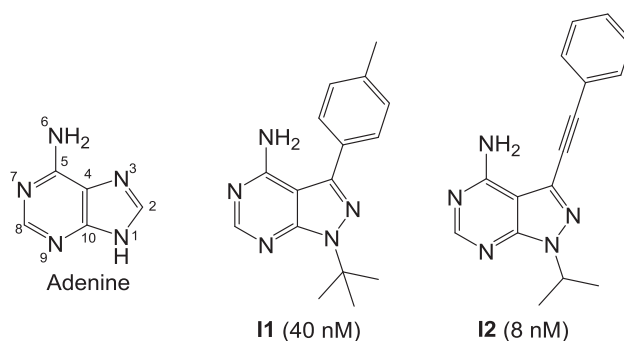

Figure 32. Structures of the nucleobase adenine and RET kinase inhibitors **I1**, and **I2**. IC_{50}-values toward RET (*in vitro*) are shown in parenthesis.

Based on the structure of **I2**, and the characteristics of the RET binding pocket, we investigated the possibility to photocontrol the inhibitory activity toward RET. To achieve this, two different approaches were pursued (Figure 33). First, a photoswitch methodology (Paper V) based on the introduction of an azo-bridge in place of the ethyne bridge of **I2**, rendering the azobenzene-derived compound **I3**, was examined. The hypothesis for discriminating binding between the two photoisomers (***E***-**I3** and ***Z***-**I3**) and RET was that the enzyme pocket would tolerate the *E*-conformation of **I3** but, upon photoswitching to the *Z*-conformation, a steric clash with the walls of the hydrophobic pocket would significantly hinder the binding, and lower the inhibitory potency.

The second approach involved attachment of a carboxylic acid functionalized 6-nitroveratroyloxycarbonyl (NVOC) caging group to the exocyclic nitrogen of **I2**, yielding the caged compound **C1** (Paper VI). NVOC-caging has been shown by Neveu *et al.* to be effective both for one- and two-photon release of retinoic acid in live zebrafish, motivating the use of this caging group also in the present study.[175] As for synthetic compliance, the NVOC-caging group has been used to cage purines in a similar fashion as in the herein reported **C1**.[176] The carboxylic acid functionality on the **C1** caging group was introduced to increase water solubility, as the corresponding methoxy compound was insufficiently soluble in water. Regarding the **C1** binding mode in the RET active site, attachment of the caging group was anticipated to both prevent hinge-binding and introduce an overall severe steric bulk in the inhibitor.
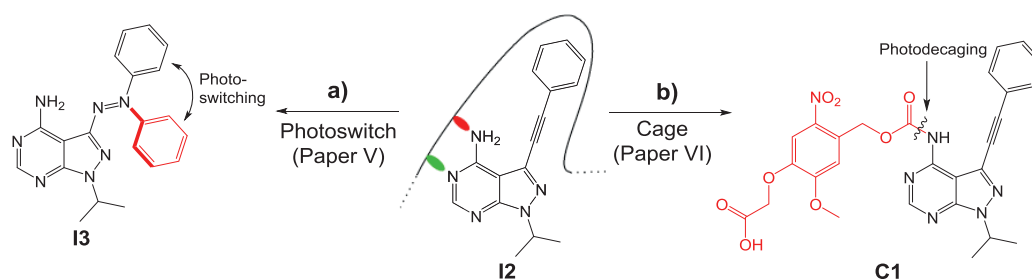

Figure 33. The two methods used for gaining photonic control over RET inhibitor activity. The line surrounding **I2** is a simplified representation of the RET kinase binding pocket (see section 4.4) depicting the hinge-region interactions (green and red ovals are H-bond acceptor and donor, respectively) and the hydrophobic pocket. **a)** Substituting the triple-bond of **I2** for an azo-bridge, renders the photoswitchable compound **I3**. **b)** Attaching a photolabile group to the exocyclic nitrogen of **I2** affords the caged compound **C1**.

5.3.2   Physicochemical Characterization

The ability of the photoresponsive compounds to control RET activity is very much dependent on the rates of the photoinduced and thermal reactions. The requirements and considerations for the two approaches (photoswitch *vs.* cage) in this respect are

notably different, as discussed in sections 4.1 and 4.2. First, the relevant photoinduced reactions (Figure 34) were studied in water.
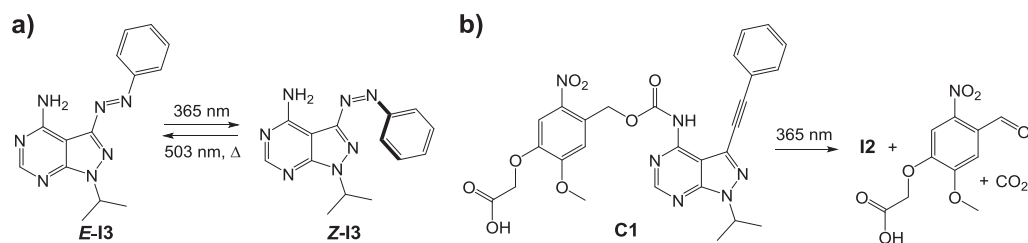

Figure 34. a) Photoswitching between the active (*E*-) and passive (*Z*-) inhibitor forms of **I3**. **b)** Liberation of active inhibitor **I2** upon decaging of **C1**.

Subjecting as-dissolved ***E*-I3** to 365 nm light enriches the sample in the *Z*-isomer (see Figure 35a for spectra), and the PSD reached is *ca.* 87% *Z*-form. Photonic ***Z*-I3 → *E*-I3** conversion can be stimulated with visible light. Here, 503 nm was used to complete the switching cycle, bringing the isomeric distribution back to >95% *E*-form. As for the **C1** decaging kinetics, aliquots were drawn during irradiation and separated using HPLC. As expected, analysis of the **C1** and **I2** concentrations with respect to irradiation time revealed a first order decaging kinetics (Figure 35b). This clearly shows that **C1** decaging (and thus liberation of the inhibitor **I2**) can be triggered with light.
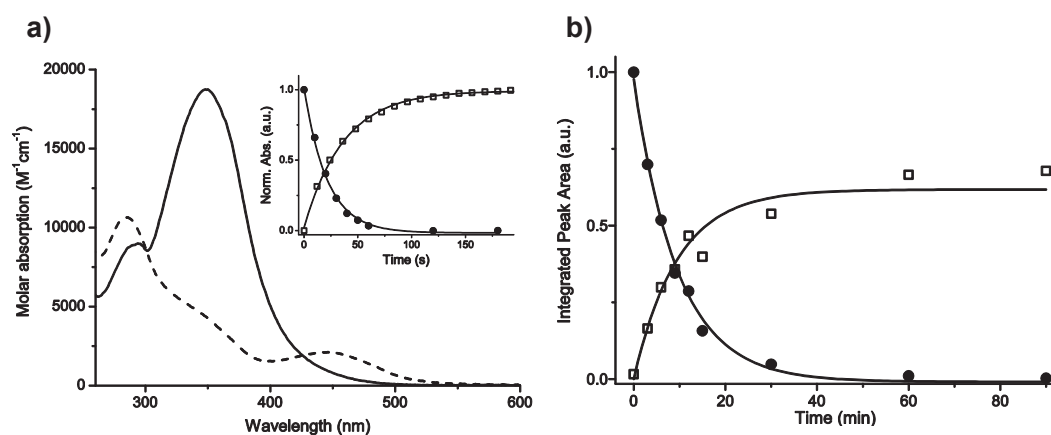

Figure 35. a) Photoswithing of **I3**. The as-dissolved ***E*-I3** (solid line) was subjected to 3 min 365 nm irradiation, yielding a PSD of 87/13 [***Z*-I3**]/[***E*-I3**] (dashed line). The inset shows the associated rates of photoswitching with time constants of 21 s (365 nm, 700 μW/cm²) and 37s (503 nm, 14 mW/cm²), for the $E \rightarrow Z$ and $Z \rightarrow E$ reaction, respectively. **b)** UV-induced decaging of **C1** where the concentrations of **C1** (solid circles) and **I2** (hollow squares) are monitored (using HPLC) as a function of irradiation time. A global first order exponential fit including both traces showed a decaging time-constant of 9.6 min (365 nm, 700 μW/cm²).

In addition to the photoreactions discussed above, thermal stability plays an important role in the performance of the photocontrolled inhibitors. As expected for azobenzene

photoswitches (section 4.1.2), the *Z*-isomer of **I3** was shown to thermally revert to ***E*-I3** with a time constant of 9.7 h at 37 °C in the absence of light. This slowly cancels the effect induced by the initial photoreaction, as the inhibitor is spontaneously "reactivated" in the dark with time. Depending on the timescale of the intended experiment, this may limit the usefullness of **I3** as an inhibitor. The cage **C1**, in contrast, was stable in aqueous solution.

5.3.3 Studies on the Isolated RET Kinase

Inhibitor studies on isolated enzymes in solution are gross simplifications of the situation in the corresponding native environment. However, because the inhibition is unperturbed by factors such as cell uptake, metabolism, and clearance, they offer the opportunity to study pure inhibitor-enzyme interactions with full control of enzyme-, substrate-, and co-factor concentrations. These systems are also free from ethical restrictions and typically more affordable than live-cell or *in vivo* assays. Thus, for establishing a biological effect of effectors, this type of study is often a preferred starting point. The RET tyrosine kinase domain has been isolated and adapted to an ATP → ADP conversion assay with luminescence readout, facilitating *in vitro* screening of RET kinase activity in the presence of effectors.[177,178] The photoswitch **I3** and cage **C1** were screened for inhibitory activity using identical incubation procedures, apart from the applied light-doses (3 min and 15 min, respectively). The incubation was outlined as follows;

  i.   The compound (*i.e.* **I3** or **C1**) was included in two identical preparations with RET kinase, substrate, and co-factors.
  ii. One preparation was exposed to 365 nm light, while the other was kept in the dark.
  iii. ATP was added, followed by incubation at room temperature for 30 min.
  iv. The relative ATP turnover was assessed by addition of luciferase-based detection reagents.†††††

The resulting dose-response curves are shown in Figure 36 below.

---

††††† For detection, several reagents were added in succession. First, the reaction was quenched, and the remaining ATP in the solution was depleted. Then, the ADP formed in the kinase reaction was converted to ATP. In the last step, a luciferease-based reagent was added to induce an [ATP]-dependent luminescence signal. Thus, the observed signal is directly proportional to the kinase activity.
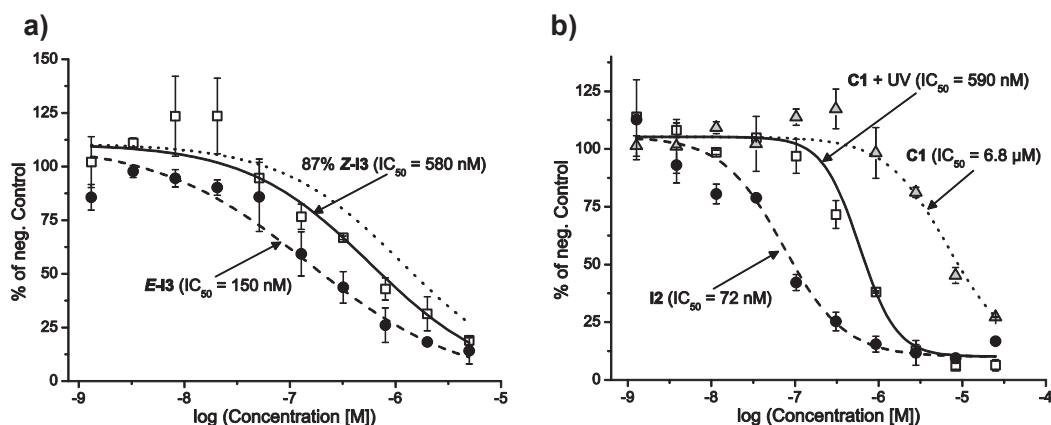
Figure 36. *In vitro* inhibition studies on the isolated RET kinase. **a)** Incubation with *E*-**I3**, before (solid circles) and after (hollow squares) 3 min 365 nm irradiation. The dotted line represents the minimum inhibitory effect of **I3**, given the 87% *Z*-form PSD, and assuming no inhibitory effect of *Z*-**I3** (see text below). **b)** Incubation with as-dissolved **C1**, before (gray triangles) and after (hollow squares) 15 min 365 nm irradiation. An identical reference incubation, albeit without light, including inhibitor **I2** (solid circles) was also performed. An irradiation control of the RET kinase assay system showed no change in kinase activity by the applied light-doses.

Photoswitching **I3** from the thermally preferred *E*-form to the *Z*-form enriched PSD causes a significantly reduced inhibitory capability (IC_{50}: 150 nM → 580 nM, Figure 36a, dashed to solid line). Because the maximum light-attainable *Z*-content is 87% (meaning that at least 13% *E*-form is present), the maximum difference in inhibitory activity for this particular photoswitch (assuming zero inhibition from the *Z*-form) is a factor of 7.7. This limit is illustrated as a dotted line in Figure 36a. In general terms, for maximum modification of inhibitory effect upon photoswitching, the inhibitor should either exhibit quantitative (PSD = 100%), bistable photoswitching and/or be completely inactive in a thermally stable, isomerically pure form. Azobenzene-derived switches designed to be passive in the *E*-conformation are uncommon, but exceptions exist; one example is the photoswitchable antibiotic recently published by the group of Feringa.[63] There is also the option of changing to a class of photoswitches with more favorable physicochemical properties. Photoswitchable enzyme inhibition has for instance been realized using the notoriously bistable DTE-type photoswitch.[118,119,179]

As for the photocage, **C1**, Figure 36b shows that irradiation significantly increases the potency of the inhibitor as the IC_{50} shifts by a factor of 12, from *ca.* 6.8 µM to 0.59 µM upon decaging. It can also be seen that the native inhibitor **I2** exhibits a considerably more potent inhibition (IC_{50} = 72 nM) than irradiated **C1**. This is expected, as the decaging of **C1** is not complete in the applied 15 min irradition (see decaging kinetics in Figure 35b). The partial inhibition exhibited by the non-irradiated caged compound **C1** is somewhat surprising given its structural incompatibility with the RET binding pocket. Although **C1** binding to the kinase active site cannot be

altogether excluded, a more likely explanation is the presence of small amounts of **I2** remaining from the synthesis of **C1** (< 0.5% by HPLC).

5.3.4   Kinase Inhibition in Live Cells

Live cells studies are a significant step up in biological complexity compared to the corresponding experiments with the purified kinase. As a conceivable application for these photocontrolled tools is for RET signal transductions studies,[4] it is required that they can be shown to be effective also in a living environment. The performance was evaluated in a live cell RET assay utilizing a β-galactosidase-based enzyme fragment complementation technique.[180,181] As was the case in the incubation with the purified kinase, the live cell incubation procedure was identical for the photoswitch **I3** and photocage **C1**, except for the applied irradiation times (3 min and 15 min, respectively). The incubation protocol was as follows;

  i. The compound was added to acclimatized live cells in two identical preparations, followed by preincubation for 3 h at 37 °C.

  ii. One preparation was exposed to 365 nm light, while the other was kept in the dark.

  iii. The growth factor Neurturin was added, followed by incubation for 3 h at 22 °C.

  iv. RET activity was assessed by addition of the supplemented detection reagents.

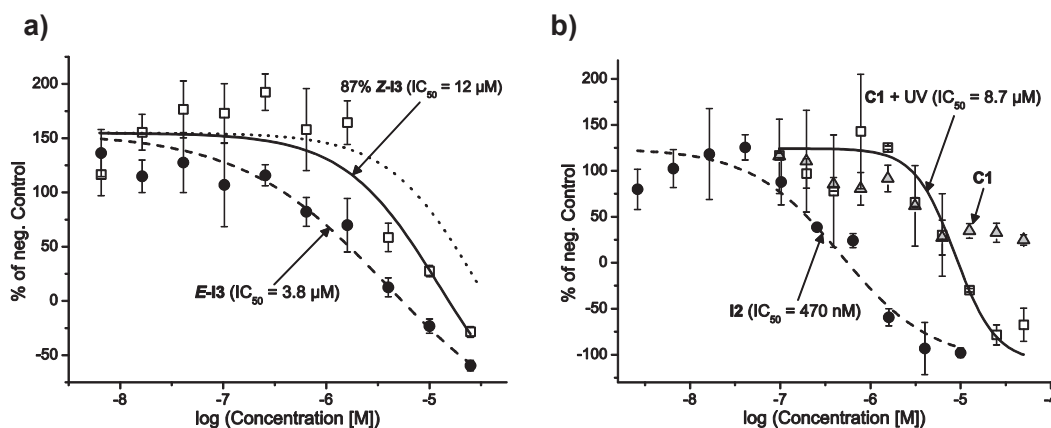The resulting dose-response curves are shown in Figure 37 below.

Figure 37. *In vitro* inhibition studies on live-cells expressing RET. **a)** Incubation with as-dissolved ***E*-I3**, before (solid circles) and after (hollow squares) 3 min 365 nm irradiation. The dotted line represents the minimum inhibitory effect of **I3**, given the 87% Z-form PSD, and assuming no inhibitory effect of ***Z*-I3**. **b)** Incubation with as-dissolved **C1**, before (gray triangles) and after (hollow squares) 15 min 365 nm irradiation. An identical reference incubation, albeit without light, including inhibitor **I2** (solid circles) was also performed. An irradiation control of the live cells showed no change in RET activity by the applied light-doses.

For the live cell incubation with the photoswitch **I3**, a 3.2-fold decrease in inhibitor potency is observed upon ***E*-I3 → *Z*-I3** isomerization (dashed to solid line in Figure 37a), which is consistent with the studies on the isolated kinase. In the incubation with the caged compound **C1** (Figure 37b), we were unable to extract meaningful IC_{50}-values with the data from the non-irradiated **C1** included in the fit. This was due to low inhibition for **C1**, even at the highest screened concentrations. It is clear, however, that irradiation results in increased inhibitory potency at higher concentrations. Again, the original compound **I2** shows a significantly lower IC_{50} compared to the irradiated **C1** (dashed *vs.* solid line in Figure 37b), due to incomplete decaging.

5.3.5 Inhibiting RET in Live Zebrafish

The last part in the investigation of photocontrolled RET inhibition was to evaluate the effect in a live organism. The zebrafish (*Danio rerio*) is a popular model organism for studying developmental biology, due to its rapid early development, transparency to light, and mapped genome. The RET gene is strongly expressed in primary motoneurons of humans[182] as well as zebrafish[183], which indicates a role in their development. We therefore reasoned that inhibition of RET during embryonic growth could result in phenotypes associated to the motoneurons of the zebrafish. To illustrate this, a transgenic tg(*olig2:dsRed*)[184] zebrafish line was used, which labels ventral spinal cord precursor cells (that in turn produces motoneurons and oligodendrocytes) with a fluorescent protein.[185] This allowed for assessment of the morphologies of these

neuronal structures by means of confocal microscopy. Because of the extensive incubation time in the zebrafish assay (*ca.* two days, 28.5 °C), and the rate of the thermal *Z*-**I3** → *E*-**I3** isomerization (time constant = 9.7 h at 37 °C), we opted not to include the photoswitch in this part of the study. Instead, we focused on the inhibitory capabilities of **C1** in the absence and presence of decaging stimulus. The zebrafish incubation protocol was as follows;

i. Compound **C1** (50 μM) was added to the zebrafish embryo solution 3 hours post fertilization (hpf) in three identical preparations, followed by incubation at 28.5 °C.

ii. To ensure efficient uptake of the cage, the embryos were washed with fresh medium before irradiation (15 min, 365 nm). One preparation was irradiated at 14 hpf, one at 24 hpf, while the third was kept in the dark.

iii. The embryos were left to develop until 48 hpf, whereafter their spinal cords were scanned with confocal imaging. ####
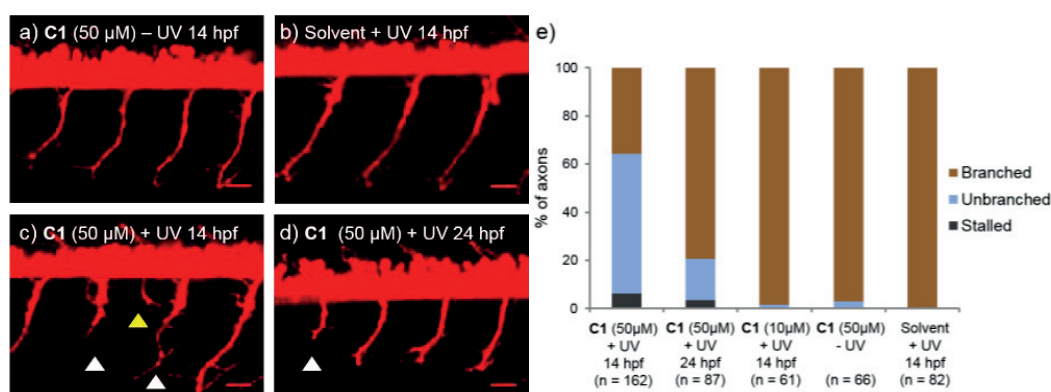

Figure 38. *In vivo* RET inhibition studies on live zebrafish treated with **C1**. The left panel (**a-d**) shows confocal image stacks of motoneurons in live tg(*olig2:dsRed*) zebrafish, with triangles indicating stalled (white) and erroneous (yellow) axons. Scale bar = 20 μM. **e)** Quantification of axonal phenotypes in the different incubations and controls; n = number of axonal processes quantified.

The results from the zebrafish incubations (Figure 38) show that embryos incubated with **C1** and irradiated at 14 hpf, display shortened and malformed axons, while the corresponding non-irradiated **C1** sample had no detrimental effect on the motoneuron axonal development.§§§§§§ Interestingly, the timing of the decaging event seems to be important, as 24 hpf decaging induced similar, but less severe and significantly fewer

---

A control experiment with irradiated, untreated zebrafish (only compound solvent added) was also performed, as well as an incubation (including the irradiation step) at a lower **C1** concentration (10 μM), see Figure 38e.

§§§§§§ The observed phenotypes could also be induced using the native inhibitor **I2** at 10 μM concentration (not shown).

abnormalities. Importantly, apart from the observed phenotypes, the zebrafish embryos exposed to the inhibitor appeared to develop normally, indicating specificity toward the RET kinase. In terms of **C1** performance, these results show that the compound can be taken up and maintained in the zebrafish, and photonically activated inside the live organism.

5.3.6 Discussion and Conclusions

Two conceptually divergent methodologies have successful been implemented to convert knowledge on established drug-target interactions into photocontrolled applications. Here, the specific binding interactions of non-photoactive RET kinase inhibitors have inspired the design of a photoswitchable and caged inhibitor, shown to be effective in three biological assays. Several differences between the two approaches can be identified from the presented results and will be discussed below.

Regarding the change in inhibitor potency upon exposure to light, it is shown that the RET activity was reduced by a factor of 12 using the cage, **C1**. This effect is higher even than the theoretical maximum effect (factor of 7.7 given the observed PSD) of the photoswitch, **I3**. This illustrates the significance of the PSD and how it can limit the use of photoswitches. For **I3**, the difference between the observed and theoretical maximum switching factor (3.9 *vs.* 7.7 in the kinasse assay) could be explained by a combination of thermal $Z \rightarrow E$ isomerization (dark reactivation of the inhibitor), and non-zero inhibition of the Z-form. The latter explaination highlights another difference between the two strategies; infering zero activity by attaching a caging group is arguably easier due to the size of the introduced photolabile substituent. The comparatively small changes in azobenzene stericity upon photoisomerization, may make the photoswitch approach more challenging in this respect.

Another noteworthy point relates to the rates of the photoreactions. The slow **C1** decaging rate neccesitated an extended irradiation time for **C1** compared to **I3** (15 min *vs.* 3 min, respectively). Longer irradiation time or higher light-flux (although deemed impractical in the applied assays) would increase the observed effect of **C1** as complete decaging was not triggered by the applied light-dose. For the photoswitch, the rates of the photoreaction was not an issue, as photoequilibrium was established much faster. In general, rapid activation of effectors can be crucial depending on the intended application, and it is clear that the photoswitch is better suited in terms of photokinetics under the herein applied conditions. On the other hand, the insufficient thermal stability of *Z*-**I3** toward isomerization disqualified **I3** from the zebrafish assay. This was in sharp contrast to **C1**, for which no such processes required consideration.

Another fundamental difference related to the design of the compounds is that decaging of **C1** yields the very same molecule as the original inhibitor, *i.e.* **I2**. However,

the inhibitor potency of the active form **I3** (**E-I3**, which was designed to mimic **I2**) displays a 2.1-fold lower inhibitor potency compared to **I2** in the kinase assay. This shows that the ability to photoswitch came with a cost in potency. Finally, the overall utility of developing photocontrolled inhibitors is nicely demonstrated in the zebrafish assay, as the time of inhibitor activation (14 hpf *vs.* 24 hpf) makes a dramatic difference in the incidence of neuronal phenotypes. Given the potential issues of uptake kinetics and biodistribution within the organism, this degree of temporal control is likely difficult to achieve with conventional drugs.

6 Concluding Remarks and Outlook

In this thesis I have shown how detailed knowledge on specific binding interactions can be converted into photocontrolled applications. I have used the well-known molecular transformations inherent to photoswitches and caged compounds to realize novel photocontrolled tools for biological use. The presented research was partly performed on a basic level, focusing in detail on host-guest binding interactions and the general behavior of isolated molecules in solution. From these exclusively spectroscopic studies (Papers II, III, and IV), concepts with distinct proof-of-principle character were developed and explored. The most important conclusions from these efforts are bulleted below.

- The spiropyran-CB7 system developed in Paper II did not function as a photocontrolled drug release scaffold due to loss of bistability. The CB7 binding bestowed the spiropyran with ultrastability toward hydrolysis.
- The thermal interconversions of a spiropyran in water can be described by an explicit set of rate- and protonation constants, according to the kinetic scheme proposed in Paper III.
- The capture and release of the neurotransmitter 4-aminopyridine can be photoreversibly controlled using the P_2-DTE system developed in Paper IV. The release event can be confirmed by fluorescent means.

I expect the increasing development of spiropyrans for aqueous and cellular use to guarantee some interest in the above findings; in particular the kinetic scheme, which allows for exact predictions of the time- and pH-dependent concentration profile of the various forms of the photoswitch. Considering the beneficial effects previously reported for CB7-binding (solubilization, enhancement of cell uptake *etc.*, discussed in section 5.1.3), the anchor-derived binding approach may be a viable method also for other types of photoswitches. The complexation-induced changes in thermal behavior of the spiropyran (and possibly other properties of other photoswitches) may also be molded into useful applications. However, it is difficult to predict with confidence how these findings will be used in future research.

In proof-of-principle studies, applicability is outweighed by novelty. The release-and-report scaffold presented in Paper IV serves as a good example. Although not immediately applicable to a biological setting, it signifies a noteworthy addition to existing intelligent drug delivery systems. The room for improvements is however willingly acknowledged. As discussed in section 5.1.5, making the scaffold water compatible would be a crucial step. Equally important is to improve the drug release ratio. Some structural improvements of the DTE switch could be made to possibly enhance the difference in P_2 binding strength between the isomers, to drive a more

substantial release. The scaffold is however innately limited by the fact that also the weakly binding closed isomer (**DTEc**) competes with the drug for binding sites on P_2.

The latter parts of the results (referred to as parts two and three in chapter 5) focus on photocontrolled small-molecules in living systems. In contrast to the former studies this can be considered to be closer to an actual biological application. The following conclusions are drawn.

- An apoptotic-like cytotoxic response can selectively be triggered by photoisomerizing a DNA-binding spiropyran derivative in live human cancer cells (Paper I).
- Light-controlled inhibition of the RET kinase can be achieved using an azobenzene-derived photoswitch (Paper V), or *o*-nitrobenzyl-type caged compound (Paper VI).

The live cell spiropyran study exemplifies how a biological effect (here: cytotoxicity) can be photocontrolled with *spatial* discrimination, since only irradiated cells committed to the death-program. Possible follow-up studies to this work include co-localization imaging experiment (using emissive probes *e.g.* for mitochondria) to identify preferred intracellular targets of the spiropyran. Further evidence regarding the type of death-program being triggered could likely also be gained using *e.g.* caspase-based apoptosis probes.[186]

The binding site-inspired scheme for developing the photocontrolled inhibitors presented in Papers V and VI demonstrates how established methodologies (both caging and incorporation of azo-groups into effectors are well-explored procedures) can readily be applied to novel targets. The caged compound **C1** is currently being considered for further studies in zebrafish.

As for an eventual transition of photocontrolled tools into clinical practice, it should be stressed that the current state of the field likely has some way to go. A reasonable speculation is that such development would (at least to begin with) be dominated by caged applications, as they are less sensitive to complications such as dark processes and incomplete conversion. Conceivable targets would likely include skin malignancies, due to their accessibility. On the other hand, I believe there is more immediate potential for using both caged compounds and photoswitches as biological probes to resolve spatial and temporal dynamics of *e.g.* cell signaling, and would welcome further development of these types of experimental protocols.

7 Acknowledgements

8 References

1. Edwards, I. R. & Aronson, J. K. Adverse drug reactions: definitions, diagnosis, and management. *Lancet* **356**, 1255-1259 (2000).

2. Frye, S. V. The art of the chemical probe. *Nat. Chem. Biol.* **6**, 159-161 (2010).

3. Bunnage, M. E., Chekler, E. L. P. & Jones, L. H. Target validation using chemical probes. *Nat. Chem. Biol.* **9**, 195-199 (2013).

4. Gorostiza, P. & Isacoff, E. Y. Optical Switches for Remote and Noninvasive Control of Cell Signaling. *Science* **322**, 395-399 (2008).

5. Weissleder, R. A clearer vision for in vivo imaging. *Nat. Biotech.* **19**, 316-317 (2001).

6. Velema, W. A., Szymanski, W. & Feringa, B. L. Photopharmacology: Beyond Proof of Principle. *J. Am. Chem. Soc.* **136**, 2178-2191 (2014).

7. Göstl, R., Senf, A. & Hecht, S. Remote-controlling chemical reactions by light: Towards chemistry with high spatio-temporal resolution. *Chem. Soc. Rev.* **43**, 1982-1996 (2014).

8. Szymański, W., Beierle, J. M., Kistemaker, H. A. V., Velema, W. A. & Feringa, B. L. Reversible Photocontrol of Biological Systems by the Incorporation of Molecular Photoswitches. *Chem. Rev.* **113**, 6114-6178 (2013).

9. Fehrentz, T., Schönberger, M. & Trauner, D. Optochemical Genetics. *Angew. Chem., Int. Ed.* **50**, 12156-12182 (2011).

10. Mayer, G. & Heckel, A. Biologically active molecules with a "light switch". *Angew. Chem., Int. Ed.* **45**, 4900-4921 (2006).

11. Brieke, C., Rohrbach, F., Gottschalk, A., Mayer, G. & Heckel, A. Light-Controlled Tools. *Angew. Chem., Int. Ed.* **51**, 8446-8476 (2012).

12. Deiters, A. Principles and applications of the photochemical control of cellular processes. *ChemBioChem* **11**, 47-53 (2010).

13. Pellicioli, A. P. & Wirz, J. Photoremovable protecting groups: reaction mechanisms and applications. *Photochem. Photobiol. Sci.* **1**, 441-458 (2002).

14. Ellis-Davies, G. C. R. Caged compounds: photorelease technology for control of cellular chemistry and physiology. *Nat. Methods* **4**, 619-628 (2007).

15. Klán, P. *et al.* Photoremovable Protecting Groups in Chemistry and Biology: Reaction Mechanisms and Efficacy. *Chem. Rev.* **113**, 119-191 (2012).

16. Bochet, C. G. Photolabile protecting groups and linkers. *J. Chem. Soc., Perkin Trans. 1*, 125-142 (2002).

17. Maxwell, J. C. A Dynamical Theory of the Electromagnetic Field. *Philos. Trans. R. Soc. London* **155**, 459-512 (1865).

18. Planck, M. Entropie und Temperatur strahlender Wärme. *Ann. Phys.* **306**, 719-737 (1900).

19. Lewis, G. N. The Conservation of Photons *Nature* **118**, 874-875 (1926).

20. Hertz, H. Ueber einen Einfluss des ultravioletten Lichtes auf die electrische Entladung. *Ann. Phys.* **267**, 983-1000 (1887).

21. Einstein, A. Über einen die Erzeugung und Verwandlung des Lichtes betreffenden heuristischen Gesichtspunkt. *Ann. Phys.* **322**, 132-148 (1905).

22. de Broglie, L.-V. *Ondes et Mouvements.* (Gauthier-Villars, 1926).

23. Bohr, N. On the Constitution of Atoms and Molecules. *Philos. Mag. Ser. 6* **26**, 476-502 (1913).

24. Schrödinger, E. An Undulatory Theory of the Mechanics of Atoms and Molecules. *Phys. Rev.* **28**, 1049-1070 (1926).

25. Heisenberg, W. Über den anschaulichen Inhalt der quantentheoretischen Kinematik und Mechanik. *Z. Physik* **43**, 172-198 (1927).

26. Fukui, K., Yonezawa, T. & Shingu, H. A Molecular Orbital Theory of Reactivity in Aromatic Hydrocarbons. *J. Chem. Phys.* **20**, 722-725 (1952).

27. Dirac, P. A. M. The Quantum Theory of the Emission and Absorption of Radiation. *Proc. R. Soc. London, Ser. A* **114**, 243-265 (1927).

28. Kasha, M. Characterization of electronic transitions in complex molecules. *Discuss. Faraday Soc.* **9**, 14-19 (1950).

29. Förster, T. Zwischenmolekulare Energiewanderung und Fluoreszenz. *Ann. Phys.* **437**, 55-75 (1948).

30. IUPAC. *Compendium of Chemical Terminology*, 2nd ed. (Blackwell Scientific Publications, 1997). Compiled by McNaught A. D. & Wilkinson A. XML on-line corrected version: http://goldbook.iupac.org (2006-) created by Nic M., Jirat, J., Kosata, B.; updates compiled by Jenkins, A. doi:10.1351/goldbook.

31. Lagona, J., Mukhopadhyay, P., Chakrabarti, S. & Isaacs, L. The Cucurbit[n]uril Family. *Angew. Chem., Int. Ed.* **44**, 4844-4870 (2005).

32. Davis, M. E. & Brewster, M. E. Cyclodextrin-based pharmaceutics: Past, present and future. *Nat. Rev. Drug Discov.* **3**, 1023-1035 (2004).

33. Wenz, G. Cyclodextrins as Building Blocks for Supramolecular Structures and Functional Units. *Angew. Chem., Int. Ed.* **33**, 803-822 (1994).

34. Beletskaya, I., Tyurin, V. S., Tsivadze, A. Y., Guilard, R. & Stern, C. Supramolecular Chemistry of Metalloporphyrins. *Chem. Rev.* **109**, 1659-1713 (2009).

35. Thordarson, P. Determining association constants from titration experiments in supramolecular chemistry. *Chem. Soc. Rev.* **40**, 1305-1323 (2011).

36. Yung-Chi, C. & Prusoff, W. H. Relationship between the inhibition constant (KI) and the concentration of inhibitor which causes 50 per cent inhibition (I50) of an enzymatic reaction. *Biochem. Pharmacol.* **22**, 3099-3108 (1973).

37. Lakowicz, J. R. *Principles of Fluorescence Spectroscopy.* 3rd ed, (Springer Science+Business Media, 2006).

38. Hell, S. W. & Wichmann, J. Breaking the diffraction resolution limit by stimulated emission: stimulated-emission-depletion fluorescence microscopy. *Opt. Lett.* **19**, 780-782 (1994).

39. Pawley, J. B. *Handbook of Biological Confocal Microscopy.* 3rd ed, (Springer Science+Business Media, 2006).

40. Frangioni, J. V. In vivo near-infrared fluorescence imaging. *Curr. Opin. Chem. Biol.* **7**, 626-634 (2003).

41. Smith, A. M., Mancini, M. C. & Nie, S. Bioimaging: Second window for in vivo imaging. *Nat. Nanotechnol.* **4**, 710-711 (2009).

42. Darlenski, R. & Fluhr, J. W. Photodynamic therapy in dermatology: past, present, and future. *J. Biomed. Opt.* **18**, 061208 (2013).

43. Kramer, R. H., Mourot, A. & Adesnik, H. Optogenetic pharmacology for control of native neuronal signaling proteins. *Nat. Neurosci.* **16**, 816-823 (2013).

44. Zemelman, B. V., Lee, G. A., Ng, M. & Miesenböck, G. Selective photostimulation of genetically chARGed neurons. *Neuron* **33**, 15-22 (2002).

45. Deisseroth, K. Optogenetics. *Nat. Methods* **8**, 26-29 (2011).

46. Nagel, G. *et al.* Channelrhodopsin-1: A light-gated proton channel in green algae. *Science* **296**, 2395-2398 (2002).

47. Pastrana, E. Optogenetics: controlling cell function with light. *Nat. Methods* **8**, 24-25 (2011).

48. Staff, T. N. Stepping Away From the Trees For a Look at the Forest. *Science* **330**, 1612-1613 (2010).

49. Beharry, A. A. & Woolley, G. A. Azobenzene photoswitches for biomolecules. *Chem. Soc. Rev.* **40**, 4422-4437 (2011).

50. Szobota, S., McKenzie, C. & Janovjak, H. Optical control of ligand-gated ion channels. *Methods Mol. Biol.* **998**, 417-435 (2013).

51. Engels, J. & Schlaeger, E. J. Synthesis, structure, and reactivity of adenosine cyclic 3',5'-phosphate-benzyltriesters. *J. Med. Chem.* **20**, 907-911 (1977).

52. Kaufman, H., Vratsanos, S. M. & Erlanger, B. F. Photoregulation of an Enzymic Process by Means of a Light-Sensitive Ligand. *Science* **162**, 1487-1489 (1968).

53. Asanuma, H., Liang, X., Yoshida, T. & Komiyama, M. Photocontrol of DNA duplex formation by using azobenzene-bearing oligonucleotides. *ChemBioChem* **2**, 39-44 (2001).

54. Ogasawara, S. & Maeda, M. Straightforward and Reversible Photoregulation of Hybridization by Using a Photochromic Nucleoside. *Angew. Chem., Int. Ed.* **47**, 8839-8842 (2008).

55. Liu, Q. & Deiters, A. Optochemical Control of Deoxyoligonucleotide Function Via a Nucleobase-Caging Approach. *Acc. Chem. Res.* **47**, 45-55 (2014).

56. Renner, C. & Moroder, L. Azobenzene as conformational switch in model peptides. *ChemBioChem* **7**, 868-878 (2006).

57. Kumita, J. R., Flint, D. G., Smart, O. S. & Woolley, G. A. Photo-control of peptide helix content by an azobenzene cross-linker: steric interactions with underlying residues are not critical. *Protein Eng.* **15**, 561-569 (2002).

58. Ali, A. M. & Woolley, G. A. The effect of azobenzene cross-linker position on the degree of helical peptide photo-control. *Org. Biomol. Chem.* **11**, 5325-5331 (2013).

59. Ito, H., Liang, X., Nishioka, H. & Asanuma, H. Construction of photoresponsive RNA for photoswitching RNA hybridization. *Org. Biomol. Chem.* **8**, 5519-5524 (2010).

60. Goldau, T. *et al.* Reversible Photoswitching of RNA Hybridization at Room Temperature with an Azobenzene C-Nucleoside. *Chem. - Eur. J.* **21**, 2845-2854 (2015).

61. Paramonov, S. V., Lokshin, V. & Fedorova, O. A. Spiropyran, chromene or spirooxazine ligands: Insights into mutual relations between complexing and photochromic properties. *J. Photochem. Photobiol., C* **12**, 209-236 (2011).

62. Zhang, J., Wang, J. & Tian, H. Taking orders from light: progress in photochromic bio-materials. *Mater. Horiz.* **1**, 169-184 (2014).

63. Velema, W. A. *et al.* Optical control of antibacterial activity. *Nat. Chem.* **5**, 924-928 (2013).

64. Stafforst, T. & Hilvert, D. Kinetic characterization of spiropyrans in aqueous media. *Chem. Commun.*, 287-288 (2009).

65. Boulègue, C., Löweneck, M., Renner, C. & Moroder, L. Redox Potential of Azobenzene as an Amino Acid Residue in Peptides. *ChemBioChem* **8**, 591-594 (2007).

66. Sheng, Y. *et al.* Comprehensive Theoretical Study of the Conversion Reactions of Spiropyrans: Substituent and Solvent Effects. *J. Phys. Chem. B* **108**, 16233-16243 (2004).

67. Görner, H. Photochromism of nitrospiropyrans: effects of structure, solvent and temperature. *Phys. Chem. Chem. Phys.* **3**, 416-423 (2001).

68. Görner, H., Atabekyan, L. S. & Chibisov, A. K. Photoprocesses in spiropyran-derived merocyanines: Singlet versus triplet pathway. *Chem. Phys. Lett.* **260**, 59-64 (1996).

69. Bletz, M., Pfeifer-Fukumura, U., Kolb, U. & Baumann, W. Ground- and First-Excited-Singlet-State Electric Dipole Moments of Some Photochromic Spirobenzopyrans in Their Spiropyran and Merocyanine Form. *J. Phys. Chem. A* **106**, 2232-2236 (2002).

70. Wojtyk, J. T. *et al.* Elucidating the mechanisms of acidochromic spiropyran-merocyanine interconversion. *J. Phys. Chem. A* **111**, 2511-2516 (2007).

71. Hammarson, M., Andersson, J., Li, S., Lincoln, P. & Andréasson, J. Molecular AND-logic for dually controlled activation of a DNA-binding spiropyran. *Chem. Commun.* **46**, 7130-7132 (2010).

72. Remón, P. *et al.* Molecular Implementation of Sequential and Reversible Logic Through Photochromic Energy Transfer Switching. *Chem. - Eur. J.* **17**, 6492-6500 (2011).

73. Andersson, J., Li, S., Lincoln, P. & Andréasson, J. Photoswitched DNA-Binding of a Photochromic Spiropyran. *J. Am. Chem. Soc.* **130**, 11836-11837 (2008).

74. Hammarson, M., Nilsson, J. R., Li, S., Lincoln, P. & Andréasson, J. DNA-Binding Properties of Amidine-Substituted Spiropyran Photoswitches. *Chem. - Eur. J.* **20**, 15855-15862 (2014).

75. Bälter, M. *et al.* Reversible Energy-Transfer Switching on a DNA Scaffold. *J. Am. Chem. Soc.* **137**, 2444-2447 (2015).

76. Brieke, C. & Heckel, A. Spiropyran Photoswitches in the Context of DNA: Synthesis and Photochromic Properties. *Chem. - Eur. J.* **19**, 15726-15734 (2013).

77. Asanuma, H. *et al.* Spiropyran as a Regulator of DNA Hybridization with Reversed Switching Mode to That of Azobenzene. *Chem. Lett.* **30**, 108-109 (2001).

78. Beyer, C. & Wagenknecht, H.-A. Synthesis of DNA with Spirobenzopyran as an Internal Covalent Modification. *Synlett* **2010**, 1371-1376 (2010).

79. Young, D. D. & Deiters, A. Light-Regulated RNA–Small Molecule Interactions. *ChemBioChem* **9**, 1225-1228 (2008).

80. Zhang, X., Zhang, J., Ying, Y.-L., Tian, H. & Long, Y.-T. Single molecule analysis of light-regulated RNA:spiropyran interactions. *Chem. Sci.* **5**, 2642-2646 (2014).

81. Koçer, A., Walko, M., Meijberg, W. & Feringa, B. L. A Light-Actuated Nanovalve Derived from a Channel Protein. *Science* **309**, 755-758 (2005).

82. Marriott, G. *et al.* Optical lock-in detection imaging microscopy for contrast-enhanced imaging in living cells. *Proc. Natl. Acad. Sci. U. S. A.* **105**, 17789-17794 (2008).

83. Bandara, H. M. D. & Burdette, S. C. Photoisomerization in different classes of azobenzene. *Chem. Soc. Rev.* **41**, 1809-1825 (2012).

84. Merino, E. Synthesis of azobenzenes: the coloured pieces of molecular materials. *Chem. Soc. Rev.* **40**, 3835-3853 (2011).

85. Bullock, D. J. W., Cumper, C. W. N. & Vogel, A. I. 989. Physical properties and chemical constitution. Part XLIII. The electric dipole moments of azobenzene, azopyridines, and azoquinolines. *J. Chem. Soc. (Resumed)*, 5316-5323 (1965).

86. Crecca, C. R. & Roitberg, A. E. Theoretical study of the isomerization mechanism of azobenzene and disubstituted azobenzene derivatives. *J. Phys. Chem. A* **110**, 8188-8203 (2006).

87. Fujino, T., Arzhantsev, S. Y. & Tahara, T. Femtosecond Time-Resolved Fluorescence Study of Photoisomerization of trans-Azobenzene. *J. Phys. Chem. A* **105**, 8123-8129 (2001).

88. Nishimura, N., Tanaka, T., Asano, M. & Sueishi, Y. A volumetric study on the thermal cis-to-trans isomerization of 4-(dimethylamino)-4[prime or minute]-nitroazobenzene and 4,4[prime or minute]-bis(dialkylamino)azobenzenes: evidence of an inversion mechanism. *J. Chem. Soc., Perkin Trans. 2*, 1839-1845 (1986).

89. Brode, W. R., Gould, J. H. & Wyman, G. M. The Relation between the Absorption Spectra and the Chemical Constitution of Dyes. XXVI. Effect of Solvent and of Temperature on the cis—trans Isomerization of Azo Dyes. *J. Am. Chem. Soc.* **75**, 1856-1859 (1953).

90. Nishimura, N. *et al.* Thermal Cis-to-Trans Isomerization of Substituted Azobenzenes II. Substituent and Solvent Effects. *Bull. Chem. Soc. Jpn.* **49**, 1381-1387 (1976).

91. Bléger, D., Schwarz, J., Brouwer, A. M. & Hecht, S. o-Fluoroazobenzenes as Readily Synthesized Photoswitches Offering Nearly Quantitative Two-Way Isomerization with Visible Light. *J. Am. Chem. Soc.* **134**, 20597-20600 (2012).

92. Knie, C. *et al.* ortho-Fluoroazobenzenes: Visible Light Switches with Very Long-Lived Z Isomers. *Chem. - Eur. J.* **20**, 16492-16501 (2014).

93. Beharry, A. A., Sadovski, O. & Woolley, G. A. Azobenzene Photoswitching without Ultraviolet Light. *J. Am. Chem. Soc.* **133**, 19684-19687 (2011).

94. Samanta, S. *et al.* Photoswitching Azo Compounds in Vivo with Red Light. *J. Am. Chem. Soc.* **135**, 9777-9784 (2013).

95. De Boni, L. *et al.* Two-photon absorption in azoaromatic compounds. *Chem. Phys. Lett.* **361**, 209-213 (2002).

96. Jiang, D.-L. & Aida, T. Photoisomerization in dendrimers by harvesting of low-energy photons. *Nature* **388**, 454-456 (1997).

97. Izquierdo-Serra, M. *et al.* Two-Photon Neuronal and Astrocytic Stimulation with Azobenzene-Based Photoswitches. *J. Am. Chem. Soc.* **136**, 8693-8701 (2014).

98. Beharry, A. A., Wong, L., Tropepe, V. & Woolley, G. A. Fluorescence Imaging of Azobenzene Photoswitching In Vivo. *Angew. Chem., Int. Ed.* **50**, 1325-1327 (2011).

99. Schönberger, M., Damijonaitis, A., Zhang, Z., Nagel, D. & Trauner, D. Development of a New Photochromic Ion Channel Blocker via Azologization of Fomocaine. *ACS Chem. Neurosci.* **5**, 514-518 (2014).

100. Bartels, E., Wassermann, N. H. & Erlanger, B. F. Photochromic Activators of the Acetylcholine Receptor. *Proc. Natl. Acad. Sci. U. S. A.* **68**, 1820-1823 (1971).

101. Pittolo, S. *et al.* An allosteric modulator to control endogenous G protein-coupled receptors with light. *Nat. Chem. Biol.* **10**, 813-815 (2014).

102. Stein, M. *et al.* Azo-Propofols: Photochromic Potentiators of GABA(A) Receptors. *Angew. Chem., Int. Ed.* **51**, 10500-10504 (2012).

103. Irie, M. Diarylethenes for Memories and Switches. *Chem Rev* **100**, 1685-1716 (2000).

104. Irie, M., Fukaminato, T., Matsuda, K. & Kobatake, S. Photochromism of Diarylethene Molecules and Crystals: Memories, Switches, and Actuators. *Chem. Rev.* **114**, 12174-12277 (2014).

105. Tian, H. & Wang, S. Photochromic bisthienylethene as multi-function switches. *Chem. Commun.*, 781-792 (2007).

106. Tian, H. & Yang, S. Recent progresses on diarylethene based photochromic switches. *Chem. Soc. Rev.* **33**, 85-97 (2004).

107. Mallory, F. B. & Mallory, C. W. *Photocyclization of Stilbenes and Related Molecules*, in *Organic Reactions*, p. 1-456 (John Wiley & Sons, Inc., 2005).

108. Kellogg, R. M., Groen, M. B. & Wynberg, H. Photochemically induced cyclization of some furyl- and thienylethenes. *J. Org. Chem.* **32**, 3093-3100 (1967).

109. Yamaguchi, T., Uchida, K. & Irie, M. Asymmetric Photocyclization of Diarylethene Derivatives. *J. Am. Chem. Soc.* **119**, 6066-6071 (1997).

110. Hanazawa, M., Sumiya, R., Horikawa, Y. & Irie, M. Thermally irreversible photochromic systems. Reversible photocyclization of 1,2-bis (2-methylbenzo[b]thiophen-3-yl)perfluorocyclocoalkene derivatives. *Chem. Commun.* 206-207 (1992).

111. Woodward, R. B. & Hoffmann, R. Stereochemistry of Electrocyclic Reactions. *J. Am. Chem. Soc.* **87**, 395-397 (1965).

112. Murguly, E., Norsten, T. B. & Branda, N. R. Nondestructive Data Processing Based on Chiroptical 1,2-Dithienylethene Photochromes. *Angew. Chem., Int. Ed.* **40**, 1752-1755 (2001).

113. Pace, T. C. S., Müller, V., Li, S., Lincoln, P. & Andréasson, J. Enantioselective Cyclization of Photochromic Dithienylethenes Bound to DNA. *Angew. Chem., Int. Ed.* **52**, 4393-4396 (2013).

114. Takeshita, M. & Irie, M. Enhancement of the photocyclization quantum yield of 2,2[prime or minute]-dimethyl-3,3[prime or minute]-(perfluorocyclopentene-1,2-diyl)bis(benzo[b]- thiophene-6-sulfonate) by inclusion in a cyclodextrin cavity. *Chem. Commun.* 2265-2266 (1997).

115. Irie, M. & Mohri, M. Thermally irreversible photochromic systems. Reversible photocyclization of diarylethene derivatives. *J. Org. Chem.* **53**, 803-808 (1988).

116. Lv, G. *et al.* Diarylethene based fluorescent switchable probes for the detection of amyloid-[small beta] pathology in Alzheimer's disease. *Chem. Commun.* **51**, 125-128 (2015).

117. Soh, N. *et al.* A fluorescent photochromic compound for labeling biomolecules. *Chem. Commun.* 5206-5208 (2007).

118. Falenczyk, C. *et al.* Chromo-pharmacophores: photochromic diarylmaleimide inhibitors for sirtuins. *Chem. Sci.* **5**, 4794-4799 (2014).

119. Vomasta, D., Högner, C., Branda, N. R. & König, B. Regulation of human carbonic anhydrase I (hCAI) activity by using a photochromic inhibitor. *Angew. Chem., Int. Ed.* **47**, 7644-7647 (2008).

120. Al-Atar, U., Fernandes, R., Johnsen, B., Baillie, D. & Branda, N. R. A Photocontrolled Molecular Switch Regulates Paralysis in a Living Organism. *J. Am. Chem. Soc.* **131**, 15966-15967 (2009).

121. Barrois, S. & Wagenknecht, H.-A. Diarylethene-modified nucleotides for switching optical properties in DNA. *Beilstein J. Org. Chem.* **8**, 905-914 (2012).

122. Cahová, H. & Jäschke, A. Nucleoside-Based Diarylethene Photoswitches and Their Facile Incorporation into Photoswitchable DNA. *Angew. Chem., Int. Ed.* **52**, 3186-3190 (2013).

123. Kramer, R. H., Fortin, D. L. & Trauner, D. New photochemical tools for controlling neuronal activity. *Curr. Opin. Neurobiol.* **19**, 544-552 (2009).

124. Kaplan, J. H., Forbush, B. & Hoffman, J. F. Rapid photolytic release of adenosine 5'-triphosphate from a protected analog: utilization by the sodium:potassium pump of human red blood cell ghosts. *Biochemistry* **17**, 1929-1935 (1978).

125. Gatterdam, V., Stoess, T., Menge, C., Heckel, A. & Tampé, R. Caged Glutathione – Triggering Protein Interaction by Light. *Angew. Chem., Int. Ed.* **51**, 3960-3963 (2012).

126. Callaway, E. M. & Katz, L. C. Photostimulation using caged glutamate reveals functional circuitry in living brain slices. *Proc. Natl. Acad. Sci. U. S. A.* **90**, 7661-7665 (1993).

127. Pirrung, M. C. & Huang, C.-Y. A General Method for the Spatially Defined Immobilization of Biomolecules on Glass Surfaces Using "Caged" Biotin. *Bioconjugate Chem.* **7**, 317-321 (1996).

128. Amatrudo, J. M. *et al.* Wavelength-Selective One- and Two-Photon Uncaging of GABA. *ACS Chem. Neurosci.* **5**, 64-70 (2013).

129. Kantevari, S., Matsuzaki, M., Kanemoto, Y., Kasai, H. & Ellis-Davies, G. C. R. Two- color, two-photon uncaging of glutamate and GABA. *Nat. Methods* **7**, 123-125 (2010).

130. Kohl-Landgraf, J. *et al.* Mechanism of the Photoinduced Uncaging Reaction of Puromycin Protected by a 6-Nitroveratryloxycarbonyl Group. *J. Am. Chem. Soc.* **136**, 3430-3438 (2014).

131. Schaper, K., Etinski, M. & Fleig, T. Theoretical investigation of the excited states of 2-nitrobenzyl and 4,5-methylendioxy-2-nitrobenzyl caging groups. *Photochem. Photobiol.* **85**, 1075-1081 (2009).

132. Pettit, D. L., Wang, S. S. H., Gee, K. R. & Augustine, G. J. Chemical two-photon uncaging: a novel approach to mapping glutamate receptors. *Neuron* **19**, 465-471 (1997).

133. Furuta, T. *et al.* Brominated 7-hydroxycoumarin-4-ylmethyls: Photolabile protecting groups with biologically useful cross-sections for two photon photolysis. *Proc. Natl. Acad. Sci. U. S. A.* **96**, 1193-1200 (1999).

134. Yan, B., Boyer, J.-C., Branda, N. R. & Zhao, Y. Near-Infrared Light-Triggered Dissociation of Block Copolymer Micelles Using Upconverting Nanoparticles. *J. Am. Chem. Soc.* **133**, 19714-19717 (2011).

135. Carling, C.-J., Nourmohammadian, F., Boyer, J.-C. & Branda, N. R. Remote-Control Photorelease of Caged Compounds Using Near-Infrared Light and Upconverting Nanoparticles. *Angew. Chem., Int. Ed.* **49**, 3782-3785 (2010).

136. Oshovsky, G. V., Reinhoudt, D. N. & Verboom, W. Supramolecular chemistry in water. *Angew. Chem., Int. Ed.* **46**, 2366-2393 (2007).

137. Hou, L., Zhang, X., Pijper, T. C., Browne, W. R. & Feringa, B. L. Reversible Photochemical Control of Singlet Oxygen Generation Using Diarylethene Photochromic Switches. *J. Am. Chem. Soc.* **136**, 910-913 (2014).

138. Presa, A. *et al.* Photoswitching the Cytotoxic Properties of Platinum(II) Compounds. *Angew. Chem., Int. Ed.* (2015), doi: 10.1002/anie.201412157.

139. Baroncini, M. *et al.* Light Control of Stoichiometry and Motion in Pseudorotaxanes Comprising a Cucurbit[7]uril Wheel and an Azobenzene-Bipyridinium Axle. *Chem. - Eur. J.* **20**, 10737-10744 (2014).

140. Kim, Y., Ko, Y. H., Jung, M., Selvapalam, N. & Kim, K. A new photo-switchable "on-off" host-guest system. *Photochem. Photobiol. Sci.* **10**, 1415-1419 (2011).

141. Zhao, J., Zhang, Y.-M., Sun, H.-L., Chang, X.-Y. & Liu, Y. Multistimuli-Responsive Supramolecular Assembly of Cucurbituril/Cyclodextrin Pairs with an Azobenzene-Containing Bispyridinium Guest. *Chem. - Eur. J.* **20**, 15108-15115 (2014).

142. Zhang, L. *et al.* Host-guest interaction between fluoro-substituted azobenzene derivative and cyclodextrins. *RSC Adv.* **5**, 12007-12014 (2015).

143. Han, M. *et al.* Light-Triggered Guest Uptake and Release by a Photochromic Coordination Cage. *Angew. Chem., Int. Ed.* **52**, 1319-1323 (2013).

144. Manning, G., Whyte, D. B., Martinez, R., Hunter, T. & Sudarsanam, S. The Protein Kinase Complement of the Human Genome. *Science* **298**, 1912-1934 (2002).

145. Bridges, A. J. Chemical Inhibitors of Protein Kinases. *Chem. Rev.* **101**, 2541-2572 (2001).

146. Krause, D. S. & Van Etten, R. A. Tyrosine Kinases as Targets for Cancer Therapy. *N. Engl. J. Med.* **353**, 172-187 (2005).

147. Liu, Y. & Gray, N. S. Rational design of inhibitors that bind to inactive kinase conformations. *Nat. Chem. Biol.* **2**, 358-364 (2006).

148. Zhang, J., Yang, P. L. & Gray, N. S. Targeting cancer with small molecule kinase inhibitors. *Nat. Rev. Cancer* **9**, 28-39 (2009).

149. Morckel, A. R. *et al.* A photoactivatable small-molecule inhibitor for light-controlled spatiotemporal regulation of Rho kinase in live embryos. *Development* **139**, 437-442 (2012).

150. Wood, J. S., Koszelak, M., Liu, J. & Lawrence, D. S. A Caged Protein Kinase Inhibitor. *J. Am. Chem. Soc.* **120**, 7145-7146 (1998).

151. Kuil, J., van Wandelen, L. T. M., de Mol, N. J. & Liskamp, R. M. J. A photoswitchable ITAM peptidomimetic: Synthesis and real time surface plasmon resonance (SPR) analysis of the effects of cis–trans isomerization on binding. *Bioorg. Med. Chem.* **16**, 1393-1399 (2008).

152. Kuil, J., van Wandelen, L. T., de Mol, N. J. & Liskamp, R. M. Switching between low and high affinity for the Syk tandem SH2 domain by irradiation of azobenzene containing ITAM peptidomimetics. *J. Pept. Sci.* **15**, 685-691 (2009).

153. Takahashi, M., Ritz, J. & Cooper, G. M. Activation of a novel human transforming gene, ret, by DNA rearrangement. *Cell* **42**, 581-588 (1985).

154. Lemmon, M. A. & Schlessinger, J. Cell signaling by receptor-tyrosine kinases. *Cell* **141**, 1117-1134 (2010).

155. Santoro, M., Melillo, R. M., Carlomagno, F., Vecchio, G. & Fusco, A. Minireview: RET: normal and abnormal functions. *Endocrinology* **145**, 5448-5451 (2004).

156. Mulligan, L. M. RET revisited: expanding the oncogenic portfolio. *Nat. Rev. Cancer* **14**, 173-186 (2014).

157. Plaza-Menacho, I. *et al.* Targeting the receptor tyrosine kinase RET sensitizes breast cancer cells to tamoxifen treatment and reveals a role for RET in endocrine resistance. *Oncogene* **29**, 4648-4657 (2010).

158. Winters, M. U. *et al.* Control of Electron Transfer in a Conjugated Porphyrin Dimer by Selective Excitation of Planar and Perpendicular Conformers. *Chem. - Eur. J.* **13**, 7385-7394 (2007).

159. Hennig, A., Bakirci, H. & Nau, W. M. Label-free continuous enzyme assays with macrocycle-fluorescent dye complexes. *Nat. Meth.* **4**, 629-632 (2007).

160. Kärnbratt, J. *et al.* Photochromic Supramolecular Memory With Nondestructive Readout. *Angew. Chem., Int. Ed.* **49**, 1854-1857 (2010).

161. Müller, M., Dierkes, P. W. & Schlue, W.-R. Ionic mechanism of 4-aminopyridine action on leech neuropile glial cells. *Brain Res.* **826**, 63-73 (1999).

162. Appel, E. A. *et al.* Enhanced stability and activity of temozolomide in primary glioblastoma multiforme cells with cucurbit[n]uril. *Chem. Commun.* **48**, 9843-9845 (2012).

163. Hettiarachchi, G. *et al.* Toxicology and Drug Delivery by Cucurbit[n]uril Type Molecular Containers. *PLoS One* **5**, e10514 (2010).

164. Uzunova, V. D., Cullinane, C., Brix, K., Nau, W. M. & Day, A. I. Toxicity of cucurbit[7]uril and cucurbit[8]uril: an exploratory in vitro and in vivo study. *Org. Biomol. Chem.* **8**, 2037-2042 (2010).

165. Li, Z. *et al.* The use of a near-infrared RNA fluorescent probe with a large Stokes shift for imaging living cells assisted by the macrocyclic molecule CB7. *Biomaterials* **34**, 6473-6481 (2013).

166. Miskolczy, Z. & Biczók, L. Photochromism in Cucurbit[8]uril Cavity: Inhibition of Hydrolysis and Modification of the Rate of Merocyanine–Spiropyran Transformations. *J. Phys. Chem. B* **115**, 12577-12583 (2011).

167. Miskolczy, Z. & Biczók, L. Selective Acceleration of the Protonated Merocyanine-Spiropyran Photochromic Transformation by Inclusion in Cucurbit[7]uril. *Photochem. Photobiol.* **88**, 1461-1466 (2012).

168. Andraos, J. A Streamlined Approach to Solving Simple and Complex Kinetic Systems Analytically. *J. Chem. Educ.* **76**, 1578-1583 (1999).

169. Kuimova, M. K. *et al.* Imaging intracellular viscosity of a single cell during photoinduced cell death. *Nat. Chem.* **1**, 69-73 (2009).

170. Montcourrier, P. *et al.* Characterization of very acidic phagosomes in breast cancer cells and their association with invasion. *J. Cell. Sci.* **107**, 2381-2391 (1994).

171. Movia, D., Prina-Mello, A., Volkov, Y. & Giordani, S. Determination of spiropyran cytotoxicity by high content screening and analysis for safe application in bionanosensing. *Chem. Res. Toxicol.* **23**, 1459-1466 (2010).

172. Mills, J. C., Stone, N. L. & Pittman, R. N. Extranuclear apoptosis. The role of the cytoplasm in the execution phase. *J. Cell. Biol.* **146**, 703-708 (1999).

173. Dinér, P., Alao, J. P., Söderlund, J., Sunnerhagen, P. & Grøtli, M. Preparation of 3-Substituted-1-Isopropyl-1H-pyrazolo[3,4-d]pyrimidin-4-amines as RET Kinase Inhibitors. *J. Med. Chem.* **55**, 4872-4876 (2012).

174. Knowles, P. P. *et al.* Structure and chemical inhibition of the RET tyrosine kinase domain. *J. Biol. Chem.* **281**, 33577-33587 (2006).

175. Neveu, P. *et al.* A caged retinoic acid for one- and two-photon excitation in zebrafish embryos. *Angew. Chem., Int. Ed.* **47**, 3744-3746 (2008).

176. Alvarez, K., Vasseur, J.-J., Beltran, T. & Imbach, J.-L. Photocleavable Protecting Groups as Nucleobase Protections Allowed the Solid-Phase Synthesis of Base-Sensitive SATE-Prooligonucleotides. *J. Org. Chem.* **64**, 6319-6328 (1999).

177. Auld, D. S. *et al.* A basis for reduced chemical library inhibition of firefly luciferase obtained from directed evolution. *J. Med. Chem.* **52**, 1450-1458 (2009).

178. Jia, Y., Quinn, C. M., Kwak, S. & Talanian, R. V. Current in vitro kinase assay technologies: the quest for a universal format. *Curr. Drug. Discov. Technol.* **5**, 59-69 (2008).

179. Chen, X. *et al.* Acetylcholinesterase Inhibitors with Photoswitchable Inhibition of beta-Amyloid Aggregation. *ACS Chem. Neurosci.* **5**, 377-389 (2014).

180. Forsell, P. *et al.* The use of TrkA-PathHunter assay in high-throughput screening to identify compounds that affect nerve growth factor signaling. *J. Biomol. Screen.* **18**, 659-669 (2013).

181. Smith, G. K. & Wood, E. R. Cell-based assays for kinase drug discovery. *Drug Discovery Today: Technol.* **7**, e13-e19 (2010).

182. Widenfalk, J., Widmer, H. R. & Spenger, C. GDNF, RET and GFRalpha-1-3 mRNA expression in the developing human spinal cord and ganglia. *Neuroreport* **10**, 1433-1439 (1999).

183. Bisgrove, B. W., Raible, D. W., Walter, V., Eisen, J. S. & Grunwald, D. J. Expression of c-ret in the zebrafish embryo: potential roles in motoneuronal development. *J. Neurobiol.* **33**, 749-768 (1997).

184. Shin, J., Park, H. C., Topczewska, J. M., Mawdsley, D. J. & Appel, B. Neural cell fate analysis in zebrafish using olig2 BAC transgenics. *Methods Cell. Sci.* **25**, 7-14 (2003).

185. Park, H. C., Shin, J. & Appel, B. Spatial and temporal regulation of ventral spinal cord precursor specification by Hedgehog signaling. *Development* **131**, 5959-5969 (2004).

186. Slee, E. A., Adrain, C. & Martin, S. J. Serial killers: ordering caspase activation events in apoptosis. *Cell Death Differ.* **6**, 1067-1074 (1999).